



Review

# Anticancer Ruthenium(III) Complexes and Ru(III)-Containing Nanoformulations: An Update on the Mechanism of Action and Biological Activity

Claudia Riccardi <sup>1</sup>, Domenica Musumeci <sup>1</sup>, Marco Trifuoggi <sup>1</sup>, Carlo Irace <sup>2</sup>, Luigi Paduano <sup>1</sup> and Daniela Montesarchio <sup>1,\*</sup>

<sup>1</sup> Department of Chemical Sciences, University of Naples Federico II, Via Cintia 21, I-80126 Naples, Italy; claudia.riccardi@unina.it (C.R.); domenica.musumeci@unina.it (D.M.); marco.trifuoggi@unina.it (M.T.); luigi.paduano@unina.it (L.P.)

<sup>2</sup> Department of Pharmacy, University of Naples Federico II, Via D. Montesano 49, I-80131 Naples, Italy; carlo.irace@unina.it

\* Correspondence: daniela.montesarchio@unina.it

Received: 31 August 2019; Accepted: 23 September 2019; Published: 26 September 2019



**Abstract:** The great advances in the studies on metal complexes for the treatment of different cancer forms, starting from the pioneering works on platinum derivatives, have fostered an increasingly growing interest in their properties and biomedical applications. Among the various metal-containing drugs investigated thus far, ruthenium(III) complexes have emerged for their selective cytotoxic activity *in vitro* and promising anticancer properties *in vivo*, also leading to a few candidates in advanced clinical trials. Aiming at addressing the solubility, stability and cellular uptake issues of low molecular weight Ru(III)-based compounds, some research groups have proposed the development of suitable drug delivery systems (e.g., taking advantage of nanoparticles, liposomes, etc.) able to enhance their activity compared to the naked drugs. This review highlights the unique role of Ru(III) complexes in the current panorama of anticancer agents, with particular emphasis on Ru-containing nanoformulations based on the incorporation of the Ru(III) complexes into suitable nanocarriers in order to enhance their bioavailability and pharmacokinetic properties. Preclinical evaluation of these nanoaggregates is discussed with a special focus on the investigation of their mechanism of action at a molecular level, highlighting their pharmacological potential in tumour disease models and value for biomedical applications.

**Keywords:** Ruthenium(III) complexes; nanocarriers; nanoaggregates; drug delivery; anticancer therapy; preclinical evaluation

## 1. Introduction

### 1.1. From Platinum(II) to Ruthenium(III)-based Complexes: The Importance of Nanoformulations in Metallo Drug Delivery

The interest in metal-based complexes for the treatment of cancer started with the serendipitous discovery of the anti-tumour properties of *cis*-diamminedichloroplatinum(II) (*cDDP* or cisplatin) in the early 1960s [1,2]. Approved in 1978 by the Food and Drug Administration [3], cisplatin is used in the treatment of a broad spectrum of human cancer malignancies either as single agent (cervical, bladder, head, and neck cancer) or in combination treatments (testicular, bladder, head and neck cancer) [4]. The cytotoxicity of cisplatin is due to its interaction with DNA, forming adducts preferentially with adjacent guanines, thus interfering with replication and transcription processes and ultimately triggering apoptosis, as main cell death pathway [5–8]. Unfortunately, dose-limiting

side effects (nephrotoxicity, ototoxicity and peripheral neurotoxicity) and its intrinsic or acquired resistance hindered its widespread use [4,9,10], stimulating the search for new, safer metal-based anticancer agents.

Second- and also third-generation Pt(II) complexes have been developed over the last 50 years, with about more than 20 Pt(II)-based compounds entered in clinical trials. Of these, only two (carboplatin [11] and oxaliplatin [12]) obtained international marketing approval, respectively, in 1992 and 2002, and three others (nedaplatin, lobaplatin and heptaplatin) were approved only in individual countries (Japan, China and Korea, respectively) [13–15].

Afterwards, novel anticancer agents based on metals different from platinum were developed, as extensively reported in several review articles [16–23]. Among all the metal derivatives thus far investigated, ruthenium complexes in the +2 and +3 oxidation states gained increasing attention as valuable alternatives to Pt(II)-based ones [24–33].

However, clinical application of metallodrugs, when administered via conventional intravenous methods, has been hampered by their limited aqueous solubility and short in vivo half-lives, resulting in inadequate bioavailability and low accumulation in the tumour masses. Thus, several approaches have been proposed to address these issues, particularly exploiting nanotechnology-based strategies [34–37]. The main advantages of using nanosystems for drug delivery include their high stability, notable loading capacity and possibility to achieve controlled or sustained drug release. This approach can significantly increase the circulation time in the body, limit the susceptibility to chemical and/or enzymatic degradation, target specific tumour sites and reduce the toxic side effects associated with drug administration [28,37–42].

As far as Ru(II)-based complexes are concerned, their preparation, encapsulation into different nanosystems and studies on their mechanism of action have been comprehensively described in recent overviews [43,44].

In this review we report the state-of-the-art on anticancer Ru(III)-based complexes including the ad hoc designed nanoformulations to incorporate and deliver these antiproliferative agents. Particular emphasis is given to the emerging strategies to facilitate the application of Ru(III)-based drugs in vivo, aimed at enhancing their solubility and bioavailability, as well as improving their delivery to cancer cells. In addition, the biological activity of these Ru(III)-containing nanosystems and, where known, their mechanism of action is discussed, focusing on the contribution of our group in this field and the most recent literature examples.

### *1.2. Anticancer Activity and Mechanism of Action of the Lead Low Molecular Weight Ru(III)-Based Compounds*

To the best of our knowledge, three Ru(III)-containing compounds entered in clinical trials: NAMI-A [45,46], KP1019 [47–53], as well as its sodium salt analogue named IT-139, formerly known as NKP-1339 [54–58]. Despite their structural similarities (Figure 1), these complexes dramatically differ in their bioactivity [59]. In fact, preclinical studies demonstrated that NAMI-A was essentially inactive against primary tumours but proved to specifically affect tumour metastases, preventing their development and growth [45,46]. In contrast, KP1019 exhibited marked cytotoxic activity in vitro in cisplatin-resistant human colon carcinoma cell lines, as well as significant anti-tumour effects in vivo against a wide variety of tumour xenografts through induction of apoptosis [47–53]. NKP-1339 is the most recent compound entered in clinical trials against solid cancer forms, showing a manageable safety profile with absence of neurotoxicity and dose-limiting haematological toxicity [54–58].

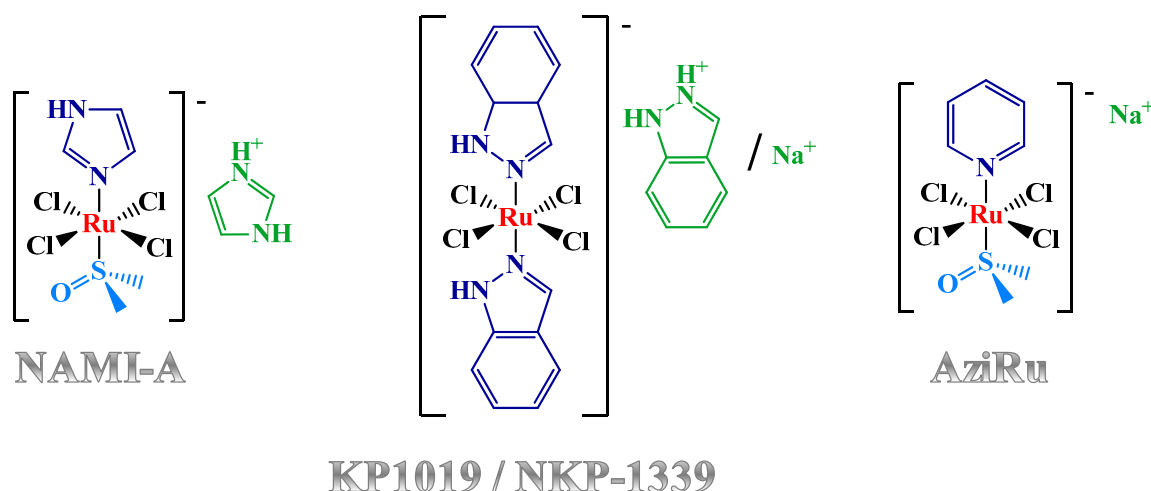


**Figure 1.** Chemical structures of NAMI-A, KP1019, NKP-1339 and AziRu. Here, ruthenium ions are indicated in red, the counterions in green, while the N- and S-donor ligands in dark and light blue, respectively.

Many preclinical studies have investigated the mechanism of action of these complexes. A large body of evidence has been gathered proving that these Ru(III) complexes are able to interact with plasma proteins—particularly with serum albumin [60–64] and transferrin [65–69]—and/or bind nucleic acids [70–73]. The extensive binding to serum proteins for KP1019 and NAMI-A was also reflected by their low distribution volume in clinical phase I evaluation [45,51].

As concerns the interaction with cancer cells, X-ray fluorescence imaging measurements revealed a wide intracellular distribution of KP1019 both in cytosol and in the nuclear region after treatment; conversely, following NAMI-A administration *in vitro*, ruthenium was not detected inside the cells, suggesting its strong interaction with cell membranes as well as alternative mechanisms of action [74].

Stimulated by the positive impact of Ru(III) complexes in the panorama of known anticancer agents, Walsby et al. [75,76] as well as our group [77] independently and almost simultaneously described a NAMI-A-like complex carrying a pyridine residue in place of the imidazole ligand, and sodium replacing imidazolium as the counterion (Figure 1, right). This novel compound, called NAMI-Pyr by the first research group and AziRu by the second one, overall proved to be poorly cytotoxic, similarly to the parent NAMI-A, however showing  $IC_{50}$  values half that of NAMI-A on human breast MCF-7 and cervical HeLa cancer cell lines (Table 1) [77–79].

The overall higher cytotoxicity observed for this pyridine-containing Ru complex vs. NAMI-A was explained by the chemical properties of the nitrogen ligand, which compared to imidazole confers higher lipophilicity and, thus, expectedly improved cellular uptake [75,80–82].

Analogously to its congeners, AziRu proved to bind both nucleic acids and proteins [83–86]. Detailed spectroscopic and mass spectrometric investigations showed AziRu to be more reactive towards DNA model systems—both single stranded and duplex oligonucleotides—than NAMI-A [85]. Moreover, its capability to interact with model proteins—such as bovine pancreatic ribonuclease A (RNase A) [84] and hen egg white lysozyme (HEWL) [83]—was investigated by X-ray crystallography and Raman microscopy studies. In both model proteins, crystal structure analysis indicated that the protein conformation was not dramatically affected by Ru complexation and that the metal lost all its original ligands upon binding [83,84]. In particular, experiments with HEWL protein also underlined the ability of AziRu, upon aging, to form polyoxo species containing Ru–O–Ru bond [83,87].

More recently, studies aimed at identifying AziRu release conditions from bound proteins were carried out, using a Raman-assisted crystallographic approach to investigate the AziRu/HEWL complex as a case study. Crystallography was used to identify the protein structural changes and metal release occurring upon  $Ru^{III} \rightarrow Ru^{II}$  reduction by alternative exposure to different reducing agents,

while Raman microscopy on protein crystals allowed identifying the spectral changes attributable to the reduction of Ru(III) bound to the protein [86]. These studies clearly indicated a Ru reduction in the protein complex, followed by a Ru release mechanism dependent on the reducing agent: reduction with hydrazine produced a native-like lysozyme crystal with a Raman spectrum identical to the wild-type protein, suggesting the complete Ru release from the protein upon reduction. In contrast, the Raman analysis on AziRu/HEWL crystals treated with ascorbate suggested that in this case the  $\text{Ru}^{\text{III}} \rightarrow \text{Ru}^{\text{II}}$  reduction occurred without Ru release. The observed differences in the hydrazine- and ascorbate-induced action indicated a two-step Ru reduction-release mechanism [86]. To better understand this process, a pH-dependent, spectroelectrochemical surface-enhanced Raman scattering (SERS) study was also performed on AziRu-functionalized Au electrodes as a surrogate and simple model system mimicking the anticancer Ru(III)-based drugs. This SERS study allowed determining a  $\text{pK}_a$  of  $6.0 \pm 0.4$  for the aquated AziRu complex in the  $\text{Ru}^{\text{III}}$  state, which corresponds to the pH values characteristic of the external microenvironment of most cancer cells, significantly differing from healthy ones. These experiments also indicated a dramatic shift of the redox potential ( $E_0$ ) by  $> 600$  mV for the aquated AziRu species toward more positive potentials upon acidification, suggesting a selective AziRu reduction in cancer environments but not in normal ones [86].

### 1.3. Nucleolipid and Aminoacyl Lipid-based Structures Incorporating AziRu, a NAMI-A-Like Ruthenium Compound

All the described ruthenium complexes proved to be poorly stable in aqueous media, where the most labile ligands, typically chloride ions, are easily and relatively rapidly replaced by hydroxide ions and/or water molecules, resulting in hydrolysis of the complexes [85,88–95], also leading to poly-oxo species formation [83,89,96,97]. Although it has been reported, at least for NAMI-A, that the presence of these oligomeric species does not really impair the overall anti-tumour activity [89,98], the premature formation of aquated species in the extracellular medium could deactivate, or activate too early, most of the administered drug, thus reducing the available active forms which ultimately interact with the biological targets (proteins or DNA) [3,99]. For this reason, the effective biomedical potential of these low molecular weight ruthenium complexes, administered as such, has been recently reconsidered. Taking into account that the ligand exchange process could also represent a potential mechanism of action of the Ru(III)-based drugs, or of activation in case they behave as prodrugs of the more reactive Ru(II) congeners, several efforts have been made to retard the ligand exchange processes in the extracellular environment so to ensure their occurrence once the drug has reached the cell.

Following the investigations carried out on KP1019 and NAMI-A [72], in a recent study the subcellular accumulation of AziRu was determined by inductively coupled plasma-mass spectrometry (ICP-MS) analysis performed on various biological samples taken from MCF-7 breast cancer cell cultures (culture medium, cellular pellet, cytosolic fraction, nuclear fraction and DNA samples) after 24 h of in vitro ruthenium treatment [100]. About 80% of the administered ruthenium was found in the culture medium, while only a very small amount (less than 10%) was detected in the nuclear fraction [100]. This result corroborated the hypothesis of a massive early drug deactivation in the extracellular environment and/or a poor ability to penetrate the cell membranes, reinforcing the need to protect the metal core in Ru-based drugs in order to obtain more efficient cell internalization.

Thus, in order to produce more effective Ru(III)-based anticancer agents, able to cross the biological barriers, our research group proposed a prodrug approach. In this design, the active unit, AziRu, has been incorporated into highly functionalized nucleolipid-based scaffolds [101] able to form, under physiological conditions, stable self-assembling aggregates efficiently protecting the metal complex from biological degradation and conveying it through the cell phospholipidic bilayers [77,79,102–109].

In detail, the low molecular weight complex AziRu was decorated using ribo- and deoxyribonucleosides as starting building blocks, functionalized with suitable hydrophilic (oligoethylene glycol moieties) and lipophilic (oleoyl or cholesteroxyacetyl groups) chains,

obtaining a mini-library of amphiphilic nanovectors to enhance the Ru(III) delivery in vivo. Within this approach, the nucleolipid-based Ru(III) complexes—named ToThyRu, HoThyRu, DoHuRu [77,106], ToThyCholRu [79,105], the fluorescently-labelled HoThyDansRu [100,106] and the second-generation HoUrRu [107] (Figure 2)—were successfully prepared and evaluated in their physico-chemical properties (for a recent review covering their design, synthesis and characterization, see Riccardi et al. [35]).

### Nucleolipid-based Ru(III) complexes

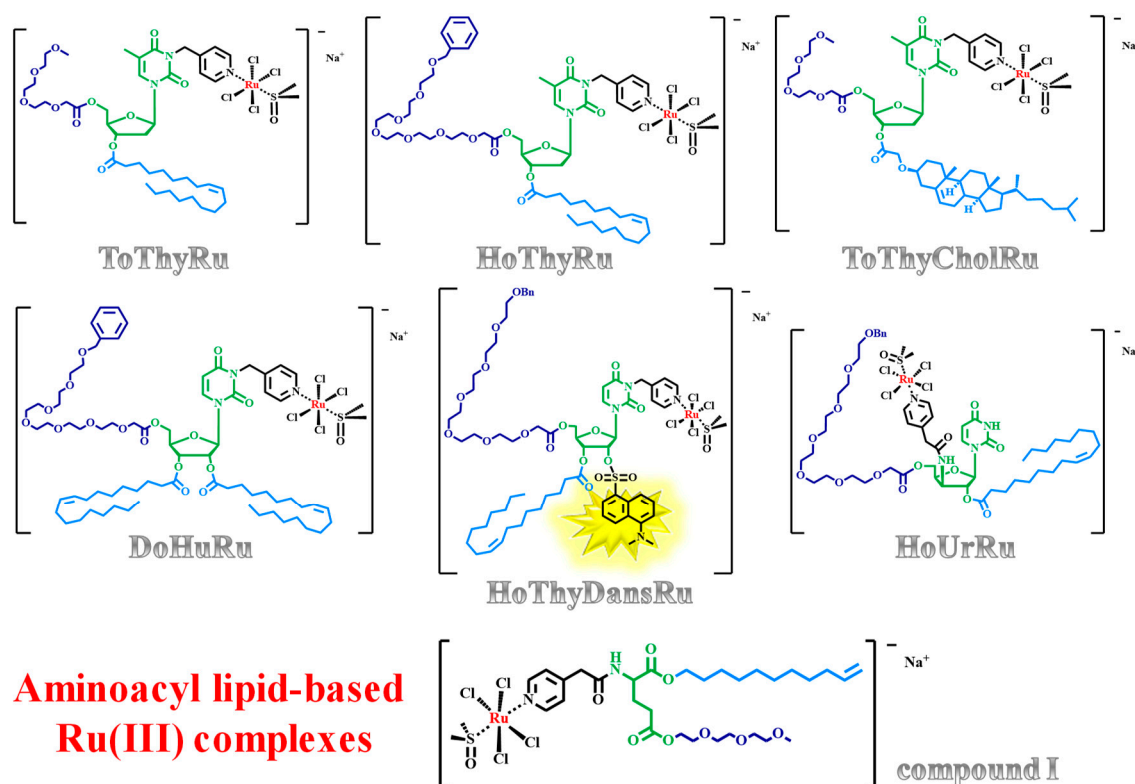


**Figure 2.** Chemical structures of the proposed nucleolipid and aminoacyl lipid-based Ru(III)-complexes. In the figures, ruthenium ions are indicated in red, the central scaffolds in green, while the hydrophilic and lipophilic chains in dark and light blue, respectively. In the HoThyDansRu molecular structure, the fluorescent dansyl group is highlighted in yellow (Bn = benzyl group).

In order to further expand the chemical diversity of the available amphiphilic Ru(III) complexes, a central core alternative to the nucleolipidic one, i.e., the trifunctional  $\alpha$ -amino acid glutamic acid, was explored to build the nanocarrier for the Ru(III) metal core [110]. The novel aminoacyl lipidic Ru(III) complex I (Figure 2) showed a slower hydrolysis kinetics compared to AziRu, demonstrating that also an aminoacyl lipid is a suitable scaffold to protect the Ru(III) complex from the aquation processes [110].

## 2. Ru(III)-Containing Formulations as Efficient Drug Delivery Systems

### 2.1. KP1019-Hosting Nanosystems

In order to overcome the poor stability observed for KP1019 in aqueous solutions, especially at physiological pH, Keppler et al. proposed an interesting approach [111]. KP1019 was entrapped in poly(lactic acid) nanoparticles (PLA NPs) in the presence of two different non-ionic surfactants: the poloxamer Pluronic F-68 and polysorbate Tween 80 (Figure 3a), in order to evaluate the contribution of the surfactant on the chemical stability and encapsulation properties of the final nanoaggregates [111].

These formulations, prepared by a single oil-in-water (o/w) emulsion and characterized by dynamic light scattering (DLS) and transmission electron microscopy (TEM) analyses, were essentially based on physical encapsulation, which exploits the affinity between the carrier and the drug to entrap the latter one in a suitable matrix.

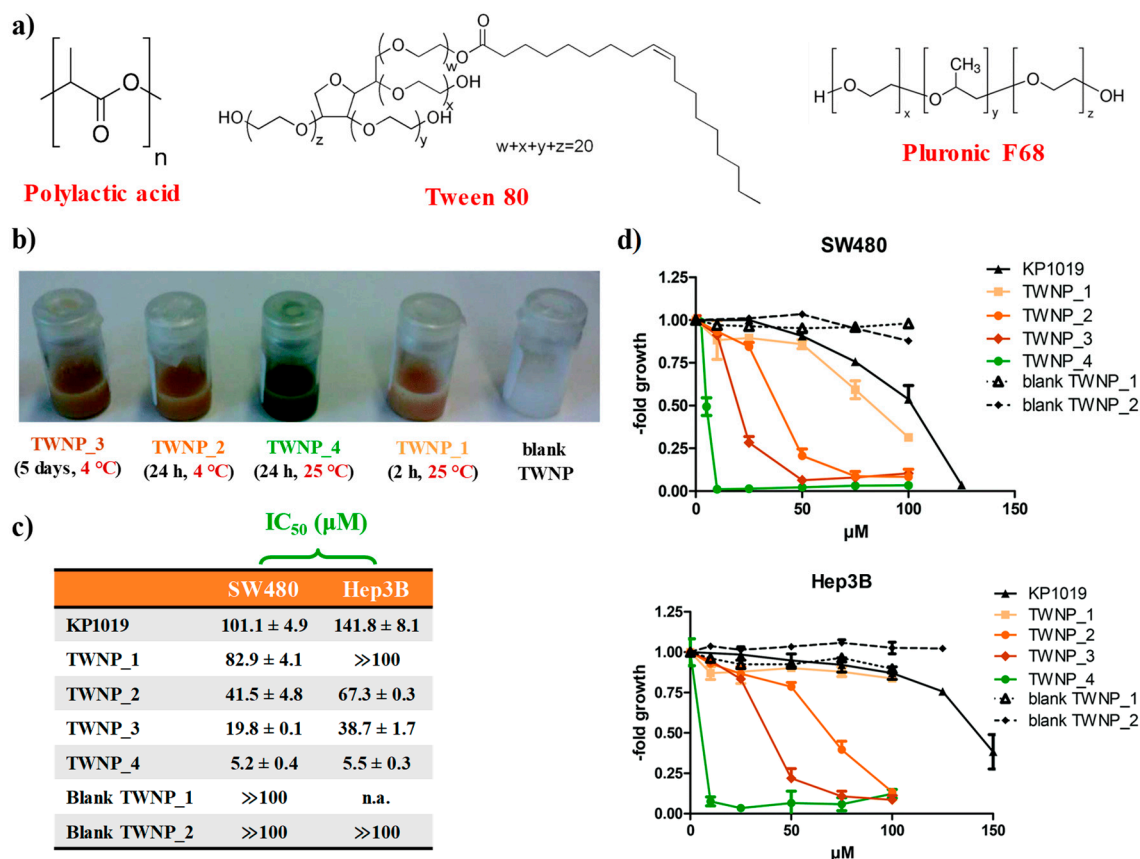


**Figure 3.** KP1019 incorporation into poly(lactide) nanoparticles (PLA NPs): (a) chemical structures of poly(lactide) acid and of the surfactant used in the formulation (poloxamer Pluronic F-68 and polysorbate Tween 80); (b) nanoparticle appearance after different temperature and period storage: TWNP\_3 (5 d, 4 °C), TWNP\_2 (24 h, 4 °C), TWNP\_4 (24 h, 25 °C), TWNP\_1 (2 h, 25 °C), blank TWNP, from left to right; (c) IC<sub>50</sub> values (μM) of the different KP1019 nanoformulations prepared in comparison with naked KP1019. Blank TWNP\_1 (1 month, 4 °C), Blank TWNP\_2 (2 h, 25 °C); IC<sub>50</sub> values are reported as mean ± SEM. (d) dose-response curves of colon carcinoma SW480 and the hepatoma Hep3B cancer cell lines with the indicated drugs as determined by MTT assay after 72 h treatment. Figures were adapted from [111] published by The Royal Society of Chemistry.

The Ru-containing nanoaggregates based on Pluronic F-68 (indicated as PLNP) clearly showed a brown drug precipitation after ca. 15 h, suggesting that KP1019 diffused out of the PLNP and therefore this kind of nanoformulation was not further explored [111].

On the contrary, the use of Tween 80 allowed preventing drug precipitation with very high KP1019 loading efficiency, ranging from 92% to 95% with respect to the initial amount. When stored at 4 °C, the obtained formulations (indicated as TWNP) did not show settling of particles, indicating a substantial stability without agglomerate formation for about 1 month. In turn, these polysorbate-containing NPs, when left at r.t., showed a remarkable colour change from brown to deep green after ca. seven days, indicative of the reduction of the Ru(III) centre (Figure 3b) [111].

This hypothesis was then investigated by kinetic studies: ESI-MS experiments demonstrated the replacement of a chloride ligand by Tween 80, involving its moderately basic oxygen groups. This exchange reaction was also accompanied by reduction of the paramagnetic Ru(III) to the

diamagnetic Ru(II) ion, as revealed by electron spin resonance (ESR) spectra, and explained by the well-known autoxidation ability of polysorbates [111].

The evaluation of the *in vitro* anticancer properties performed on colon carcinoma SW480 and hepatoma Hep3B cell lines indicated a modest increase of the antiproliferative activity for the stable NPs (stored at 4 °C), along with a markedly higher cytotoxic activity for the NPs left at r.t. (Figure 3c,d). Indeed, green NP solutions showed a 20- and 26-fold increased cytotoxic activity with respect to the naked KP1019 drug, respectively on SW480 and Hep3B cancer cells. Thus, surprisingly, longer storage period distinctly increased the activity of the KP1019-loaded TWNP particles [111].

For KP1019, the same research group also proposed a strategy alternative to the physical encapsulation, based on the chemical conjugation of the ruthenium complex with a selected polymer [112]. In particular, KP1019 was loaded into micelle-like carriers (MC-KP1019) formed by an ad hoc synthesized PEGylated polymer. Indeed, micelles proved to be highly biocompatible and efficient [113,114]. The obtained micelles were fully characterized by TEM and zeta potential measurements in order to determine their size range and surface charge. In addition, MC-KP1019 solutions (0.3 mg/mL KP1019) proved to be stable at 4 °C, with no precipitation for more than three months [112].

Then, the anticancer activity of MC-KP1019 was evaluated following 72 h drug incubation and compared with naked KP1019 on different human cancer cell lines, i.e., the colon carcinoma cell line HCT116 and its subline HCT116 (p53/ko) with a deleted p53 gene, the non-small cell lung carcinoma cell line SW1573 with its ABCC1- and LRP-overexpressing subline 2R120, and its ABCB1- and ABCC1-overexpressing subline 2R160, the epidermal carcinoma cell line KB-3-1 and its ABCB1-overexpressing subline KBC-1, the breast cancer cell model MCF-7 and its ABCB1-overexpressing subline MCF-7/adr, along with the human colon adenocarcinoma Lovo and its ABCB1- overexpressing subline Lovo/dox. In all cases, KP1019-containing micelles were found to be more active than naked KP1019, showing IC<sub>50</sub> values between 1.6- and 22.7-fold lower compared to the free Ru compound (IC<sub>50</sub> values ~100 µM or above) [112].

Notably, in the SW1573 sublines 2R160 and 2R120, both being distinctly resistant to KP1019, the micellar formulation of KP1019 was able to overcome this resistance, showing very interesting cytotoxicity [112]. Moreover, the micelle-based nanosystems facilitated the cellular accumulation of KP1019, as determined by ICP-MS measurements. Concerning their mode of action, increased cell cycle arrest in G2/M phase (PI-staining), DNA damage (Comet assay) as well as enhanced levels of apoptotic cell death (caspase 7 and PARP cleavage) were found in HCT116 cells treated with the MC-KP1019 nanoformulations [112].

## 2.2. NAMI-A-Hosting Nanosystems

The micellization approach has been explored to enhance also the *in vivo* delivery of NAMI-A.

Stenzel and coworkers reported the polymerization of 4-vinyl imidazole (VIm) using a trithiocarbonate RAFT agent, i.e., 2-[(dodecylthio-carbonothioyl)thio]-2-methylpropanoic acid, and the subsequent chain extension with poly(ethylene glycol)methyl ether acrylate (PPEGMEA) to obtain a biocompatible amphiphilic block copolymer capable to self-assemble into polymeric micelles and incorporate NAMI-A (indicated as P(NAMI-A)-PPEGMEA, Figure 4a) [115].

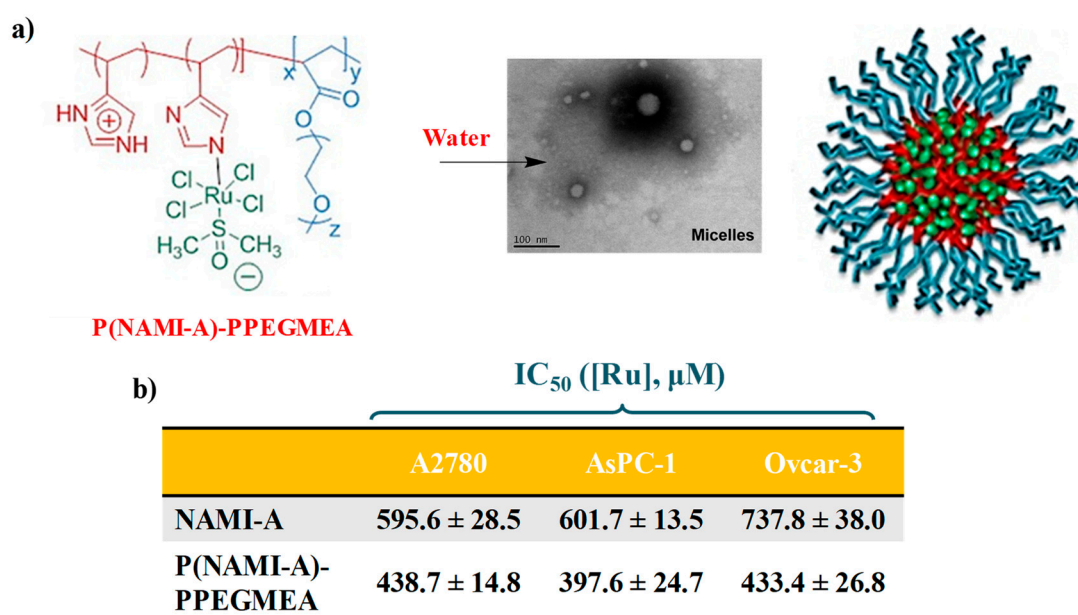


**Figure 4.** NAMI-A conjugation to polymeric micelles: (a) chemical structure of the amphiphilic block copolymer P(NAMI-A)-PPEGMEA and schematic representation of its micellization in water; (b) cytotoxicity and IC<sub>50</sub> values (μM, expressed in terms of ruthenium concentration) of NAMI-A and P(NAMI-A)-PPEGMEA against ovarian A2780 and Ovcar-3 and pancreatic AsPC-1 cancer cell lines. IC<sub>50</sub> values are reported as mean ± SEM. Figures were adapted with permission from [115] Copyright 2014 from American Chemical Society.

The polymerization reaction was followed by SEC analysis monitoring the retention time changes due to the increased polymer size over time and the resulting micelles were then characterized by DLS and TEM experiments (Figure 4a) [115].

When tested on ovarian (A2780 and Ovcar-3) and highly aggressive pancreatic AsPC-1 cancer cell lines, a 1.5-times increase in cytotoxicity was found in all the tested cell lines for the polymeric NAMI-A-containing micelles compared to the naked ruthenium complex (Figure 4b) [115].

Notably, polymeric micelles significantly improved also the NAMI-A antimetastatic potential, with increased inhibitory effects on both the migration and invasion of human breast cancer cells [115]. In particular, the influence of the polymeric P(NAMI-A)-PPEGMEA micelles on the migration processes of three cell lines (invasive cancerous MDA-MB-231, noninvasive cancerous MCF-7 cancerous noncancerous CHO) was evaluated when a chemical (chemotaxis) and a contact (haptotaxis) stimulus was applied to promote cell movements. Both the chemotactic and haptotactic migration of breast cancer cells were inhibited in a massive way with respect to the nontumorigenic CHO cells, with statistically significant effects observed for the invasive MDA-MB-231 cell line [115].

### 2.3. AziRu-Hosting Nanosystems

Recently, Tesauro and colleagues proposed a variant of the well-known AziRu (indicated in this work as RuPy by the authors) containing a fully protected sugar moiety as decoration for the ruthenium-coordinating pyridine moiety (named RuPyTry, Figure 5a) aiming at increasing the Ru(III) complex cell internalization [116]. This novel complex, fully characterized by ESI-MS, IR and <sup>1</sup>H NMR spectroscopy, showed a faster hydrolysis in aqueous solution with respect to its parent compound, with formation of the respective mono aqua complex, probably favoured by the hydrogen-bonding properties of the nitrogen atoms in the triazole moiety facilitating the access of water molecules to the metal [116].

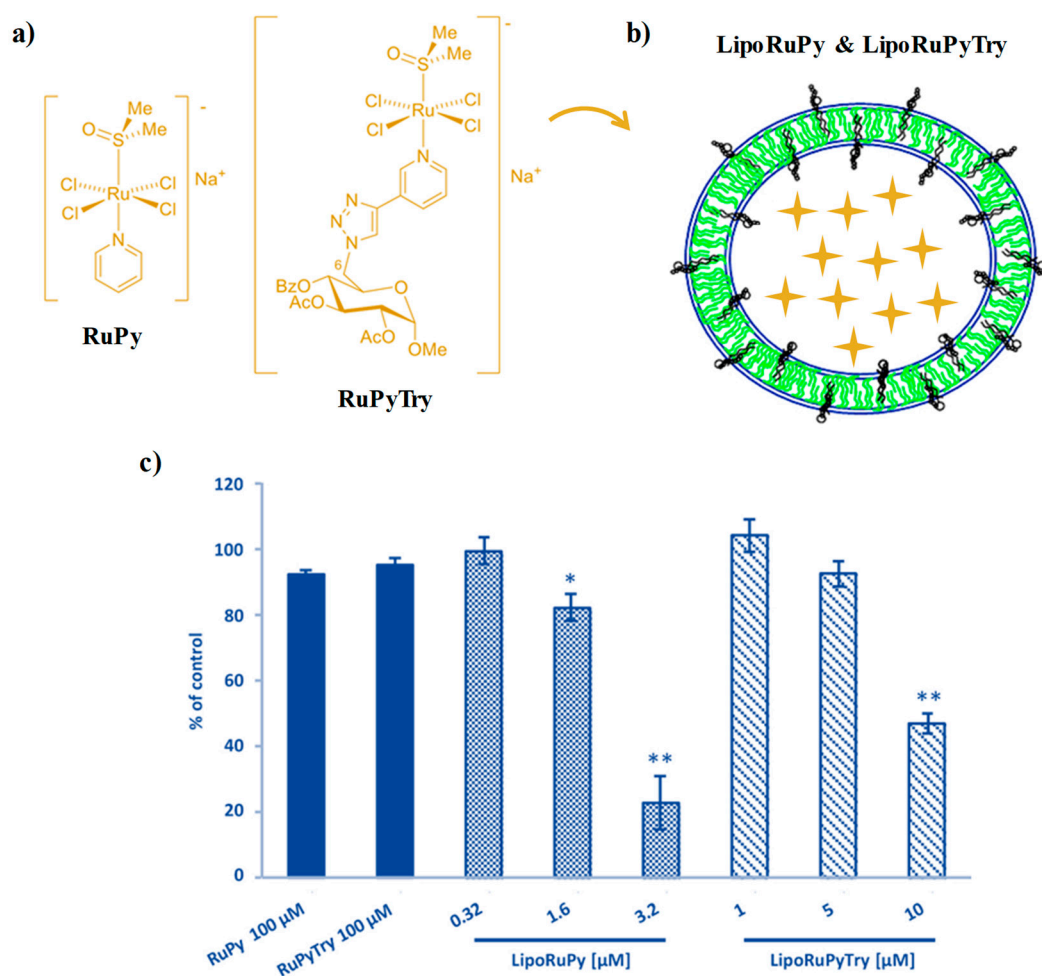


**Figure 5.** Pyridine-containing Ru(III) complexes inserted in liposome systems: (a) chemical structure of the proposed RuPy and RuPyTry compounds; (b) schematic representation of liposomal nanoaggregates containing the pyridine-based Ru(III) complexes; (c) dose-response histograms reporting the cytotoxic effects observed for the naked Ru(III) compounds and their liposomal formulations in PC-3 cancer cells after 48 h treatment. Figures are adapted from [116].

Then, Ru-containing liposome formulations were prepared mixing phosphatidylcholine (PC)/cholesterol (Chol)/DSPEPeg2000 in 57/38/5 molar ratio (Figure 5b). The obtained liposomes, with ca. 100 nm size, exhibited very slow ruthenium release kinetics, with only 4% of the complex released in serum over 72 h monitoring [116].

These Ru(III) complexes as such, as well as their liposomal nanoaggregates, LipoRuPy and LipoRuPyTry, were evaluated for their anticancer activity analysing the inhibition of cell proliferation on human prostate cancer PC-3 cells and human dermal fibroblasts (NHDF).

The naked Ru(III) complexes did not show significant cytotoxic effects on cancer PC-3 cells even when tested at 100  $\mu\text{M}$  concentration (Figure 5c); a slight decrease in cell viability was found only at concentrations >500  $\mu\text{M}$ . Conversely, the liposomal formulations exhibited relevant cytotoxicity under the same conditions. The observed reduction in cell viability was found to be concentration-dependent and more marked for the RuPy-containing liposomes (LipoRuPy, Figure 5c). In turn, when tested on normal NHDF cells, these formulations did not affect cell viability even at 100  $\mu\text{M}$  concentration, demonstrating their selectivity and promising bioactivity [116].

#### 2.4. Mononuclear and Dinuclear Ru(III)-Dithiocarbamato Complexes Encapsulated in Nanosized Carriers

Fregona et al. [117] proposed novel mono- and dinuclear Ru(III)-complexes with aromatic and non-aromatic dithiocarbamates as ligands: in particular, carbazolyldithiocarbamato derivatives (CDT) and pyrrolidinedithiocarbamate (PDT) analogues were prepared (Figure 6a). These compounds were fully characterized by physico-chemical techniques such as elemental analysis, ESI-MS spectrometry,  $^1\text{H}$  NMR UV-VIS and FT-IR spectroscopic studies [117].

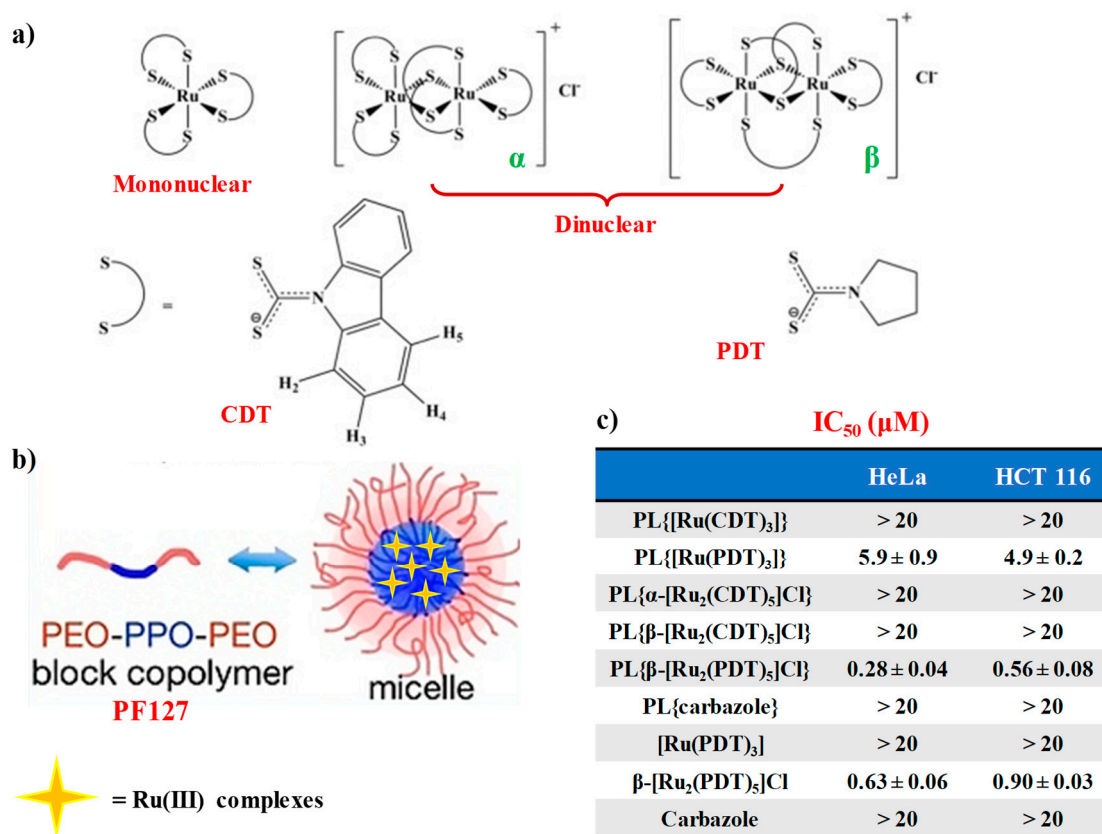


**Figure 6.** (a) Chemical structures of mononuclear and dinuclear Ru(III)-dithiocarbamato complexes and of the investigated dithiocarbamato ligands: pyrrolidyl dithiocarbamate (PDT) and carbazolyldithiocarbamate (CDT); (b) schematic representation of the Pluronic® F127 block copolymer and micelle formation with Ru(III) complex internalization; (c)  $\text{IC}_{50}$  values ( $\mu\text{M}$ ) evaluated after 72 h treatment with free Ru(III)-dithiocarbamato complexes and their micelles formulations (indicated as PL{compound}).  $\text{IC}_{50}$  values are reported as mean  $\pm$  SEM. Figures are adapted from [117].

In order to address the solubility issues typically associated with ruthenium drugs under physiological conditions, both CDT and PDT Ru(III)-based derivatives were encapsulated in water-soluble micellar carriers by using the biocompatible copolymer Pluronic® F127 [117].

Such block copolymer is a non-ionic surfactant consisting of hydrophilic poly(ethylene oxide) (PEO) and hydrophobic poly(propylene oxide) (PPO), arranged in A-B-A tri-block structure which comprise a hydrophobic PPO region covered by a hydrophilic shell, made up of PEO chains [118].

The incorporation of the selected Ru(III)-based compounds during the micellization process was driven by the hydrophobic interactions established between the compounds and the PPO domain of the selected copolymer, hence preventing unwanted release of the loaded compounds (Figure 6b for the schematic representation of the micelle formation) [117]. As verified by UV-VIS analysis in saline solution (NaCl 0.9% *w/v*), the prepared Ru(III)-incorporating micellar nanocarriers did not show significant changes in the UV spectra over time, at least over 72 h monitoring [117].

Both naked CDT- or PDT-based ruthenium compounds as well as their nanoformulations were then tested in preliminary bioactivity assays on two human tumour epithelial cell lines, i.e., HeLa (cervix adenocarcinoma) and HCT 116 (colon carcinoma) over 72 h treatment, using cisplatin as the control [117].

Interestingly, the  $\beta$  form of the PDT dinuclear complex ( $[\text{Ru}_2(\text{PDT})_5]\text{Cl}$ ) evidenced a ca. two-fold higher activity when loaded into Pluronic<sup>®</sup> F-127 micelles compared to its naked form. This occurred also for the mononuclear PDT complex, showing a three-fold increased anticancer activity (Figure 6c) [117]. Notably, all the PDT-based compounds proved to be more efficient against cervical HeLa than on colon carcinoma HCT116 cancer cell lines, as also found for the Ru(III)-containing nanosystems [109]. Conversely, both mononuclear and dinuclear Ru(III)-CDT complexes encapsulated in Pluronic<sup>®</sup> F127 micelles were not active on the tested cell lines [117].

### 2.5. Liposome-Based Systems Containing Nucleolipid or Aminoacyl Lipid-Based Ru(III) Complexes

As in the case of low molecular weight Ru(III) compounds, also the nucleolipid- or aminoacyl lipid-based complexes incorporating AziRu, here described in paragraph 1.3, when dissolved in aqueous solutions, showed tendency to hydrolyse over time, even if sensibly reduced compared to naked AziRu [77,105,110]. In order to further increase their stability and obtain liposome-based delivery systems incorporating specific amounts of the selected Ru(III) complex, our group studied the co-aggregation of both nucleolipid- and aminoacyl lipid-based Ru(III) complexes with either the zwitterionic phospholipid POPC (1-palmitoyl-2-oleoyl-sn-glycero-3-phosphocholine) or the cationic lipid DOTAP (1,2-dioleoyl-3-trimethylammoniumpropane). A schematic representation of the obtained liposome-based nanosystems is reported in Figure 7.

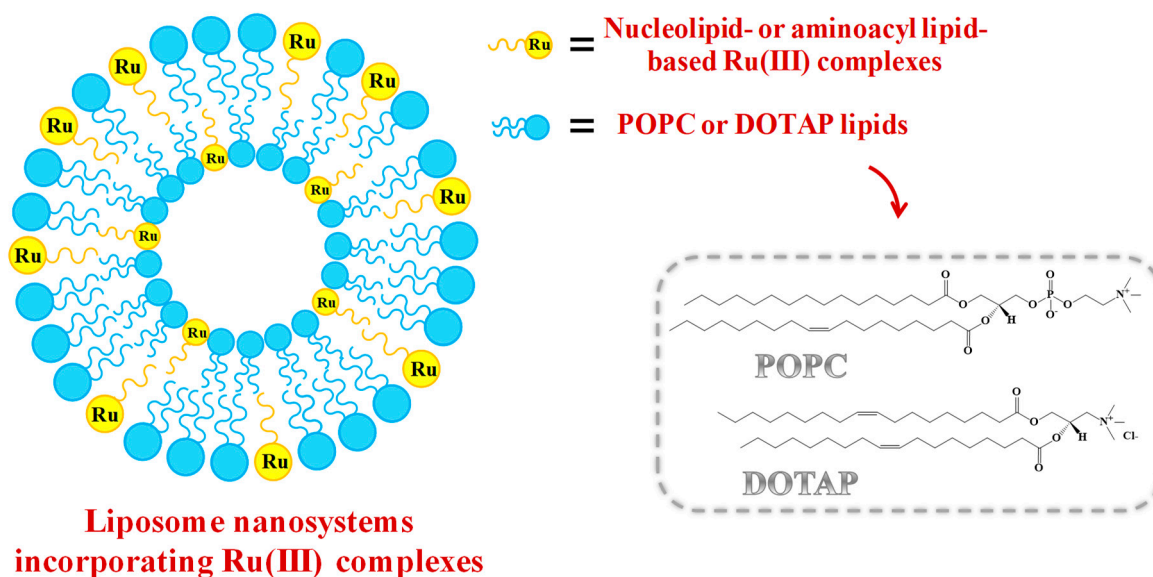


**Figure 7.** Schematic representation of liposomal POPC- or DOTAP-based nanoaggregates containing nucleolipid- or aminoacyl lipid-based Ru(III) complexes.

Liposomes, discovered in the 1960s, consist in phospholipid-based nanovesicles having a morphology very similar to cellular membranes, with an aqueous core surrounded by lipid bilayers [119–121]. Thanks to their peculiar structure, liposomes are considered ideal nanosystems to encapsulate both hydrophilic and lipophilic drugs, respectively in the aqueous core and within the lipid bilayer [122–124]. To date, liposomes also represent the most successful drug delivery systems [125], with several formulations approved by FDA for anticancer therapy and also available in clinical use [119,126–129], such as lipoplatin, a liposomal cisplatin formulation approved by FDA for pancreatic and lung cancer treatment [130].

Thus, POPC and DOTAP lipids were chosen as Ru(III) complexes stabilizing agents on the basis of their proved biocompatibility [77,105,106,131,132]. In particular, POPC liposomes are efficiently used in a broad range of biotechnological applications [133], while liposomes formed by the cationic lipid DOTAP showed noteworthy transfection efficiency both *in vitro* and *in vivo* [131], probably due to the favourable interactions with the negatively charged membranes.

The use of phospholipids—forming ordered bilayers in which the Ru complexes can be easily lodged—allowed obtaining Ru(III)-containing formulations stable for months in physiological media, in which the incorporated metal amount can be finely modulated.

On the other hand, the selected lipids allowed exploiting different interactions for the Ru-complex embedding (mostly hydrophobic for POPC, and both hydrophobic and electrostatic for DOTAP), thus providing a basis to evaluate a structure-activity rationale.

Generally, the Ru(III)-containing POPC formulations were prepared mixing the Ru complex and the lipid in 15:85 molar ratio [77,105,107]. In turn, liposomes based on cationic DOTAP lipid were able to incorporate a higher amount of the nucleolipid- or aminoacyl lipid-based Ru complex, providing stable DOTAP co-aggregates with up to 30% in moles of ToThyCholRu [79] or the aminoacyl lipid compound I [110], and 50% in moles of ToThyRu, HoThyRu, DoHuRu or HoUrRu [106,107]. Both Ru(III)-containing liposomes showed effectively retarded ligand exchange processes in physiological solutions [105,110].

On these Ru(III)-containing liposomes detailed preclinical studies were then carried out in order to assess their anticancer activity and disclose their mechanism of action, so to evaluate their potential in cancer treatments.

### 3. Antiproliferative Effects of Liposome-Based Systems Containing Nucleolipid or Aminoacyl Lipid-Based Ru(III) Complexes: Insight into Their Mode of Action

#### 3.1. *In Vitro* Bioactivity

In order to verify the antiproliferative efficacy of the nucleolipid- or aminoacyl lipid-based Ru(III) complexes inserted in POPC- and DOTAP-based formulations, detailed investigations on their *in vitro* bioactivity were performed in comparison with naked AziRu [77,79,100,105–107,110,134]. A selected panel of human and non-human cancer cell lines was chosen, particularly focusing on cells of different histopathological origin and widely used in anticancer research due to their replicative potential and malignancy, such as MCF-7 (human breast adenocarcinoma cell line), WiDr (human epithelial colorectal adenocarcinoma cell line), HeLa (human cervical cancer cells) and C6 (tumour rat glioma cells) [134–136]. In parallel experiments, some of these formulations were also tested on normal cell lines, such as L6 (rat muscle cells) and HaCaT (human keratinocytes cells), representing useful models to assess possible biological effect on healthy cells [137]. The experimental procedures here adopted involved the estimation of the anticancer activity by means of a “cell survival index”, arising from the combination of a mitochondrial functional assay *in vitro* for the evaluation of the metabolic activity with an automated cell count. From the resulting concentration/effect curves, IC<sub>50</sub> values were determined (Table 1).

In line with our expectations, liposomes exclusively composed by POPC or DOTAP did not interfere with cell viability and proliferation [77,105,106]. On the contrary, all the tested Ru(III)-containing POPC- and DOTAP-based formulations inhibited cancer cell proliferation at least one order of magnitude more effectively than naked AziRu, with IC<sub>50</sub> values in the low  $\mu\text{M}$  range, indicative of a significant activity in reducing cancer cells growth (Table 1) [35,77,79,100,105–107,110,134].

**Table 1.** IC<sub>50</sub> values (μM) relative to AziRu and to the effective ruthenium concentration inserted in the Ru(III)-incorporating POPC- and DOTAP-based liposomes in the indicated cell lines following 48 or 72 h of incubation in vitro. IC<sub>50</sub> values are reported as mean ± SEM.

	IC <sub>50</sub> (μM)					
	MCF-7	WiDr	C6	HeLa	L6	HaCaT
NAMI-A [78]	620 ± 30	-	-	626 ± 45	-	-
AziRu [77,79]	305 ± 16 [77]	441 ± 20 [77]	318 ± 12 [77]	382 ± 19 [79]	> 500 [79]	> 500 [79]
POPC-based formulations						
ToThyRu/POPC [77,134]	27.8 ± 0.1 [134]	75 ± 4 [77]	36 ± 8 [77]	-	-	-
HoThyRu/POPC [77]	7 ± 4	40 ± 5	81 ± 7	-	-	-
DoHuRu/POPC [77,134]	18.9 ± 0.1 [134]	99 ± 5 [77]	24 ± 5 [77]	-	-	-
ToThyCholRu/POPC [79,105]	70 ± 12 [105]	165 ± 10 [105]	-	-	>500 [79]	>500 [79]
HoUrRu/POPC [107]	14 ± 7	20 ± 8	-	-	-	-
DOTAP-based formulations						
ToThyRu/DOTAP [106,134]	10.1 ± 0.1 [134]	50 ± 11 [106]	54 ± 8 [106]	-	-	-
HoThyRu/DOTAP [100,106]	13 ± 4 [100]	65 ± 8 [106]	43 ± 11 [106]	-	-	-
DoHuRu/DOTAP [106,134]	10.3 ± 0.2 [134]	41 ± 10 [106]	34 ± 9 [106]	-	-	-
ToThyCholRu/DOTAP [79]	13 ± 2	23 ± 8	-	34 ± 4	187 ± 1	377 ± 3
HoUrRu/DOTAP [107]	8 ± 5	12 ± 5	-	-	-	-
I/DOTAP [110]	31.2 ± 2.7	-	35.4 ± 2.7	45.6 ± 3	-	>150

Thus, the insertion of AziRu into highly functionalized scaffolds (nucleolipid or aminoacyl lipid structures), along with the subsequent liposome encapsulation, allowed us converting a very weakly cytotoxic compound into effective antiproliferative agents, with IC<sub>50</sub> values from ~4 to ~50 times lower than the parent metal complex [35,77,79,100,105–107,110,134].

The higher anticancer activity observed for the tested formulations with respect to the naked AziRu suggested an enhanced cellular uptake efficiency for the Ru(III)-incorporating liposomes due to nanovectorization [35,77,79,100,105–107,110,134]. Interestingly, when tested on healthy cell lines, as human HaCaT keratinocytes and rat L6 muscle cells, the Ru(III)-containing liposomal formulations did not show toxicity even at very high concentrations, demonstrating a selective cytotoxicity against highly proliferative malignant cells (Table 1).

These in vitro outcomes placed these Ru(III)-containing liposomal formulations among the most promising Ru-based anticancer agents currently described in the literature [35,77,79,100,105–107,110,134], with only few reported cases showing similar in vitro antiproliferative activity [80,111,116,117,138–141].

Furthermore, in most investigated cancer cells, the IC<sub>50</sub> values for the DOTAP formulations were significantly lower than those calculated for the same Ru(III) complex lodged in POPC liposomes [35,79,100,106,107,134]. This indicates that, under identical experimental conditions, the cationic DOTAP liposomes greatly enhanced the anticancer activity of the nucleolipidic Ru(III) complexes, likely due to the positive net superficial charge of the nanocarriers which can promote the interaction with cell membranes and, consequently, the drug internalization.

Interestingly, the differences among the various nucleolipidic Ru(III) complexes incorporated in the liposomal formulations were not very significant, consistently with the rationale that the metal centre is the effectively bioactive species and the different nucleolipids simply represent useful variants of the carrier molecules [35].

From these bioscreens, MCF-7 breast cancer cells proved to be the most sensitive to ruthenium treatments in vitro: for this reason, the evaluation of the cellular response to the exposure to some of the developed Ru(III)-containing formulations was extended to other in vitro models of human breast cancer cells (BCC), worldwide the most common invasive cancers in women [142–144]. In particular,

ToThyRu and DoHuRu-containing liposomes (both POPC and DOTAP formulations) [134] as well as HoThyRu/DOTAP formulations [100] were further investigated focusing on well-established breast cancer cell lines: in addition to the epithelial-like breast adenocarcinoma MCF-7 cells, MDA-MB-231, MDA-MB-436, MDA-MB-468 and CG5 cells were inserted into a panel of human breast cancer models for preclinical evaluations (Table 2). The endocrine-responsive (ER) breast adenocarcinoma MCF-7 and the triple-negative breast adenocarcinoma (TNBC) MDA-MB-231 cell models account for the great majority of investigations on breast cancer cells and are considered the most reliable in vitro models of breast cancer together with their variants CG5, MDA-MB-436 and MDA-MB-468, respectively [145–147].

**Table 2.** IC<sub>50</sub> values (μM) relative to cisplatin (cDDP), AziRu and the effective ruthenium concentration inserted in the Ru(III)-incorporating POPC- and DOTAP-based liposomes in the indicated BCC lines following 48 h of incubation in vitro. IC<sub>50</sub> values are reported as mean ± SEM.

	IC <sub>50</sub> (μM)					
	MCF-7	MDA-MB-231	MDA-MB-436	MDA-MB-468	CG-5	MCF 10A
cDDP [100,134]	17 ± 5 [100]	−19 ± 4 [100]	-	24 ± 1 [134]	-	-
AziRu [100,134]	>250	>250	>250	>250	>250	>250
POPC-based formulations						
ToThyRu/POPC [134]	27.8 ± 0.1	36 ± 3	>37.5	15.7 ± 0.1	19.4 ± 0.2	-
DoHuRu/POPC [134]	18.9 ± 0.1	15 ± 1	37 ± 1	20.4 ± 0.8	30.6 ± 0.8	-
DOTAP-based formulations						
ToThyRu/DOTAP [134]	10.1 ± 0.1	10.8 ± 0.2	15.0 ± 0.2	14.7 ± 0.1	4.1 ± 0.2	-
DoHuRu/DOTAP [134]	10.3 ± 0.2	12.1 ± 0.3	20.0 ± 0.2	14.2 ± 0.1	3.3 ± 0.2	-
HoThyRu/DOTAP [100]	13 ± 4	12 ± 3	-	-	-	>100

According to the reported IC<sub>50</sub> values (Table 2), all the liposome formulations were effective in reducing cell growth and proliferation, proving the high sensitivity of BCC to the action of Ru(III)-based nanoaggregates, mainly of DOTAP-based formulations [134]. Notably, HoThyRu/DOTAP was basically inactive when tested on MCF-10A cells (IC<sub>50</sub> higher than 100 μM considering the effective ruthenium concentration), used as a reliable model for normal human mammary epithelial cells. Taken together, these outcomes proved a significant selectivity of these Ru(III)-hosting nanosystems towards BCC lines, without significant biological effects on healthy counterparts of mammary gland as epithelial cells [100,134].

### 3.2. Cellular Uptake Studies on Ru(III)-Containing Liposomes by Fluorescence Microscopy

In vitro preliminary investigations demonstrated that all the Ru(III)-containing liposomes were endowed with significant antiproliferative activity toward cancer cells of different histological origin, with particular efficacy on in vitro models of breast cancer cells.

Since one possible mechanism of action of the ruthenium-based anticancer drugs was suggested to be the nuclear DNA binding [148,149], the cellular uptake and nuclear entry ability were investigated, being a key element to induce inhibition of cancer cell proliferation [72].

Thus, time-course fluorescence microscopy experiments were performed to evaluate the Ru(III)-containing liposome uptake and their subcellular localization in carcinoma cells at different incubation times. In particular, ToThyRu/POPC formulations as well as DOTAP-based liposomes containing either DoHuRu or ToThyCholRu were evaluated in parallel experiments as representatives respectively of POPC and DOTAP-based nanoaggregates [77,79,106]. In the case of the cellular uptake evaluation of ToThyRu/POPC and DoHuRu/DOTAP nanoformulations, breast MCF-7 cancer cells were selected. In turn, the in vitro uptake of ToThyCholRu/DOTAP nanosystems was evaluated on both MCF-7 and colorectal WiDr cancer cell lines, in order to verify possible differences toward cancer cells of different histological origin.

In these experiments, the liposomes were loaded also with the fluorescent rhodamine-B (Rhod) dye, allowing to reveal their fusion with the membranes and cellular uptake; the blue fluorescent stain DAPI was used to label DNA, in order to detect the position of the nuclei; finally, merged images, arising from overlapped fluorophore emissions of DAPI and Rhod from the same cell monolayers, gave a clear and unambiguous indication on the overall cellular uptake process and its kinetics.

For all the investigated formulations, independently from the analysed cancer cell line, a marked fluorescence was detected into cells already after 1 h incubation. After typically 3 and 6 h, fluorescence localized widespread in the nuclei, cytoplasm and close to the membranes, indicating that the liposomes were significantly taken up by cancer cells [77,79,106]. Few differences in the cell uptake were found on varying the lipid used in the formulation: indeed, in the case of DOTAP nanoaggregates hosting DoHuRu or ToThyCholRu complexes, a massive cell uptake was already observed after 30 min incubation [77,79,106]. Therefore, in all cases these formulations showed a high propensity to cross the cell membranes along the uptake process in the tested cancer cell lines [77,79,106].

Aiming at a deeper insight into the cell internalization process and metabolic fate of the liposomal formulations, additional *in vitro* fluorescence experiments were performed on MCF-7 cancer cells treated with an ad hoc prepared dansyl-labelled ruthenium complex named HoThyDansRu (Figure 2), co-aggregated with DOTAP analogously to the other described nucleolipid-based complexes. Monitoring the dansyl fluorescence, the fate of the active ruthenium complex could be directly assessed, examining its localization after cells treatment. Cationic liposomes hosting the fluorescently labelled HoThyDansRu rapidly localized within the cells, showing relevant cytoplasm dansyl-dependent fluorescence emission already after 30 min incubation and increasing accumulation over time, reaching the maximum fluorescence emission after 2 h (Figure 8a) [106]. A marked tendency to accumulate in proximity of the nuclei was detected (Figure 8a), suggesting possible interaction of the active metal also with nucleic acids [106].

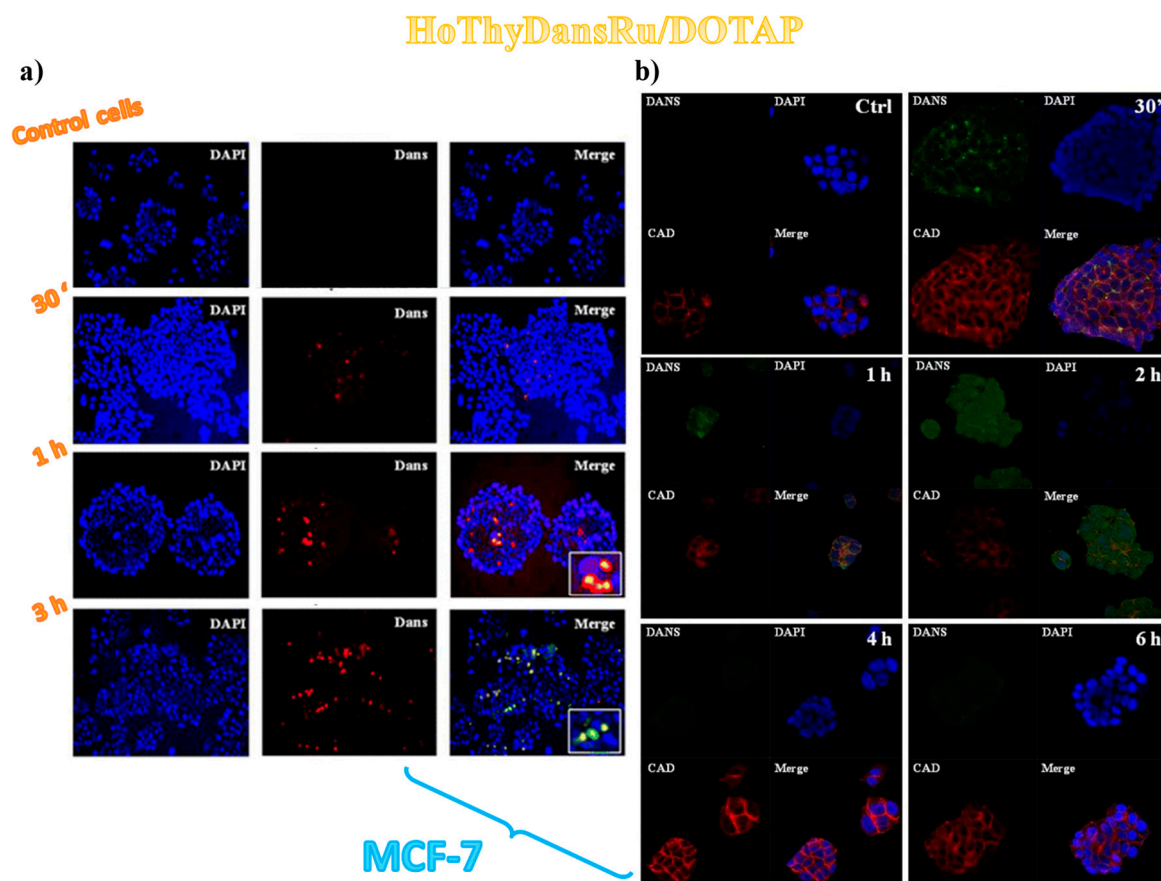


**Figure 8.** Human MCF-7 breast adenocarcinoma cells incubated with 100  $\mu\text{M}$  HoThyDansRu/DOTAP liposome formulations and followed at different times: (a) fluorescent photomicrographs of cell monolayers showing the cellular localization of the fluorescent HoThyDansRu/DOTAP liposomes; (b) confocal microscopy bioimaging showing the cellular uptake of the fluorescent HoThyDansRu/DOTAP nanosystem. DAPI was used as a nuclear stain (shown in blue). Dansyl-dependent fluorescence (Dans) of HoThyDansRu/DOTAP liposomes is shown in red (a) or as green dots (b). E-cadherine-associated fluorescence (CAD), defining cell shape, is shown in red (b). In merged images (Merge), the two fluorescent emission patterns are overlapped. Insets in panel a represent higher magnifications of merged images showing cellular location of fluorescent dansylated ruthenium complexes. Figures were adapted with permission from [106] Copyright (2013) American Chemical Society (a) and from [100] (b).

Overall, analysis of the dansyl-dependent fluorescence emission over time indicated that the HoThyDansRu/DOTAP nanoaggregates first localized within the cell membranes, then entered the cytoplasm, spreading to the whole cell, including perinuclear and nuclear compartments (Figure 8b) [100].

The fluorescence detection suggested an intracellular release of the ruthenium derivative from the liposomes: at longer incubation times (i.e., 4 and 6 h), a significant decrease in the dansyl-dependent fluorescence signal intensity occurred (Figure 8b), supporting the hypothesis that the liposome released the active ruthenium complex inside the cell [100]. In fact, it was demonstrated that the fluorescence intensity of the dansyl probe is largely influenced by the external environment: the fluorescence of dansyl group is marked in hydrophobic environments, while poor fluorescence emission is detected when the probe is exposed to water [150–152]. Accordingly, the marked fluorescence intensity of HoThyDansRu in the first monitoring indicated that the dansyl dye was inserted in the apolar DOTAP lipid bilayer; its progressively less and less intense fluorescence (Figure 8b) suggested that the nucleolipid Ru-complex was released in the intracellular media [100].

All these findings were thus corroborated in MCF-7 cells by fluorescence experiments using confocal microscopy coupled to Red E-cadherine-associated fluorophore, a 120-kDa transmembrane glycoprotein able to highlight adherens junctions and cell-cell contacts in epithelial clusters [100].

Overall, these data highlighted the crucial role played by the cellular uptake process in determining the anticancer efficacy of Ru(III)-based drugs, showing both POPC and DOTAP-based liposomes as very efficient nanocarriers for the stabilization of Ru complexes in aqueous media and their effective transport in cells. Particularly relevant was their clear detection in the nucleus, differently from other known Ru(III) complexes, able to accumulate in the cytoplasm but not in the nuclear region [153]. Notably, for these systems cationic DOTAP nanoaggregates proved to be more effective as Ru(III)-based drugs carriers, showing faster uptake kinetics [77,79,100,106].

### 3.3. Sub-Cellular Accumulation of the Ru(III) Complexes

Ruthenium intracellular amount was determined by ICP-MS analysis performed on subcellular fractions (culture medium, cellular pellet, cytosolic fraction, nuclear fraction and DNA sample) of MCF-7 cells, after 24 h *in vitro* treatment with HoThyRu/DOTAP nanoaggregates [100]. AziRu was also included as suitable control, demonstrating the vital importance of nanoformulations for an efficient ruthenium cellular uptake and internalization [100]. In fact, after 24 h exposure, about 80% of the administered AziRu was found in the culture medium, while 85% of the administered HoThyRu/DOTAP liposomes amount was revealed at cellular level.

Furthermore, analysis of the isolated subcellular fractions indicated for the HoThyRu/DOTAP formulations a broad ruthenium distribution among the intracellular compartments, above all in the nucleus. Almost 50% of the ruthenium administered as liposomal nanosystem was found bound to nuclear DNA vs. <10% of the metal from the naked AziRu detected in the nuclear fraction bound to DNA [100].

### 3.4. Cell Morphological Changes Induced by *in Vitro* Treatment with Ru(III)-Containing Liposomes

To further support the relationship between cell viability and ruthenium-induced cytotoxicity, subconfluent cultures of the selected cancer cell lines throughout the *in vitro* experiments were also examined by phase-contrast light microscopy to monitor the dynamic morphological changes occurring during cell death. Thus, confluent MCF-7, WiDr and C6 cancer cells were evaluated after incubation with ToThyRu/POPC liposomes and MCF-7, WiDr and HeLa cells were examined after *in vitro* treatments with ToThyCholRu/DOTAP formulations, as representative example of POPC and DOTAP-based nanoaggregates, respectively.

In all cases, after 48 h *in vitro* treatments of the selected cancer cell lines, morphological modifications of the cell monolayers were clearly evident [77,79], with distinctive hallmarks of apoptosis (Figure 9a,b) [154]. Indeed, besides losing their normal morphology, apoptotic features—as membrane blebs and cell shrinkage [154]—appeared in the treated cells together with a significant increase of the number of rounded-up cells after exposure to the Ru(III)-containing liposomes [77,79].

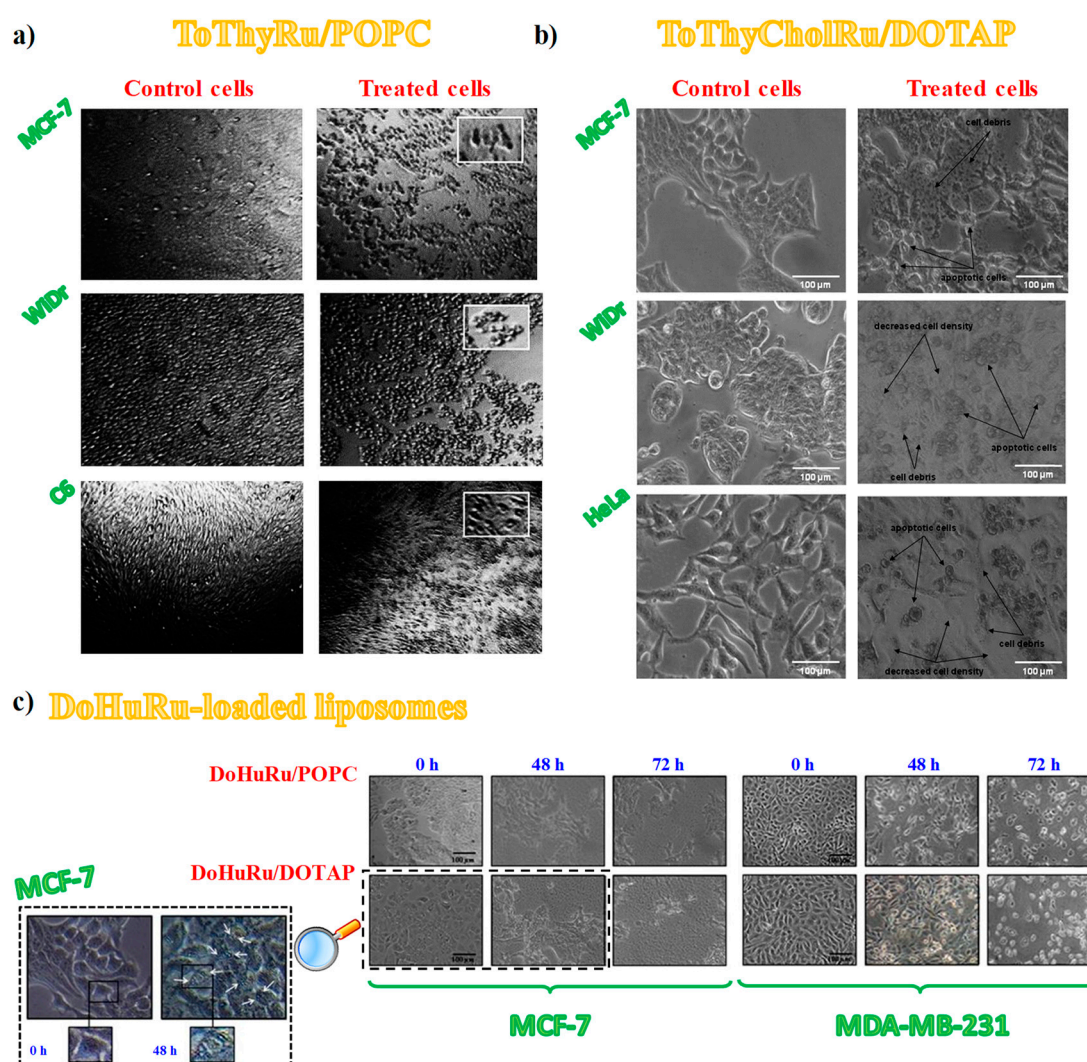


**Figure 9.** Representative photomicrographs by phase-contrast light microscopy showing the cellular morphological changes and cytotoxic effects on cellular monolayers: untreated (left column in panels **a** and **b**) or treated for 48 h with ToThyRu/POPC (**a**) or ToThyCholRu/DOTAP (**b**) formulations. For ToThyRu/POPC nanosystems, MCF-7, WiDr and C6 cancer cell lines were examined (**a**); in turn, for ToThyCholRu/DOTAP nanocarriers, MCF-7, WiDr and HeLa cancer cell lines were analysed (**b**). Insets in (**a**) represent higher magnifications of injured cells following incubations with ToThyRu/POPC liposomes. (**c**) MCF-7 and MDA-MB-231 breast cancer cells treated for 48 and 72 h with ruthenium  $IC_{50}$  concentrations of DoHuRu-containing liposomes. The inset in (**c**) represents higher magnifications at 0 (left panel) and 48 h (right panel) DoHuRu/DOTAP treated MCF-7 cells, showing the formation of autophagic vacuoles detectable in cell cytoplasm. Figures are adapted from [77] (**a**), [79] (**b**) and [134] (**c**).

In the case of cytomorphological modifications induced by the treatment with the aminoacyl lipid Ru(III) compound **I** hosted in DOTAP liposomes, not only malignant cells such as MCF-7, HeLa and C6 but also normal cell lines as 3T3-L1 (mouse embryo fibroblast) and HaCaT (human keratinocytes) were analysed by phase-contrast light microscopy in the absence and presence of the drug. Notably, while the cell distribution and cytomorphology were substantially unaffected on the healthy cells after 48 h of *in vitro* treatment, under the same conditions the cell monolayers integrity was strongly perturbed, with distinctive hallmarks of apoptotic cell death, such as membrane blebs, cell shrinkage, formation of balloon-like structures and cell contraction [154], in the case of the cancer cells [110].

More recently, cellular cytomorphological changes induced by Ru(III)-containing liposome administration were specifically investigated in two different breast adenocarcinoma cell lines,

i.e., MCF-7 and MDA-MB-231 cells [146,147]. Indeed, in the presence of DoHuRu/POPC and DoHuRu/DOTAP formulations at 48 or 72 h [134], photomicrographs indicated the characteristic cell shrinkage as well as loss of cell-cell contacts, diagnostic of apoptosis (Figure 9c) [154].

Therefore, the overall morphological analysis outcomes provided strong evidence of an apoptosis-inducing activity, in line with several *in vitro* studies supporting apoptotic events to explain the anticancer properties of different ruthenium derivatives, both in their +2 and +3 oxidation states [47,78,112,140,141,153,155–161]. However, also other different molecular pathways can be involved in the cell death process [153]. In fact, in the case of MCF-7 cells treated with the DoHuRu/DOTAP liposomes at  $IC_{50}$  conc., in addition to apoptotic hallmarks, also autophagic vacuoles were clearly detectable, suggesting morphological changes associated with autophagy activation (Figure 9c, inset) [134].

### 3.5. Insight into the Ru(III)-Containing Liposomes Mode of Action: Identification of Molecular Cell Death Pathways

#### 3.5.1. Pro-Apoptotic Effects in Breast Cancer Cells Evaluated by FACS Analysis

The observed changes both in the cell morphology and in the monolayers appearance suggested that Ru(III)-containing liposomal formulations might exert their antiproliferative effects in BCC by activation of specific cell death pathways, such as apoptosis and/or autophagy mechanisms [77,79,110,134].

To investigate the apoptosis induction in MCF-7 and MDA-MB-231 cancer cells, both DoHuRu-hosting POPC and DOTAP formulations were analysed by fluorescence-activated cell sorting (FACS) analysis by using Annexin V-FITC (fluorescein isothiocyanate) along with the propidium iodide (PI) dye, a very sensitive method to differentiate apoptotic (Annexin V-FITC positive, PI negative) from necrotic (Annexin V-FITC positive, PI positive) cells [162].

Both DoHuRu-incorporating lipid formulations induced exceptional pro-apoptotic effects, more marked for the DOTAP-based nanoaggregates, without observing significant increased necrosis (Figure 10) [134]. In particular, for MCF-7 cells, after 48 h of treatment at  $IC_{50}$  conc. of the tested formulations, 46% and 36% of total cell population, respectively, for DoHuRu/DOTAP and DoHuRu/POPC formulations, were found in early stages of apoptosis (Annexin V-FITC positive and PI negative). Additional 24 h treatment resulted in 82% and 37% of cell population, respectively, for DoHuRu/DOTAP and DoHuRu/POPC formulations, in late apoptosis phase (positive for both Annexin V-FITC binding and for PI uptake). Under the same conditions, similar trend and percentage of cell population in the different apoptotic stages were found also for MDA-MB-231 cells, once again with stronger pro-apoptotic effects for DOTAP- than POPC-based formulations (Figure 10) [134]. Indeed, these results further corroborated the increased *in vitro* efficacy—especially as a trend over time—of the cationic DOTAP nanocarriers with respect to the zwitterionic POPC liposomes hosting the same nucleolipidic Ru(III)-complex, likely due to different cellular uptake kinetics.

### DoHuRu-loaded liposomes

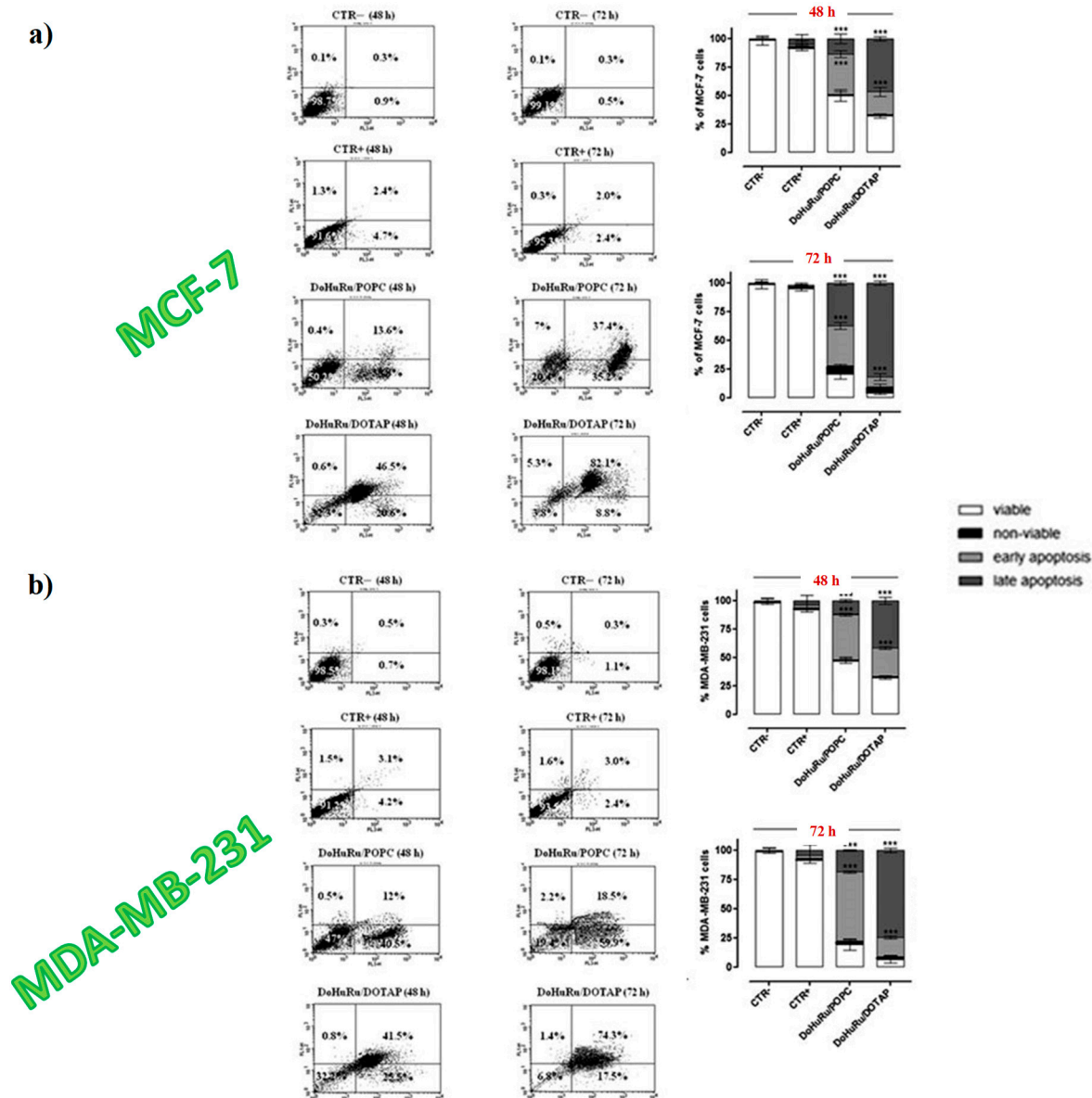


**Figure 10.** Induction of apoptosis in MCF-7 (a) and MDA-MB-231(b) breast cancer cells, evaluated by FACS analysis (right on each panel), after cell labelling with propidium iodide (PI) and FITC-Annexin V. Cells were both unlabelled and untreated (CTR -), labelled and not treated (CTR +), treated with IC<sub>50</sub> doses of DoHuRu-incorporating POPC or DOTAP liposomes for 48 and 72 h, as indicated. The quantitative analysis of viable, non-viable (necrotic), early and late apoptotic cells after drug exposure is represented (bar graphs on the right of each panel). Viable cells are negative for both PI and FITC-Annexin V binding; non-viable, necrotic cells are negative for FITC-Annexin V binding and positive for PI uptake; cells in early apoptosis are FITC-Annexin V positive and PI negative; cells in late apoptosis are positive for both FITC-Annexin V binding and PI uptake. Figures were adapted from [134].

#### 3.5.2. DNA Fragmentation Assay

It is generally accepted that apoptosis activation and subsequent DNA cleavage represent the main cytotoxic mode of action of metal-based antiproliferative drugs [4,141]. In addition to shrinkage and fragmentation of cells and nuclei, the apoptotic processes are also accompanied by a marked

degradation of the chromosomal DNA in the nucleosomal area. Late events of apoptosis typically lead to DNA fragmentation, resulting in a “ladder” formation easily detectable by agarose gel electrophoresis [163]. Thus DNA cleavage extent in cultured cells is directly correlated with the amount of apoptotic cells and this kind of investigation has been already explored for other Ru(III) complexes after *in vitro* treatment of MCF-breast cancer cells [112,141,153].

To further sustain the evidence that Ru(III)-containing formulations were able to trigger apoptosis in cancer cell lines, DNA degradation on genomic DNA samples obtained from treated cells was also investigated. In particular, ToThyCholRu/DOTAP liposomes were evaluated for their DNA fragmentation activity on MCF-7, WiDr and HeLa cancer cells (Figure 11a) [79]; while DoHuRu-hosting lipid formulations were specifically evaluated on both MCF-7 and MDA-MB-231 breast cancer cells (Figure 11b) [134].

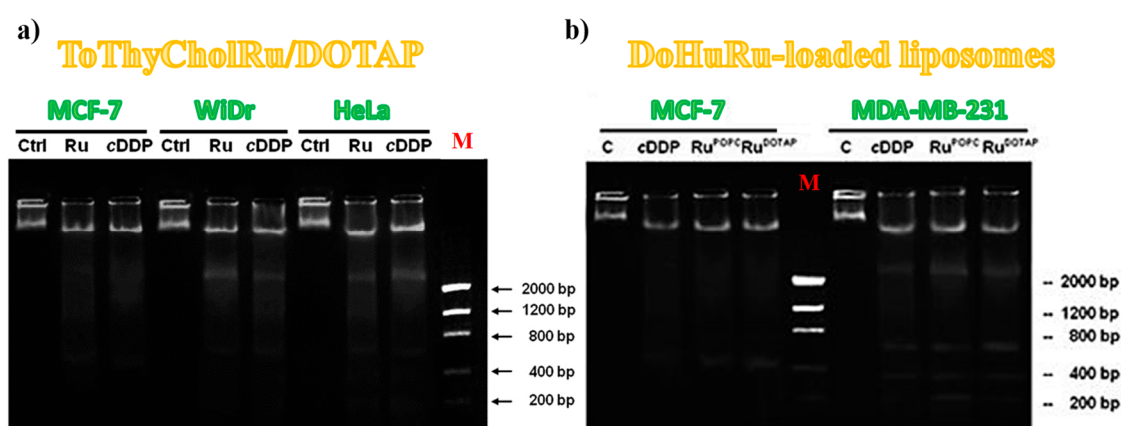


**Figure 11.** 1.5% agarose gels representing the DNA fragmentation assay on MCF-7, WiDr and HeLa cells, treated or not (Ctrl) for 48 h with IC<sub>50</sub> doses of ToThyCholRu–DOTAP liposomes (indicated as Ru) (a) and MCF-7 and MDA-MB-321 cells treated or not (C) with IC<sub>50</sub> concentrations of DoHuRu/POPC (Ru<sup>POPC</sup>) and DoHuRu/DOTAP (Ru<sup>DOTAP</sup>) for 48 h (b). In both experiments, the selected cell lines were also treated with IC<sub>50</sub> conc. of cisplatin (cDDP) used as a control. Lane M corresponds to the molecular weight markers. Figures are adapted from [79] (a) and [134] (b).

In all cases, the DNA extracted from cells following 48 h of incubation with IC<sub>50</sub> doses of Ru(III)-containing formulations strongly indicated fragmentation, accompanied by typical internucleosomal DNA laddering. The DNA cleavage extent was very close to that induced by cisplatin, used as positive control [163], while no relevant DNA fragmentation was found in untreated cancer cells (Figure 11) [79,134].

However, in all the tested formulations, the nuclear fragmentation pattern observed for MCF-7 cancer cells was not typical. This was explained considering that this cell line is particularly resistant to chemotherapeutics due to deletion in the CASP-3 gene, leading to an inherited caspase-3 deficiency expression [164]. Caspase-3 proteins are commonly activated by different death signals and are therefore responsible of cleavage of important cellular proteins and ultimately of apoptotic DNA damage [165]. In this case, MCF-7 cells undergo cell death triggered by apoptotic stimuli in the absence of canonical DNA fragmentation and thus activating mechanisms independent of caspase-3 but associated with different effector caspases, such as caspase-6 or -7 [166,167].

### 3.5.3. Apoptotic-Related Protein Expression in Breast Cancer Cells

In addition to the fundamental role of caspase-3 in the DNA damage induction, all the intracellular caspases and BCL-2 (B-cell lymphoma-2) family proteins represent key elements for cancer response to chemotherapeutic intervention due to their involvement in the fine regulation of the apoptotic cell death machinery [168]. In particular, the family of BCL-2 contains protein factors playing a critical role in controlling dynamic cellular processes, decision-making between life and commitment to the

mitochondrial apoptosis (intrinsic apoptotic pathway). BCL-2 was discovered as a new oncoprotein in acute lymphoblastic leukaemia, protecting cells from programmed cell death as apoptosis inhibitor and promoting cellular survival by inhibition of Bax and Bid action on mitochondria [169]. Many BCL-2 proteins with anti-apoptotic activities have been discovered, including B-cell lymphoma-extra-large (BCL-xL), BCL-2-like protein 2 (BCL-w), BCL-2-like protein 10 (BCL-B), myeloid cell leukemia 1 (MCL-1) and BCL-2 related gene A1 (A1). Conversely, the pro-apoptotic effectors of the BCL-2 family members, such as Bax and Bid, can commit a cell to its programmed death by promoting the permeabilization of its mitochondrial outer membrane (MOM) and the activation of the caspase cascade [170]. As a consequence, cytc and other intermembrane space (IMS) mitochondrial proteins are released into the cytosol, playing a central role in the apoptosome formation that subsequently activates caspase 9. In turn, caspase 9 activates effector caspases 3, 6 and 7, cleaving vital cellular proteins and ultimately ensuring cellular demolition (Figure 12, right). The intrinsic pathway is typically activated by intracellular stress signals [165,171]. Several clinical studies demonstrated that the overexpression of the antiapoptotic BCL-2 protein is a negative prognostic marker in various tumours [172]; while high Bax expression was associated with a better response to chemotherapy in many cancers forms [173,174].

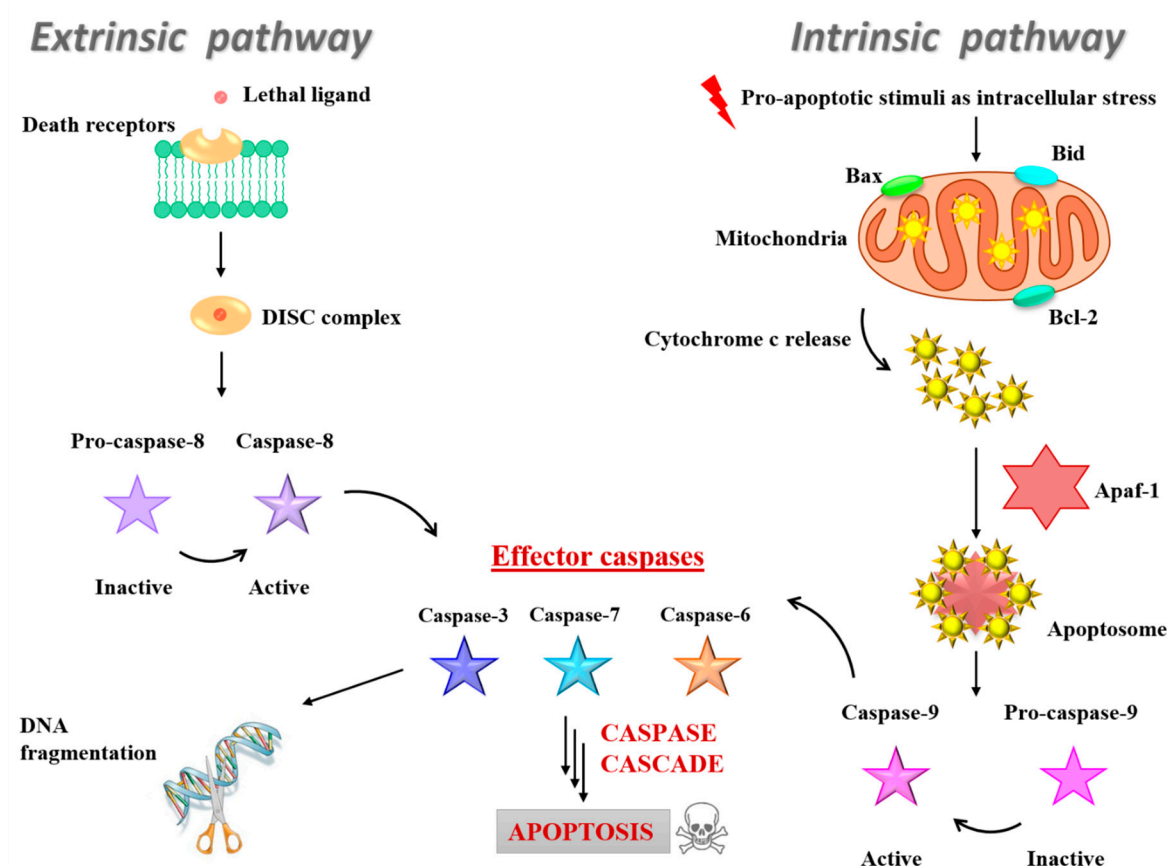


**Figure 12.** Schematic representation of the intrinsic (or mitochondrial) and the extrinsic (or death receptor) apoptotic pathways.

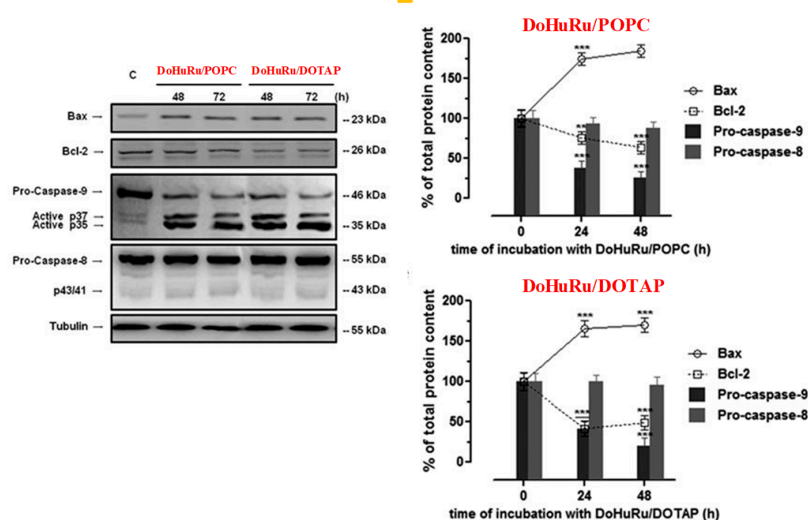
Conversely, the extrinsic pathway is generally activated by extracellular ligands able to bind to death receptors on the cell surface, leading to the formation of the death-inducing signalling complex (DISC). Formation of DISC—typically triggered by members of the death receptor superfamily, such as CD95 and tumour necrosis factor receptor—induces in turn caspase-8 activation and thereby the downstream caspase cascade (Figure 12, left) [175]. Thus, specific activation of some caspases or BCL-2 factors are suggestive of the induction of distinctive apoptotic pathways [171,175].

Thus, Western blot analysis was used to investigate protein expression profile in treated MCF-7 and MDA-MB-231 cells after exposure to IC<sub>50</sub> of DoHuRu/POPC and DoHuRu/DOTAP formulations at 48 and 72 h [134]. In both the investigated BCC lines, a considerable increase in caspase-9 activity with respect to untreated cells was detected—resulting in the production of active p35 and p37 subunits, known to amplify the apoptotic response—along with a simultaneous Bax up-regulation and BCL-2 down-regulation (Figure 13) [134]. These biological responses were time-dependent and more evident after treatment in vitro with the cationic DoHuRu/DOTAP liposome [134]. The activation of pro-caspase-9, together with the changed Bax/BCL-2 ratio, suggested a Ru-dependent activation of the apoptotic intrinsic pathway, probably as a result of interactions with putative mitochondrial targets, maybe via selective ROS generation and accumulation, as already found for other Ru(II) and Ru(III)-based drugs [176].

### DoHuRu-loaded liposomes

a)

MCF-7



b)

MDA-MB-231

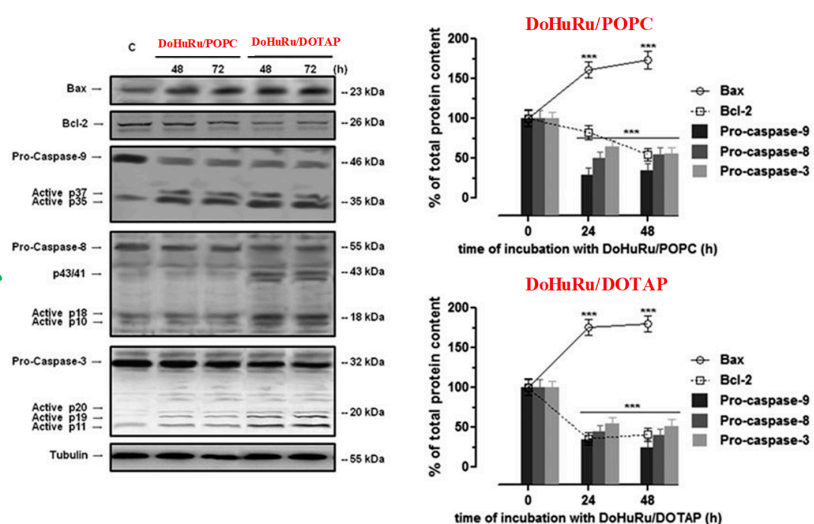


**Figure 13.** Western blot analysis showing the effects of IC<sub>50</sub> doses of DoHuRu/POPC and DoHuRu/DOTAP following 48 and 72 h of incubation in MCF-7 (a) and MDA-MB-231 (b) cells on caspases-3, -8 and -9 expression and activation, and on Bax and BCL-2 expression. Bands resulting after chemoluminescence from treated cells were extracted, quantified by densitometric analysis and then plotted (graphs on the right of each panel): solid and dotted lines for Bax and BCL-2 expression proteins, respectively, and bar graphs (caspases-3, -8 and -9) reported as percentage of control in relation to the used Ru-containing nanoaggregates. Figures are adapted from [134].

Notably, while no activation of caspase-8 appeared even after 72 h of exposure to the zwitterionic POPC-based nanosystems, the cationic DoHuRu/DOTAP nanoaggregates seemed to promote full length pro-caspase-8 cleavage, as evidenced by the formation of p10 and p18 fragments (Figure 13), fundamental active elements in the extrinsic death pathway [134].

Hence, DoHuRu/DOTAP formulations were able to concurrently trigger the induction of the two major apoptotic processes. Moreover, the activation of both apoptotic pathways (the intrinsic and the extrinsic one) seems to occur in a cell-specific manner, being evident only in MDA-MB-231 cells (Figure 13b). Possibly, the net positive surface charge of DOTAP-based nanoaggregates allows interacting in a peculiar manner with the cell membrane external bilayer, stimulating specific surface receptors involved in the activation of the death receptor pathway. However, these findings are not unprecedented since the activation of extrinsic apoptosis pathways [177], as well as the ability of some Ru(II) and Ru(III) complexes to simultaneously activate intrinsic and extrinsic apoptosis pathways, [178] have been demonstrated for other anticancer chemotherapeutics.

#### 3.5.4. Autophagy Activation in Breast Cancer Cells

In addition to apoptotic pathway, cellular suicide may also occur via non-apoptotic forms of programmed death such as autophagy [179,180]. Autophagic activity—generally low under basal conditions—can be specifically up-regulated in the presence of several physiological and non-physiological stimuli, including *in vitro* pharmacological treatments. [181,182] As in the case of apoptosis, autophagy play a crucial role in early stages of carcinogenesis, in cellular proliferation and survival [182–188]. Excessive autophagy is associated with cell death, as well as with other death pathways depending on cell types—an aspect to be taken into account as ruthenotherapy additionally activates apoptosis [189,190].

Since the activation of a pro-apoptotic response by chemotherapy can be affected by several factors, including cancer phenotypes and specific gene mutations, ultimately affecting the therapy success, the induction of alternative cell death pathway, alone or coupled to the apoptotic one [191], could represent an attractive goal in future anticancer intervention, especially in metastatic breast cancer cells [192,193]. The recent discovery of crosstalk connection among different cell death effectors and signalling pathways [194–196] will in fact offer novel effective therapeutic opportunities for targeted cancer therapies [197].

Notably, some Ru(II) complexes were found to be able to activate autophagy in cancer cells, though occasionally in antagonism to mitochondrial-mediated apoptosis [198,199]. A late step of the autophagic cell death consists of the autolysosomes formation, which is dependent on the coordinated activity of autophagy-related (Atg) proteins [186] involved in the maintenance of the cellular homeostasis [183,184,186,187,200]. Therefore, the formation of autophagic vacuoles visualized via monodansylcadaverine (MDC), a selective autofluorescent marker for autolysosomes detection [201]—in BCC treated with either DoHuRu/POPC or DoHuRu/DOTAP—was verified to evaluate the ability of Ru(III)-based compounds to induce also autophagy [134].

FACS analysis was used for the quantitative determination of MDC staining in MCF-7 and MDA-MB-231 cells exposed for 48 and 72 h to ruthenium IC<sub>50</sub> doses (Figure 14) [134]. While the treatment with DoHuRu/POPC did not reveal significant autolysosome formation, the cellular exposure to DoHuRu/DOTAP liposomes indicated a significant formation of the MDC-labelled vacuoles already after 48 h (Figure 14). These results suggest the capability of the cationic nanoaggregates to activate autophagy in the presence of apoptosis [134].

## DoHuRu-loaded liposomes

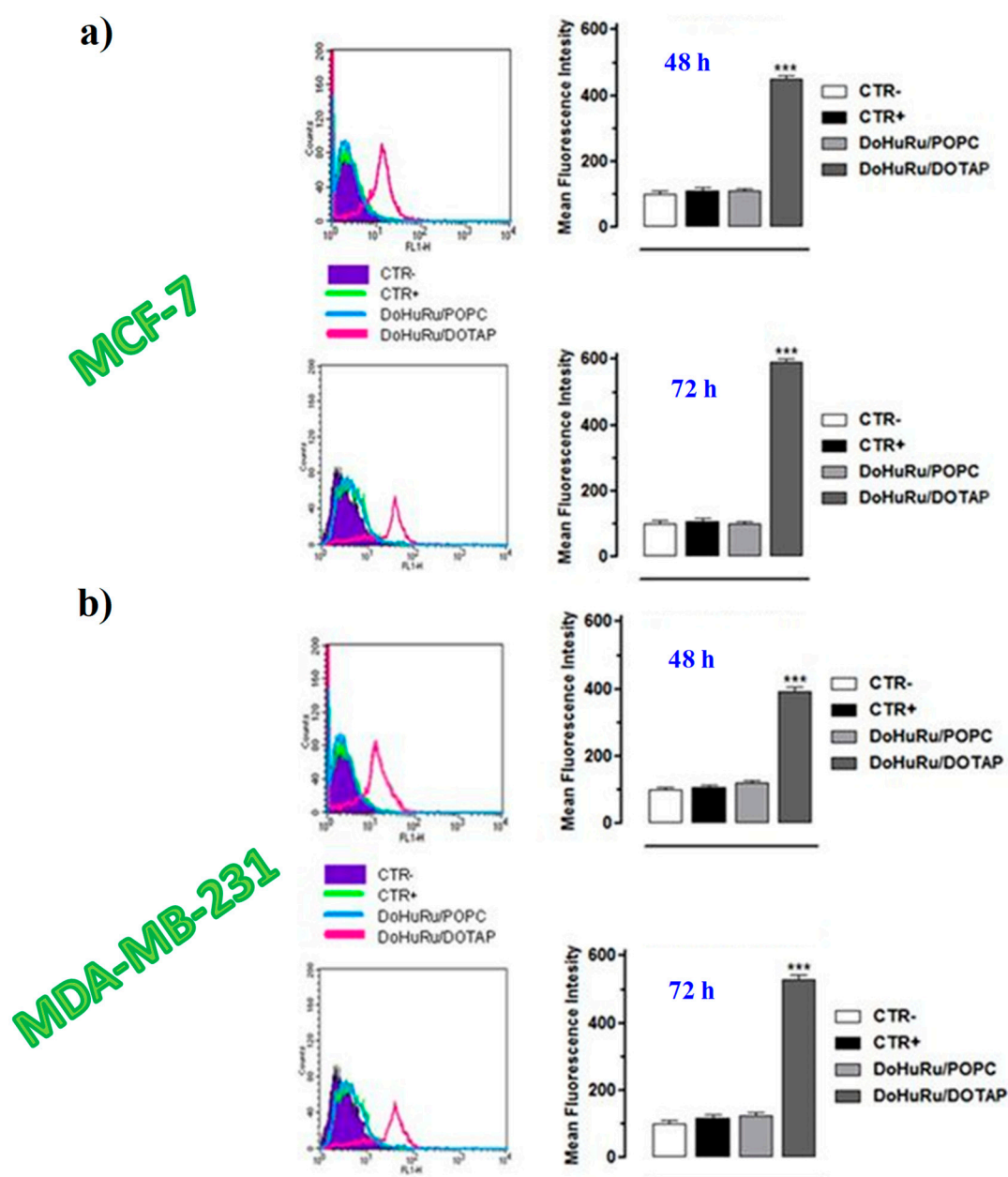


**Figure 14.** Quantitative flow cytometric analysis of autophagosomes formation (MDC incorporation) in MCF-7 (a) and MDA-MB-231 (b) breast cancer cells for the autophagy activation evaluation: unlabelled and untreated (CTR –), labelled and untreated (CTR +), treated with IC<sub>50</sub> concentrations of DoHuRu/POPC or with DoHuRu/DOTAP formulations for 48 and 72 h, as indicated. In the bar graphs, calculated main fluorescence intensities (MFIs) values are expressed as percentage of control cells. Figures are adapted from [134].

The ability of DoHuRu-hosting cationic liposomes to induce autophagy could be associated with the ruthenium-induced down-regulation of the prosurvival protein BCL-2: indeed, interferences in the interaction between Beclin-1 and BCL-2 family proteins, by which Beclin-1 is inhibited in normal conditions, stimulate autophagy [202].

To get further insight into the ability of the Ru(III)-containing formulations to induce autophagic cell death in cancer cells, MCF-7 breast cells treated with DoHuRu/DOTAP liposomes were processed

with a fluorescent autophagic detection kit able to measure autophagic vacuoles and to monitor the autophagic flux in live cells. DAPI was used to stain nuclei and FITC to visualize autophagic vesicles, such as autophagosomes and autophagolysosomes, and then the percentage of positive cells to autophagy was assessed [100]. In this way HoThyRu/DOTAP liposomes were demonstrated to strongly promote the formation of cytosolic autophagic vacuoles [100], reaching after 72 h similar effects to those induced by rapamycin, used as positive control being one of the most potent autophagy inducers [203].

### 3.5.5. Autophagy-Related Proteins Expression in Breast Cancer Cells

The formation of autophagosomes represents the last step of autophagy process in which at least 16 proteins are involved: among these, only the LC3 protein strongly associates with the membrane of autophagosomes. This protein exists in two different forms: LC3-I and LC3-II, found respectively in the cytoplasm and as membrane-bound form. LC3-phosphatidylethanolamine conjugate (LC3-II) differs from LC3-I being covalently linked to lipid moieties [204] starting from LC3-I to initiate the formation of the autophagosome vacuoles [182,184]. The autophagosomal marker LC3-II reflects autophagic activity, so that LC3 monitoring by both immunoblotting and immunofluorescence has become a consistent method for autophagy detection [205]. In addition, the Beclin-1 activity is very important in autophagy cell death pathway: this protein is a component of the phosphatidylinositol-3-kinase (PI3K) complex, which is required for autophagosome formation, and the expression of Beclin-1 was found decreased in malignant breast epithelial cells [206–208]. Recent data also suggested a lack of autophagic pathways following Beclin-1 depletion which can be induced by different conditions, including chemotherapeutic interventions [209]. As demonstrated by immunoblot analysis (Figure 15), protein samples extracted from MCF-7 and MDA-MB-231 cells, following *in vitro* treatments with HoThyRu/DOTAP liposomes for 48 and 72 h, showed a relevant increase in both LC3 proteins, and mainly in the LC3-II form [100]. In parallel, Bax was significantly increased and BCL-2 decreased, and no relevant change between untreated and treated cells was found in Beclin-1 protein content (Figure 15).

As survival factor, BCL-2 down-regulation proved to promote the activation of autophagic cell death [210–212]. In addition, the maintenance of basal amounts of Beclin-1 after exposure to cationic Ru-based nanosystems could be decisive in regulating the induction of autophagy. Indeed, fluorescent bioimaging of MCF-7 cells treated with HoThyRu-containing DOTAP formulations and stained for LC3 indicated an intense protein immunoreactivity, likely localized into autophagic vacuoles in the cytoplasm [100].

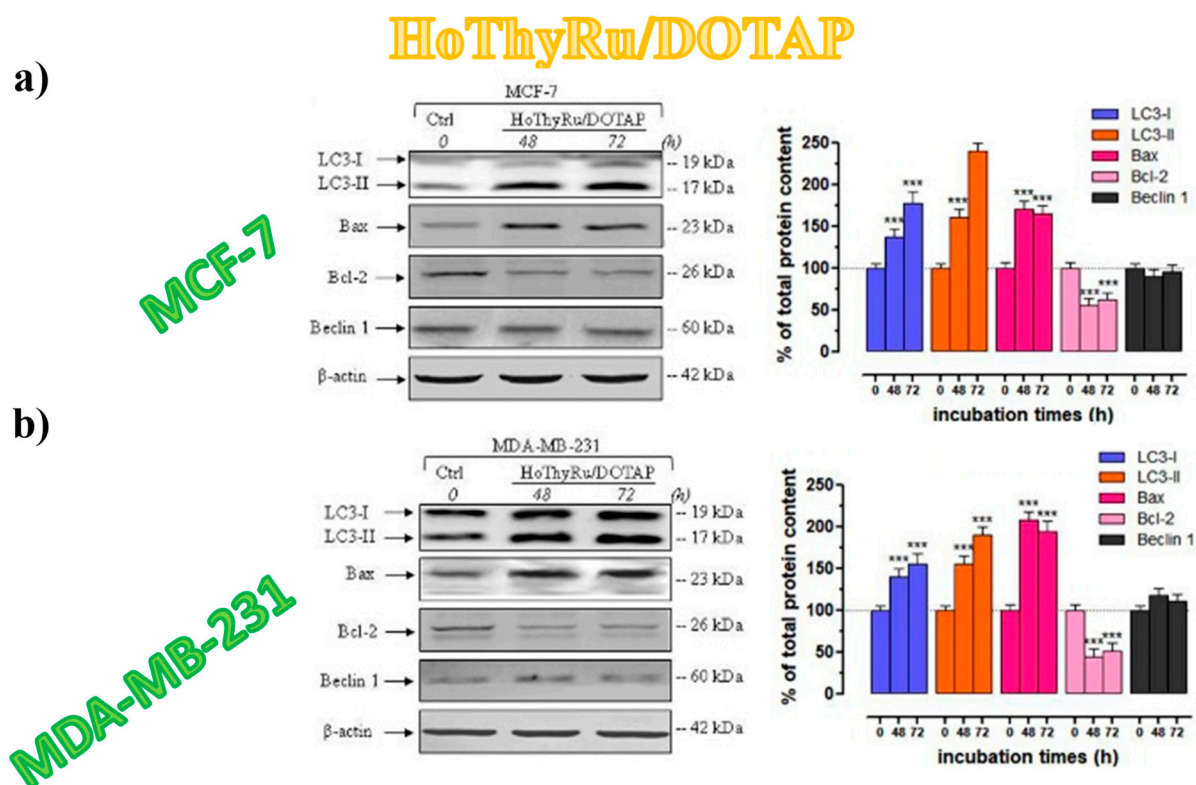


**Figure 15.** Western blot analysis showing the effects of IC<sub>50</sub> doses of HoThyRu/DOTAP liposomes following 48 and 72 h of incubation in MCF-7 (a) and MDA-MB-231 cells (b) on LC3-I, LC3-II, Bax, BCL-2, and Beclin-1 expression (Ctrl, untreated cells at the time zero). Bands resulting from MCF-7 and MDA-MB-231 cells were extracted, quantified by densitometric analysis and then plotted in bar graphs (right of each panel) as percentage of controls. Figures are adapted from [100].

### 3.6. *In Vivo* Anticancer Efficacy of Ru(III)-Containing Liposomes in Mice BCC Xenografts

In a preliminary investigation focused on *in vivo* response to HoThyRu/DOTAP formulation, athymic nude mice bearing human BCC xenografts were subcutaneously inoculated into the right flank with MCF-7 cells. Two weeks after the tumour growth, intraperitoneal injection of HoThyRu/DOTAP nanoaggregates was carried out once a week for four weeks. At the end of the schedule, the mice were sacrificed and the tumours collected (Figure 16) [100]. Subsequent analysis showed that the administration of HoThyRu/DOTAP formulation significantly inhibited breast cancer cell proliferation in mice, with a relevant reduction in both the weight and volume of tumour lesions with respect to the control group (Figure 16a–c). Notably, mice survival was 100%, and body weights were not affected by the ruthenium treatments (Figure 16d,e). Moreover, no evident toxicity was observed on the treated mice, suggesting a very good *in vivo* tolerance of the HoThyRu-hosting DOTAP nanosystems [100].

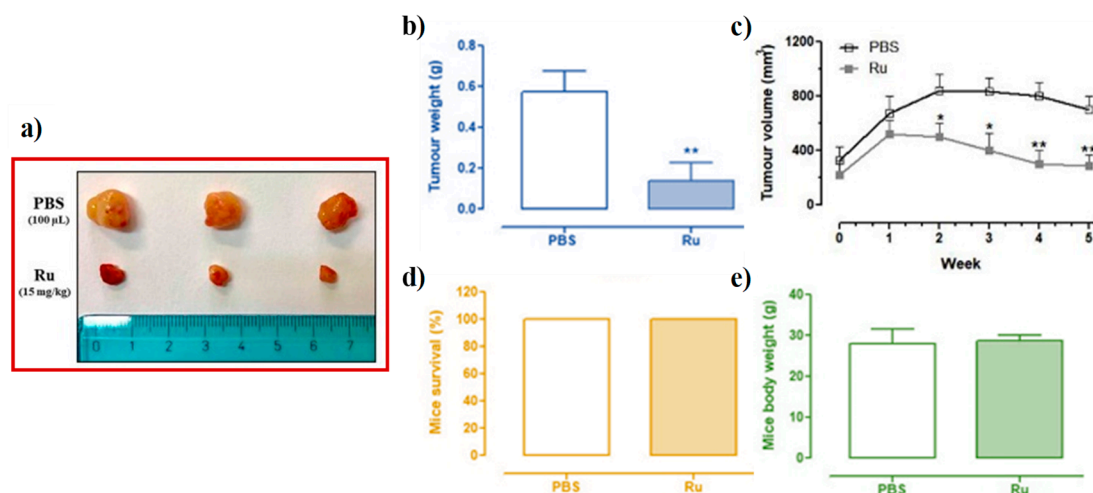


**Figure 16.** In vivo anticancer effects of HoThyRu/DOTAP nanosystems: tumour photographs after the collection (a); tumour weight (b) and tumour size (c) evaluation; mice survival (d) and body weight (e) determination (PBS control group, Ru treated group). Figures are adapted from [100].

#### 4. Improved Ru(III)-Containing Nanosystems: Introduction of Targeting and/or Diagnostic Agents for Theranostic Applications

Starting from the promising in vitro bioactivity of Ru(III)-containing POPC- and DOTAP-based liposomes, able to selectively and significantly reduce cancer cell survival, further improvements of these systems were recently proposed. In particular, two alternative approaches were reported based on varying the platform used to deliver the nucleolipid-based Ru(III)-complexes.

In a first approach, niosome vesicles were used to replace liposomes.

In detail, vesicles prepared from non-ionic surfactants [213,214], currently known as niosomes or NSVs (non-ionic surfactant vesicles), gained increasing attention as drug delivery systems, providing a cheaper and more stable alternative to phospholipids used in liposome preparation [215,216]. Niosomes are self-assembled vesicles made up of single chain non-ionic surfactants combined with cholesterol or other lipids [217,218]. Charged molecules can be also added as ingredients to better stabilize the obtained formulations and prevent their aggregation over time [214,215,218,219].

Owing to their vesicle structure, niosomes are able to incorporate both hydrophilic and hydrophobic drugs, just like liposomes do [216,218,220,221]. The drug is entrapped in a membrane resulting from the self-assembly of the surfactant + lipid molecules, generally organized in stable bilayers [222]. Niosomes can protect the loaded drugs from premature degradation or possible inactivation overcoming some major biopharmaceutical problems such as insolubility, side effects, and poor chemical stability of drugs [223,224]. Moreover, the high chemical stability of surfactants, compared with phospholipids, makes niosome purification, handling and storage much easier than those of conventional liposomes [225,226].

In our approach, the use of niosomal formulations allowed the introduction in the lipid formulation, besides the Ru(III)-based complexes, also of an active targeting agent, i.e., the oligodeoxyribonucleotide AS1411 [109]. This G-rich 26-mer, carrying the sequence  $5' \text{GGTGGTGGTGGTGGTGGTGGTGGTGG} 3'$ , entered in Phase II anticancer clinical trials, selectively targets nucleolin, a multifunctional protein involved in cell survival, growth and proliferation, overexpressed on the outer membrane of cancer cells (for a recent review covering the state-of-the-art knowledge on AS1411, see P. J. Bates et al. [227]).

Recently, AS1411 has been largely employed as a selective nucleolin-targeting agent, successfully combined with chemotherapeutic agents (such as paclitaxel [228–231], docetaxel [232–234], doxorubicin [235–244], and epirubicin) [245] onto suitable nanosystems in the context of specific recognition of cancer cells and tumour-selective delivery of therapeutic or imaging agents for cancer treatment [227].

In the proposed niosome formulations, AS1411 was for the first time associated with a Ru(III)-based chemotherapeutic drug to improve its selective delivery via specific recognition of cancer cells [109].

In a second approach, superparamagnetic iron oxide NPs (SPIONs) with a core/double shell architecture were exploited as platform for Ru incorporation, proving to be effective contrast agents for in vivo Magnetic Resonance Imaging (MRI) investigations and thus potential tools in theranostic nanomedicine, intended to provide simultaneous diagnosis and treatment of a disease, with early detection, easy monitoring, targeted therapy and minimal toxicity [246,247].

#### 4.1. Niosome-Based Systems Containing Nucleolipid-Based Ru(III) Complexes

With the aim of exploring niosome vesicles as versatile scaffolds for effective loading of multiple anticancer drugs to be used in combination therapies, Riccardi et al. [109] devised a novel formulation—mixing a cationic lipid, i.e., [2,3-di(tetradecyloxy)propan-1-aminium chloride] and the non-ionic surfactant polysorbate 80 in 3:1 molar ratio—as optimized vesicles with respect to previously described ones (Figure 17) [248,249]. Then, these niosomal formulations were decorated with the anticancer drug HoThyRu—hitherto one of the most effective ones among the nucleolipidic-based Ru(III) complexes investigated—as well as with the G-quadruplex-forming aptamer AS1411, to ensure highly specific recognition towards cancer cells (Figure 17) [109].

### AS1411/niosome\_HoThyRu

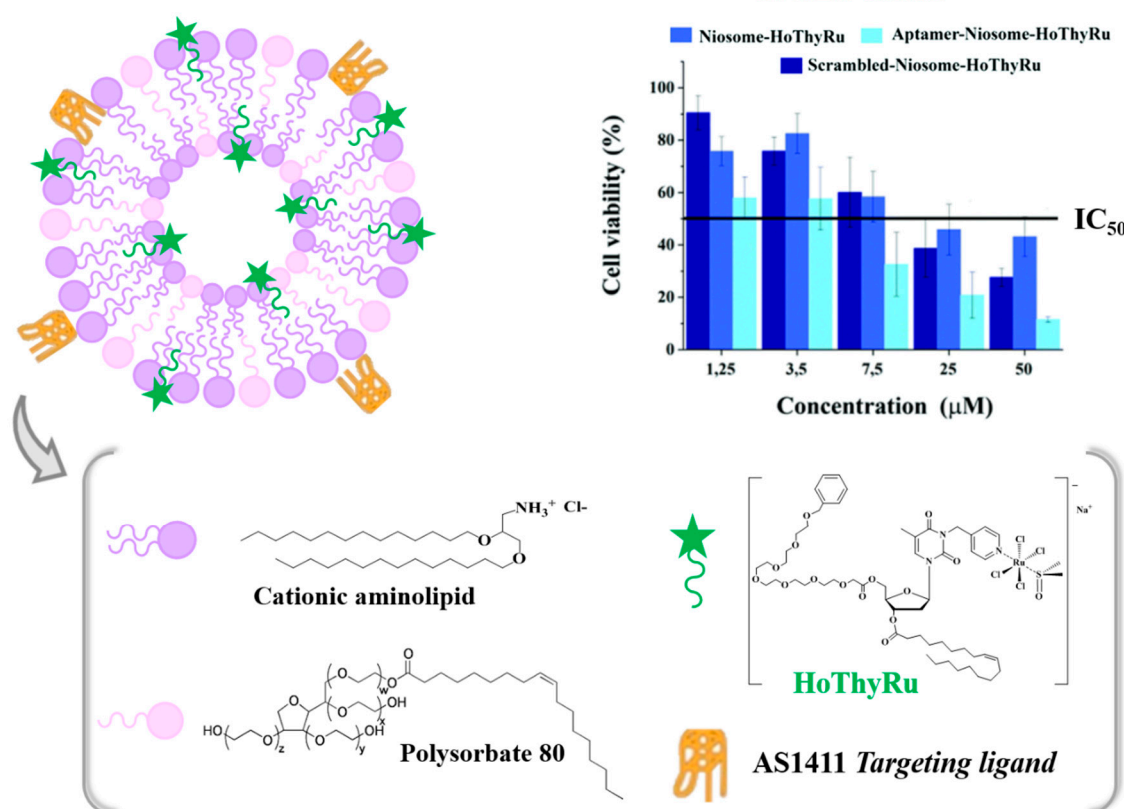


**Figure 17.** Schematic representation of niosome formulations based on a cationic aminolipid and the polysorbate 80, also containing the nucleolipid-based Ru(III) complex HoThyRu along with AS1411. On the right, the concentration/effects bar graphs obtained after in vitro treatment on HeLa cancer cells were also reported as representative examples. Figures were adapted from [109].

The morphology, average size, zeta potential, electrophoretic mobility and stability over time of the functionalized niosomes were analysed using different biophysical techniques.

In particular, both unfunctionalized and functionalized niosomes gave monodisperse vesicle-like aggregates, with typical size of ca. 100 nm, stable upon storage for one month, also able to fully incorporate both the nucleolipid Ru(III) complex HoThyRu and the oligonucleotide AS1411. The functionalization was driven by electrostatic interactions, in the case of the negatively-charged oligonucleotide, and by a combination of hydrophobic and electrostatic interactions for HoThyRu encapsulation [109].

Then, the antiproliferative activity of the niosome formulations was evaluated using the MTT assay on a selected panel of human cells including a human cervix adenocarcinoma (HeLa) and two colorectal cancer cell lines (HTB-38, HCC2998), as well as a non tumoural embryonic human cell line (HEK293T). HeLa cells were selected as a relatively drug-sensitive cell line with high nucleolin content, already proved to be responsive to niosome formulations [249] as well as to AS1411 [227]. In contrast, HTB-38 and HCC2998 colorectal cancer cell lines were chosen being highly resistant even to very effective chemotherapeutic agents such as 5-fluorouracil and camptothecin [250,251]. Finally, the embryonic cell line HEK293T was included as healthy cell line, already investigated to verify the absence of toxicity of niosome formulations [252].

Niosome formulations containing both AS1411 and HoThyRu showed increased bioactivity compared to those carrying only HoThyRu, proving the ability of the nucleolin-targeting aptamer to markedly enhance the bioactivity of the Ru(III)-containing niosomes (in Figure 17, on the right, the concentration/effect curves obtained on HeLa cells were reported as a representative example).

The obtained response was however cell-dependent, with HeLa cells more sensitive to this drug treatment than colorectal cancer cells [109]. The observed lower antiproliferative activity on both HCC2998 and HTB-38 colorectal cancer cell lines can be explained considering their generally poor sensitivity to drug treatments and low expression of nucleolin. Taken together, these results proved niosome formulations as very interesting nanocarriers to transport in cells anticancer drugs and the efficacy of AS1411 as targeting agent also in niosomal systems [109].

#### 4.2. Nanoparticle-Based Systems Containing Nucleolipid-Based Ru(III) Complexes

Stable phosphocholine-functionalized SPIONs (18LPC/SPIONs) were recently prepared through thermal decomposition method exploiting hydrophobic interactions between a suitable phosphocholine, i.e., 1-octadecyl- 2-hydroxy-*sn*-glycero-3-phosphocholine (18LPC), and an inner amphiphilic layer (composed by oleic acid and oleylamine), covering the surface of the NPs [108,253,254].

18LPC-SPIONs were further decorated with the nucleolipid-based Ru(III)-complex ToThyCholRu (18LPC-ToThyCholRu/SPIONs) [108], lodged in the external coating layer of the nanoparticle surface through reversible hydrophobic interactions (Figure 18a). Then, all the prepared SPION systems were characterized by DLS, TEM, small-angle X-ray scattering (SAXS) and wide-angle X-ray scattering (WAXS) measurements.

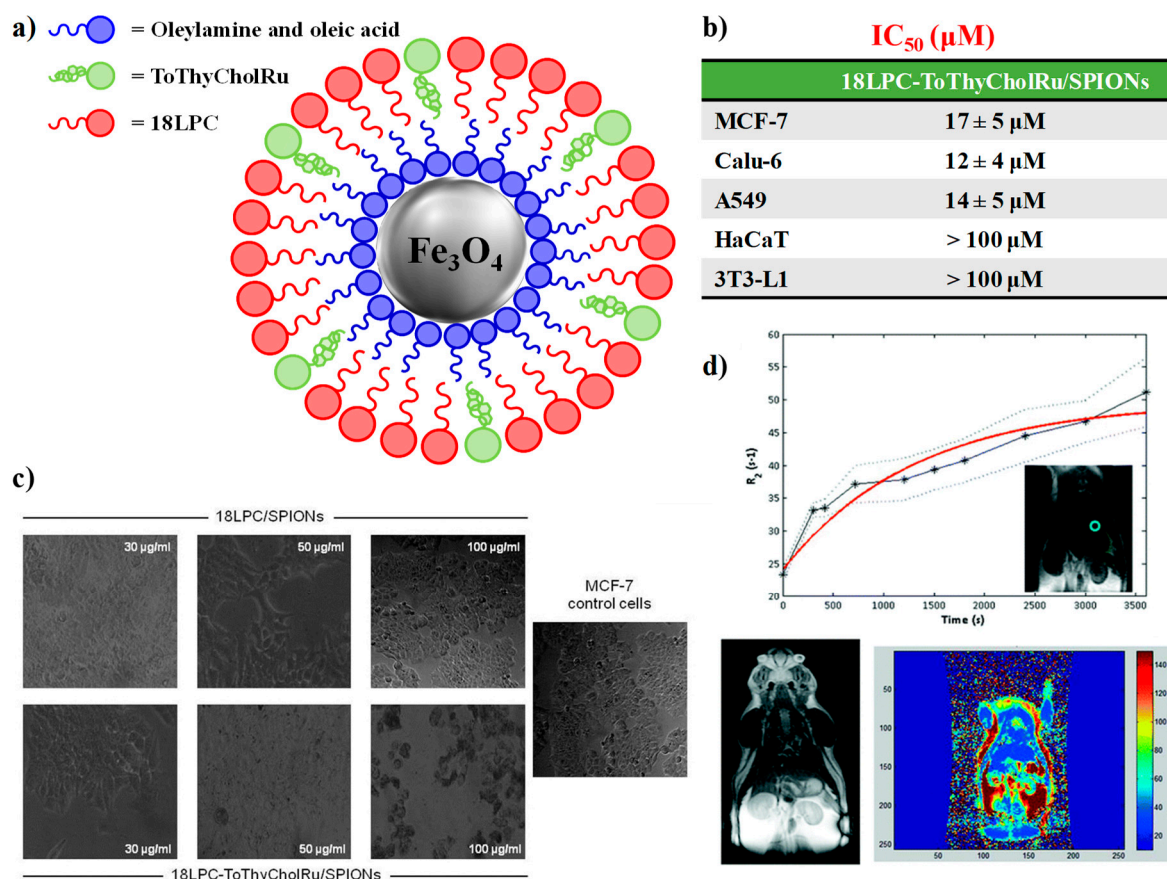


**Figure 18.** 18LPC-ToThyCholRu/SPIONs: schematic representation of NPs systems with the inner membrane layer based on oleylamine/oleic acid and the outer membrane layer composed of 18-LPC loaded with the Ru(III)-complex ToThyCholRu (a); IC<sub>50</sub> values (μM)—reported as mean ± SEM—relative to the effective ruthenium concentration carried by 18LPC-ToThyCholRu/SPIONs in the indicated cell lines following 48 h incubation (b); representative photomicrographs by phase-contrast light microscopy (c) of MCF-7 cell lines untreated (control cells, left) or treated for 48 h with the indicated iron concentration of 18LPC/SPIONs (top line) and of 18LPC-ToThyCholRu/SPIONs (bottom line); MRI measurements (d): transverse relaxation rate ( $R_2 = 1/T_2, s^{-1}$ ) measured after bolus injection in the tail vein of 18LPC/SPIONs in 0.9% NaCl solution (top) with inset representing the ROI, selected in the coronal plane covering the liver; T<sub>2</sub>-weighted image of a coronal view of the animal (Wistar rat) before injection of the 18LPC/SPIONs (bottom, left); representative T<sub>2</sub>-mapping MRI image of a coronal view after injection (t = 3 min) of the 18LPC/SPIONs (bottom, right). Figures are adapted from [108].

The successive evaluation of the bioactivity of the ToThyCholRu-functionalized SPIONs on selected human cancer and non-cancer cells (MCF-7 breast adenocarcinoma, human HaCaT keratinocytes, murine 3T3L-1 fibroblasts, human Calu-6 and A549 lung carcinoma cell lines) confirmed the potential of this system as an effective theranostic device (Figure 18b) [108]. Indeed, 18LPC/SPIONs were devoid of significant biological effects, even at 100 μg/mL iron concentration on both cancer and healthy cell lines, (Figure 18b) while the incorporation of the amphiphilic ruthenium complex ToThyCholRu in the SPION surface induced a significantly enhanced bioactivity, providing significant cytotoxic effects in cancer cells without affecting healthy cells (Figure 18b) [108]. Notably, when inserted in the SPION nanosystems, ToThyCholRu was also very effective in inhibiting MCF-7 proliferation, with ca. four-fold higher cytotoxicity compared to the same Ru(III) complex loaded in POPC; conversely the inhibition efficiency was similar to that observed after loading in cationic DOTAP-based nanoaggregates (see data reported in Table 1).

In analogy to previous investigations (Section 3.4), subconfluent breast MCF-7 culture cells were also examined by phase-contrast light microscopy indicating that the *in vitro* exposure to 18LPC/SPIONs did not alter cell morphology, whereas after Ru-loaded NPs administration, significant cytological changes of the cell monolayers clearly appeared (Figure 18c) [108].

Once assessed for their biocompatibility, 18LPC/SPIONs were also injected in the tail vein of a healthy rat, chosen as a small animal model to evaluate their *in vivo* pharmacokinetics and applicability as negative contrast agents for MRI analyses (Figure 18d). This effect is typically evaluated with the transverse proton relaxation time ( $T_2$ ) reduction or transverse proton relaxation rate ( $R_2$ ) increase [255,256].

Ten minutes after injection, a notable  $T_2$  relaxation time decrease was recorded in the liver of the animal, consistently with the nanoparticle capture by the reticuloendothelial hepatic tissue (Kupffer cells) [257], without significant variation in other organs (e.g., kidneys and heart). Then, according to the progressive accumulation of the 18LPC/SPIONs in the tissue for excretion,  $R_2$  reached a maximum value 60 min after injection [108].

Thus, 18LPC/SPIONs demonstrated to favour long circulation times with a measurable reduction in the MR signals in the rat liver, indicating a very promising potential for use as MRI negative contrast agents [108].

More recently, as additional ingredients for the SPIONs surface decoration, suitable lipophilic AS1411 conjugates were also studied [258] in order to evaluate in future studies the ability of AS1411 to enhance the Ru(III)-based compounds uptake and, thus, their overall anticancer activity also when incorporated onto SPIONs.

## 5. Conclusions

Cancer is one of the leading causes of death in the world, representing a key topic in scientific research. Cancer cells are able to accumulate multiple mutations allowing their uncontrollable growing, invasiveness, and eventually spreading to other parts of the body causing tumour metastasis formation. In addition, malignant cells typically exhibit aberrations in the physiological signalling pathways regulating various cellular processes, such as cell growth and division, as well as cell-to-cell communication. Therefore, the genetic and phenotypic heterogeneities of tumours form, making cancer a very difficult disease to treat.

Stimulated by the success of cisplatin, intense efforts have been devoted to the development of alternative transition metal-based anti-tumour compounds. Pioneering studies in this field led to promising lead Ru(III)-complexes, such as NAMI-A, KP-1019 and NKP-1339, which entered clinical trials, even though none of these have been approved yet for human use.

The difficulty of progressing lead compounds from animal studies to human clinical trials and/or effective clinical use highlights the complications involved in overcoming the pharmacokinetic and pharmacodynamic barriers in living animals. Metal compounds with proved selective anti-tumour *in vitro* activity are presumably able to reach the target tumour xenograft without causing adverse effects to the health of the animal. Nevertheless, this is not always verified since a compound active *in vitro* against cancer cell lines can fail under *in vivo* testing for several reasons. For example, the lipophilicity of complexes is determinant for effective cellular uptake. Secondly, the compound may be too unstable in human plasma or may be cleared too quickly by the liver. Alternatively, a compound may be too toxic to a particular organ, even though it may not show cytotoxicity *in vitro* against normal cell lines.

In this context, the encapsulation of Ru(III) complexes into nanostructures is an increasing research area, particularly useful to address the uptake and stability issues of these anticancer agents; therefore, some ground-breaking advances are expected in the near future. Nanoformulations can be used to enhance the efficacy of Ru complexes in cancer treatment by targeted delivery of drugs into cancer cells and reduce their adverse effects and systemic toxicity by optimization of their pharmacokinetic properties. Notably, examples have been here discussed showing the ability of Ru(III)-functionalized

liposomes to activate multiple cell death pathways, which represents a very interesting perspective in order to develop new intervention strategies in TNBC with limited chemotherapeutic options.

Although nanostructured materials functionalized with Ru complexes (micelles, liposomes, niosomes and iron oxide nanoparticles) have shown great potential in the treatment of cancer, there are still many challenges in translating basic research into clinical applications.

To reach these challenging goals, understanding the pharmacokinetic and pharmacodynamic parameters of a drug is essential for the design of dosage administration regimens, as well as to help reducing toxicity effects and enhancing target drug delivery. A more in-depth understanding of the mechanism of action of the hit/lead compounds could also potentially help to improve the potency and selectivity of the candidate drugs through rational design of optimized drugs.

Finally, significant efforts must be invested in developing extensive in vivo screenings in models that mimic human pathophysiology in order to achieve higher predictability for successful Ru(III)-drug development.

Overall, research on the encapsulation of Ru(III) complexes will undoubtedly continue to develop and, owing to the high structural variety of nanosystems and Ru derivatives, new delivery platforms will certainly be realized in the near future for anticancer therapies.

Based on the continuous efforts that worldwide researchers have invested in this field, our feeling is that it is only a matter of time before new metal complexes with superior efficacy and low toxicity will be approved as anticancer therapeutics, finally replacing longstanding metal-based anticancer drugs as cisplatin and its derivatives.

In this context, the next years will witness progress in elucidating real targets and mechanisms of action that will provide solid scientific basis for extensive preclinical development of selected Ru(III)-containing formulations.

**Author Contributions:** For research articles with several authors, a short paragraph specifying their individual contributions must be provided. The following statements should be used “conceptualization, D.M. and C.R.; methodology, D.M. and C.R.; software, C.R.; validation, D.M., L.P., C.I. and M.T.; formal analysis, D.M.; resources, C.R.; data curation, D.M. and C.R.; writing—original draft preparation, C.R., D.M., L.P., M.T., C.I. and D.M.; writing—review and editing, D.M. and C.R.; project administration, D.M.; funding acquisition, D.M.”

**Funding:** This research was funded by the Italian Association for Cancer Research (AIRC) (IG2015 n. 17,037 to D.M.).

**Conflicts of Interest:** The authors declare no conflict of interest.

## References

1. Rosenberg, B.; Vancamp, L.; Krigas, T. Inhibition of cell division in escherichia coli by electrolysis products from a platinum electrode. *Nature* **1965**, *205*, 698–699. [[CrossRef](#)] [[PubMed](#)]
2. Rosenberg, B.; van Camp, L.; Trosko, J.E.; Mansour, V.H. Platinum compounds: A new class of potent antitumour agents. *Nature* **1969**, *222*, 385–386. [[CrossRef](#)] [[PubMed](#)]
3. Kelland, L. The resurgence of platinum-based cancer chemotherapy. *Nat. Rev. Cancer* **2007**, *7*, 573–584. [[CrossRef](#)] [[PubMed](#)]
4. Dasari, S.; Bernard Tchounwou, P. Cisplatin in cancer therapy: Molecular mechanisms of action. *Eur. J. Pharm.* **2014**, *740*, 364–378. [[CrossRef](#)] [[PubMed](#)]
5. Davies, M.S.; Berners-Price, S.J.; Hambley, T.W. Slowing of cisplatin aquation in the presence of DNA but not in the presence of phosphate: Improved understanding of sequence selectivity and the roles of mono-aquated and di-aquated species in the binding of cisplatin to DNA. *Inorg. Chem.* **2000**, *39*, 5603–5613. [[CrossRef](#)] [[PubMed](#)]
6. Cepeda, V.; Fuertes, M.; Castilla, J.; Alonso, C.; Quevedo, C.; Perez, J. Biochemical mechanisms of cisplatin cytotoxicity. *Anticancer Agents Med. Chem.* **2007**, *7*, 3–18. [[CrossRef](#)] [[PubMed](#)]
7. Reedijk, J. Platinum anticancer coordination compounds: Study of DNA binding inspires new drug design. *Eur. J. Inorg. Chem.* **2009**, *10*, 1303–1312. [[CrossRef](#)]
8. Todd, R.C.; Lippard, S.J. Structure of duplex DNA containing the cisplatin 1,2-[Pt(NH<sub>3</sub>)<sub>2</sub>]<sup>2+</sup>-d(GpG) cross-link at 1.77 Å resolution. *J. Inorg. Biochem.* **2010**, *104*, 902–908. [[CrossRef](#)] [[PubMed](#)]

9. Eckstein, N. Platinum resistance in breast and ovarian cancer cell lines. *J. Exp. Clin. Cancer Res.* **2011**, *30*, 91. [[CrossRef](#)] [[PubMed](#)]
10. Oun, R.; Moussa, Y.E.; Wheate, N.J. The side effects of platinum-based chemotherapy drugs: A review for chemists. *Dalt. Trans.* **2018**, *47*, 6645–6653. [[CrossRef](#)] [[PubMed](#)]
11. Harrap, K.R. Preclinical studies identifying carboplatin as a viable cisplatin alternative. *Cancer Treat. Rev.* **1985**, *12*, 21–33. [[CrossRef](#)]
12. De Gramont, A.; Figer, A.; Seymour, M.; Homerin, M.; Hmissi, A.; Cassidy, J.; Boni, C.; Cortes-Funes, H.; Cervantes, A.; Freyer, G.; et al. Leucovorin and fluorouracil with or without oxaliplatin as first-line treatment in advanced colorectal cancer. *J. Clin. Oncol.* **2000**, *18*, 2938–2947. [[CrossRef](#)] [[PubMed](#)]
13. Galanski, M.; Jakupec, M.A.; Keppler, B.K. Update of the preclinical situation of anticancer platinum complexes: Novel design strategies and innovative analytical approaches. *Curr. Med. Chem.* **2005**, *12*, 2075–2094. [[CrossRef](#)] [[PubMed](#)]
14. Wheate, N.J.; Walker, S.; Craig, G.E.; Oun, R. The status of platinum anticancer drugs in the clinic and in clinical trials. *Dalton Trans.* **2010**, *39*, 8113–8127. [[CrossRef](#)] [[PubMed](#)]
15. Ali, I.A.; Wani, W.; Saleem, K.; Haque, A. Platinum compounds: A hope for future cancer chemotherapy. *Anticancer Agents Med. Chem.* **2013**, *13*, 296–306. [[CrossRef](#)] [[PubMed](#)]
16. Ott, I.; Gust, R. Non platinum metal complexes as anti-cancer drugs. *Arch. Pharm.* **2007**, *340*, 117–126. [[CrossRef](#)] [[PubMed](#)]
17. Gasser, G.; Ott, I.; Metzler-Nolte, N. Organometallic anticancer compounds. *J. Med. Chem.* **2011**, *54*, 3–25. [[CrossRef](#)] [[PubMed](#)]
18. Sava, G.; Bergamo, A.; Dyson, P.J. Metal-based antitumour drugs in the post-genomic era: What comes next? *Dalton Trans.* **2011**, *40*, 9069–9075. [[CrossRef](#)]
19. Bergamo, A.; Gaiddon, C.; Schellens, J.H.; Beijnen, J.H.; Sava, G. Approaching tumour therapy beyond platinum drugs: Status of the art and perspectives of ruthenium drug candidates. *J. Inorg. Biochem.* **2012**, *106*, 90–99. [[CrossRef](#)] [[PubMed](#)]
20. Ndagi, U.; Mhlongo, N.; Soliman, M.E. Metal complexes in cancer therapy – an update from drug design perspective. *Drug Des. Dev. Ther.* **2017**, *11*, 599–616. [[CrossRef](#)] [[PubMed](#)]
21. Liang, J.X.; Zhong, H.J.; Yang, G.; Vellaisamy, K.; Ma, D.L.; Leung, C.H. Recent development of transition metal complexes with in vivo antitumor activity. *J. Inorg. Biochem.* **2017**, *177*, 276–286. [[CrossRef](#)]
22. Lazarević, T.; Rilak, A.; Bugarić, Ž.D. Platinum, palladium, gold and ruthenium complexes as anticancer agents: Current clinical uses, cytotoxicity studies and future perspectives. *Eur. J. Med. Chem.* **2017**, *142*, 8–31. [[CrossRef](#)]
23. Hanif, M.; Hartinger, C.G. Anticancer metallodrugs: Where is the next cisplatin? *Future Med. Chem.* **2018**, *10*, 615–617. [[CrossRef](#)] [[PubMed](#)]
24. Bratsos, I.; Jedner, S.; Gianferrara, T.; Alessio, E. Ruthenium anticancer compounds: Challenges and expectations. *Chim. Int. J. Chem.* **2007**, *61*, 692–697. [[CrossRef](#)]
25. Levina, A.; Mitra, A.; Lay, P.A. Recent developments in ruthenium anticancer drugs. *Metallomics* **2009**, *1*, 458–470. [[CrossRef](#)]
26. Antonarakis, E.S.; Emadi, A. Ruthenium-based chemotherapeutics: Are they ready for prime time? *Cancer Chemother. Pharm.* **2010**, *66*, 1–9. [[CrossRef](#)]
27. Bergamo, A.; Sava, G. Ruthenium anticancer compounds: Myths and realities of the emerging metal-based drugs. *Dalton Trans.* **2011**, *40*, 7817–7823. [[CrossRef](#)] [[PubMed](#)]
28. Blunden, B.M.; Stenzel, M.H. Incorporating ruthenium into advanced drug delivery carriers—An innovative generation of chemotherapeutics. *J. Chem. Technol. Biotechnol.* **2015**, *90*, 1177–1195. [[CrossRef](#)]
29. Alessio, E. Thirty years of the drug candidate NAMI-A and the myths in the field of ruthenium anticancer compounds: A personal perspective. *Eur. J. Inorg. Chem.* **2017**, *2017*, 1549–1560. [[CrossRef](#)]
30. Zheng, K.; Wu, Q.; Wang, C.; Tan, W.; Mei, W. Ruthenium (II) complexes as potential apoptosis inducers in chemotherapy. *Anticancer Agents Med. Chem.* **2017**, *17*, 29–39. [[CrossRef](#)] [[PubMed](#)]
31. Thota, S.; Rodrigues, D.A.; Crans, D.C.; Barreiro, E.J. Ru (II) compounds: Next-generation anticancer metalloterapeutics? *J. Med. Chem.* **2018**, *61*, 5805–5821. [[CrossRef](#)]
32. Meier-Menches, S.M.; Gerner, C.; Berger, W.; Hartinger, C.G.; Keppler, B.K. Structure-activity relationships for ruthenium and osmium anticancer agents-towards clinical development. *Chem. Soc. Rev.* **2018**, *47*, 909–928. [[CrossRef](#)] [[PubMed](#)]

33. Coverdale, J.P.C.; Laroia-McCarron, T.; Romero-Canelón, I. Designing ruthenium anticancer drugs: What have we learnt from the key drug candidates? *Inorganics* **2019**, *7*, 31. [[CrossRef](#)]
34. Wani, W.A.; Prashar, S.; Shreaz, S.; Gómez-Ruiz, S. Nanostructured materials functionalized with metal complexes: In search of alternatives for administering anticancer metallodrugs. *Coord. Chem. Rev.* **2016**, *312*, 67–98. [[CrossRef](#)]
35. Riccardi, C.; Musumeci, D.; Irace, C.; Paduano, L.; Montesarchio, D. Ru (III) complexes for anticancer therapy: The importance of being nucleolipidic. *Eur. J. Org. Chem.* **2017**, *2017*, 1100–1119. [[CrossRef](#)]
36. Sarkar, A. Novel platinum compounds and nanoparticles as anticancer agents. *Pharm. Pat. Anal.* **2018**, *7*, 33–46. [[CrossRef](#)] [[PubMed](#)]
37. Poursharifi, M.; Wlodarczyk, M.T.; Mieszawska, A.J. Nano-based systems and biomacromolecules as carriers for metallodrugs in anticancer therapy. *Inorganics* **2019**, *7*, 2. [[CrossRef](#)]
38. Malam, Y.; Loizidou, M.; Seifalian, A.M. Liposomes and nanoparticles: Nanosized vehicles for drug delivery in cancer. *Trends Pharm. Sci.* **2009**, *30*, 592–599. [[CrossRef](#)] [[PubMed](#)]
39. Pillai, G. Nanomedicines for cancer therapy: An update of FDA approved and those under various stages of development. *SOJ Pharm. Pharm. Sci.* **2014**. [[CrossRef](#)]
40. Din, F.U.; Aman, W.; Ullah, I.; Qureshi, O.S.; Mustapha, O.; Shafique, S.; Zeb, A. Effective use of nanocarriers as drug delivery systems for the treatment of selected tumors. *Int. J. Nanomed.* **2017**, *12*, 7291–7309. [[CrossRef](#)]
41. Ventola, C.L. Progress in nanomedicine: Approved and investigational nanodrugs. *Pharm. Ther.* **2017**, *42*, 742–755.
42. Villemain, E.; Ong, Y.C.; Thomas, C.M.; Gasser, G. Polymer encapsulation of ruthenium complexes for biological and medicinal applications. *Nat. Rev. Chem.* **2019**, *3*, 261–282. [[CrossRef](#)]
43. Zeng, L.; Gupta, P.; Chen, Y.; Wang, E.; Ji, L.; Chao, H.; Chen, Z.S. The development of anticancer ruthenium(II) complexes: From single molecule compounds to nanomaterials. *Chem. Soc. Rev.* **2017**, *46*, 5771–5804. [[CrossRef](#)] [[PubMed](#)]
44. Thangavel, P.; Viswanath, B.; Kim, S. Recent developments in the nanostructured materials functionalized with ruthenium complexes for targeted drug delivery to tumors. *Int. J. Nanomed.* **2017**, *12*, 2749–2758. [[CrossRef](#)] [[PubMed](#)]
45. Rademaker-Lakhai, J.M.; van den Bongard, D.; Pluim, D.; Beijnen, J.H.; Schellens, J.H.M. A phase I and pharmacological study with imidazolium-trans-DMSO-imidazole-tetrachlororuthenate, a novel ruthenium anticancer agent. *Clin. Cancer Res.* **2004**, *10*, 3717–3727. [[CrossRef](#)] [[PubMed](#)]
46. Leijen, S.; Burgers, S.A.; Baas, P.; Pluim, D.; Tibben, M.; van Werkhoven, E.; Alessio, E.; Sava, G.; Beijnen, J.H.; Schellens, J.H.M. Phase I/II study with ruthenium compound NAMI-A and gemcitabine in patients with non-small cell lung cancer after first line therapy. *Investig. New Drugs* **2015**, *33*, 201–214. [[CrossRef](#)] [[PubMed](#)]
47. Kapitza, S.; Pongratz, M.; Jakupec, M.A.; Heffeter, P.; Berger, W.; Lackinger, L.; Keppler, B.K.; Marian, B. Heterocyclic complexes of ruthenium(III) induce apoptosis in colorectal carcinoma cells. *J. Cancer Res. Clin. Oncol.* **2005**, *131*, 101–110. [[CrossRef](#)] [[PubMed](#)]
48. Jakupec, M.A.; Arion, V.B.; Kapitza, S.; Reisner, E.; Eichinger, A.; Pongratz, M.; Marian, B.; von Keyserlingk Graf, N.; Keppler, B.K. KP1019 (FFC14A) from bench to bedside: Preclinical and early clinical development—an overview. *Int. J. Clin. Pharm. Ther.* **2005**, *43*, 595–596. [[CrossRef](#)]
49. Hartinger, C.G.; Zorbas-Seifried, S.; Jakupec, M.A.; Kynast, B.; Zorbas, H.; Keppler, B.K. From bench to bedside—Preclinical and early clinical development of the anticancer agent indazolium trans-[tetrachlorobis(1H-indazole)ruthenate(III)] (KP1019 or FFC14A). *J. Inorg. Biochem.* **2006**, *100*, 891–904. [[CrossRef](#)]
50. Hartinger, C.G.; Jakupec, M.A.; Zorbas-Seifried, S.; Groessl, M.; Egger, A.; Berger, W.; Zorbas, H.; Dyson, P.J.; Keppler, B.K. KP1019, a new redox-active anticancer agent—preclinical development and results of a clinical phase I study in tumor patients. *Chem. Biodivers.* **2008**, *5*, 2140–2155. [[CrossRef](#)]
51. Lentz, F.; Drescher, A.; Lindauer, A.; Henke, M.; Hilger, R.A.; Hartinger, C.G.; Scheulen, M.E.; Dittrich, C.; Keppler, B.K.; Jaehde, U. Pharmacokinetics of a novel anticancer ruthenium complex (KP1019, FFC14A) in a phase I dose-escalation study. *Anticancer Drugs* **2009**, *20*, 97–103. [[CrossRef](#)] [[PubMed](#)]
52. Singh, V.; Azad, G.K.; Mandal, P.; Reddy, M.A.; Tomar, R.S. Anti-cancer drug KP1019 modulates epigenetics and induces DNA damage response in *Saccharomyces cerevisiae*. *FEBS Lett.* **2014**, *588*, 1044–1052. [[CrossRef](#)] [[PubMed](#)]

53. Flocke, L.S.; Trondl, R.; Jakupec, M.A.; Keppler, B.K. Molecular mode of action of NKP-1339—A clinically investigated ruthenium-based drug—Involves ER- and ROS-related effects in colon carcinoma cell lines. *Investig. New Drugs* **2016**, *34*, 261–268. [[CrossRef](#)] [[PubMed](#)]
54. Trondl, R.; Heffeter, P.; Kowol, C.R.; Jakupec, M.A.; Berger, W.; Keppler, B.K. NKP-1339, the first ruthenium-based anticancer drug on the edge to clinical application. *Chem. Sci.* **2014**, *5*, 2925–2932. [[CrossRef](#)]
55. Burris, H.A.; Bakewell, S.; Bendell, J.C.; Infante, J.; Jones, S.F.; Spigel, D.R.; Weiss, G.J.; Ramanathan, R.K.; Ogden, A.; Von Hoff, D. Safety and activity of IT-139, a ruthenium-based compound, in patients with advanced solid tumours: A first-in-human, open-label, dose-escalation phase I study with expansion cohort. *ESMO Open* **2016**, *1*, e000154. [[CrossRef](#)] [[PubMed](#)]
56. Lizardo, M.M.; Morrow, J.J.; Miller, T.E.; Hong, E.S.; Ren, L.; Mendoza, A.; Halsey, C.H.; Scacheri, P.C.; Helman, L.J.; Khanna, C. Upregulation of glucose-regulated protein 78 in metastatic cancer cells is necessary for lung metastasis progression. *Neoplasia* **2016**, *18*, 699–710. [[CrossRef](#)]
57. Schoenhacker-Alte, B.; Mohr, T.; Pirker, C.; Kryeziu, K.; Kuhn, P.S.; Buck, A.; Hofmann, T.; Gerner, C.; Hermann, G.; Koellensperger, G.; et al. Sensitivity towards the GRP78 inhibitor KP1339/IT-139 is characterized by apoptosis induction via caspase 8 upon disruption of ER homeostasis. *Cancer Lett.* **2017**, *404*, 79–88. [[CrossRef](#)] [[PubMed](#)]
58. Blazevic, A.; Hummer, A.A.; Heffeter, P.; Berger, W.; Filipits, M.; Cibir, G.; Keppler, B.K.; Rompel, A. Electronic state of sodium trans-[tetrachloridobis (1H-indazole) ruthenate (III)] (NKP-1339) in tumor, liver and kidney tissue of a SW480-bearing mouse. *Sci. Rep.* **2017**, *7*, 40966. [[CrossRef](#)]
59. Alessio, E.; Messori, L. Anticancer drug candidates face-to-face: A case story in medicinal inorganic chemistry. *Molecules* **2019**, *24*, 1995. [[CrossRef](#)]
60. Messori, L.; Orioli, P.; Vullo, D.; Alessio, E.; Iengo, E. A spectroscopic study of the reaction of NAMI, a novel ruthenium(III) anti-neoplastic complex, with bovine serum albumin. *Eur. J. Biochem.* **2000**, *267*, 1206–1213. [[CrossRef](#)]
61. Bytzeck, A.K.; Boeck, K.; Hermann, G.; Hann, S.; Keppler, B.K.; Hartinger, C.G.; Koellensperger, G. LC- and CZE-ICP-MS approaches for the in vivo analysis of the anticancer drug candidate sodium trans-[tetrachloridobis (1H-indazole) ruthenate (III)] (KP1339) in mouse plasma. *Metallomics* **2011**, *3*, 1049–1055. [[CrossRef](#)] [[PubMed](#)]
62. Dömötör, O.; Hartinger, C.G.; Bytzeck, A.K.; Kiss, T.; Keppler, B.K.; Enyedy, E.A. Characterization of the binding sites of the anticancer ruthenium (III) complexes KP1019 and KP1339 on human serum albumin via competition studies. *J. Biol. Inorg. Chem.* **2013**, *18*, 9–17. [[CrossRef](#)] [[PubMed](#)]
63. Webb, M.I.; Walsby, C.J. Albumin binding and ligand-exchange processes of the Ru (III) anticancer agent NAMI-A and its bis-DMSO analogue determined by ENDOR spectroscopy. *Dalton Trans.* **2015**, *44*, 17482–17493. [[CrossRef](#)] [[PubMed](#)]
64. Bijelic, A.; Theiner, S.; Keppler, B.K.; Rompel, A. X-ray structure analysis of indazolium trans-[tetrachlorobis (1H-indazole) ruthenate (III)] (KP1019) bound to human serum albumin reveals two ruthenium binding sites and provides insights into the drug binding mechanism. *J. Med. Chem.* **2016**, *59*, 5894–5903. [[CrossRef](#)] [[PubMed](#)]
65. Messori, L.; Kratz, F.; Alessio, E. The interaction of the antitumor complexes Na[trans-RuCl<sub>4</sub>(DMSO)(Im)] and Na[trans-RuCl<sub>4</sub>(DMSO)(Ind)] with apotransferrin: A spectroscopic study. *Met. Based Drugs* **1996**, *3*, 1–9. [[CrossRef](#)]
66. Pongratz, M.; Schluga, P.; Jakupec, M.A.; Arion, V.B.; Hartinger, C.G.; Allmaier, G.; Keppler, B.K. Transferrin binding and transferrin-mediated cellular uptake of the ruthenium coordination compound KP1019, studied by means of AAS, ESI-MS and CD spectroscopy. *J. Anal. Atomic Spectrom.* **2004**, *19*, 46–51. [[CrossRef](#)]
67. Mazuryk, O.; Kurpiewska, K.; Lewinski, K.; Stochel, G.; Brindell, M. Interaction of apo-transferrin with anticancer ruthenium complexes NAMI-A and its reduced form. *J. Inorg. Biochem.* **2012**, *116*, 11–18. [[CrossRef](#)]
68. Spiewak, K.; Brindell, M. Impact of low- and high-molecular-mass components of human serum on NAMI-A binding to transferrin. *J. Biol. Inorg. Chem.* **2015**, *20*, 695–703. [[CrossRef](#)]
69. Ciambellotti, S.; Pratesi, A.; Severi, M.; Ferraro, G.; Alessio, E.; Merlino, A.; Messori, L. The NAMI A-human ferritin system: A biophysical characterization. *Dalton Trans.* **2018**, *47*, 11429–11437. [[CrossRef](#)]

70. Pizarro, A.M.; Sadler, P.J. Unusual DNA binding modes for metal anticancer complexes. *Biochimie* **2009**, *91*, 1198–1211. [[CrossRef](#)]
71. Alessio, E.; Balducci, G.; Lutman, A.; Mestroni, G.; Calligaris, M.; Attia, W.M. Synthesis and characterization of two new classes of ruthenium (III)-sulfoxide complexes with nitrogen donor ligands (L): Na[trans-RuCl<sub>4</sub>(R<sub>2</sub>SO)(L)] and mer, cis-RuCl<sub>3</sub>(R<sub>2</sub>SO)(R<sub>2</sub>SO)(L). The crystal structure of Na[trans-RuCl<sub>4</sub>(DMSO)(NH<sub>3</sub>)] 2DMSO, Na[trans-RuCl<sub>4</sub>(DMSO)(Im)] H<sub>2</sub>O, Me<sub>2</sub>CO (Im = imidazole) and mer, cis-RuCl<sub>3</sub>(DMSO)(DMSO)(NH<sub>3</sub>). *Inorg. Chim. Acta* **1993**, *203*, 205–217. [[CrossRef](#)]
72. Groessl, M.; Zava, O.; Dyson, P.J. Cellular uptake and subcellular distribution of ruthenium-based metallodrugs under clinical investigation versus cisplatin. *Metallomics* **2011**, *3*, 591–599. [[CrossRef](#)] [[PubMed](#)]
73. Stevens, S.K.; Strehle, A.P.; Miller, R.L.; Gammons, S.H.; Hoffman, K.J.; McCarty, J.T.; Miller, M.E.; Stultz, L.K.; Hanson, P.K. The anticancer ruthenium complex KP1019 induces DNA damage, leading to cell cycle delay and cell death in *Saccharomyces cerevisiae*. *Mol. Pharm.* **2013**, *83*, 225–234. [[CrossRef](#)] [[PubMed](#)]
74. Aitken, J.B.; Antony, S.; Weekley, C.M.; Lai, B.; Spiccia, L.; Harris, H.H. Distinct cellular fates for KP1019 and NAMI-A determined by X-ray fluorescence imaging of single cells. *Metallomics* **2012**, *4*, 1051. [[CrossRef](#)] [[PubMed](#)]
75. Webb, M.I.; Chard, R.A.; Al-Jobory, Y.M.; Jones, M.R.; Wong, E.W.Y.; Walsby, C.J. Pyridine analogs of the antimetastatic Ru(III) complex NAMI-A targeting non-covalent interactions with albumin. *Inorg. Chem.* **2012**, *51*, 954–966. [[CrossRef](#)] [[PubMed](#)]
76. Mu, C.; Chang, S.W.; Prosser, K.E.; Leung, A.W.Y.; Santacruz, S.; Jang, T.; Thompson, J.R.; Yapp, D.T.T.; Warren, J.J.; Bally, M.B.; et al. Induction of cytotoxicity in pyridine analogues of the anti-metastatic Ru(III) complex NAMI-A by ferrocene functionalization. *Inorg. Chem.* **2016**, *55*, 177–190. [[CrossRef](#)] [[PubMed](#)]
77. Mangiapia, G.; D'Errico, G.; Simeone, L.; Irace, C.; Radulescu, A.; Di Pascale, A.; Colonna, A.; Montesarchio, D.; Paduano, L. Ruthenium-based complex nanocarriers for cancer therapy. *Biomaterials* **2012**, *33*, 3770–3782. [[CrossRef](#)] [[PubMed](#)]
78. Tan, C.; Wu, S.; Lai, S.; Wang, M.; Chen, Y.; Zhou, L.; Zhu, Y.; Lian, W.; Peng, W.; Ji, L.; et al. Synthesis, structures, cellular uptake and apoptosis-inducing properties of highly cytotoxic ruthenium-norharman complexes. *Dalton Trans.* **2011**, *40*, 8611–8621. [[CrossRef](#)] [[PubMed](#)]
79. Vitiello, G.; Luchini, A.; D'Errico, G.; Santamaria, R.; Capuozzo, A.; Irace, C.; Montesarchio, D.; Paduano, L. Cationic liposomes as efficient nanocarriers for the drug delivery of an anticancer cholesterol-based ruthenium complex. *J. Mater. Chem. B* **2015**, *3*, 3011–3023. [[CrossRef](#)]
80. Łakomska, I.; Fandzloch, M.; Muzioł, T.; Lis, T.; Jezierska, J. Synthesis, characterization and antitumor properties of two highly cytotoxic ruthenium(III) complexes with bulky triazolopyrimidine ligands. *Dalton Trans.* **2013**, *42*, 6219. [[CrossRef](#)]
81. Webb, M.I.; Wu, B.; Jang, T.; Chard, R.A.; Wong, E.W.Y.; Wong, M.Q.; Yapp, D.T.T.; Walsby, C.J. Increasing the bioavailability of Ru(III) anticancer complexes through hydrophobic albumin interactions. *Chem. Eur. J.* **2013**, *19*, 17031–17042. [[CrossRef](#)] [[PubMed](#)]
82. Chang, S.W.; Lewis, A.R.; Prosser, K.E.; Thompson, J.R.; Gladkikh, M.; Bally, M.B.; Warren, J.J.; Walsby, C.J. CF<sub>3</sub> derivatives of the anticancer Ru(III) complexes KP1019, NKP-1339, and their imidazole and pyridine analogues show enhanced lipophilicity, albumin interactions, and cytotoxicity. *Inorg. Chem.* **2016**, *55*, 4850–4863. [[CrossRef](#)] [[PubMed](#)]
83. Vergara, A.; D'Errico, G.; Montesarchio, D.; Paduano, L.; Merlino, A. Interaction of anticancer ruthenium compounds with proteins high-resolution X-ray structures and raman microscopy studies of the adduct between hen egg white lysozyme and AziRu. *Inorg. Chem.* **2013**, *52*, 4157–4159. [[CrossRef](#)]
84. Vergara, A.; Russo Krauss, I.; Montesarchio, D.; Paduano, L.; Merlino, A. Investigating the ruthenium metalation of proteins: X-ray structure and Raman microspectroscopy of the complex between RNase A and AziRu. *Inorg. Chem.* **2013**, *52*, 10714–10716. [[CrossRef](#)] [[PubMed](#)]
85. Musumeci, D.; Rozza, L.; Merlino, A.; Paduano, L.; Marzo, T.; Massai, L.; Messori, L.; Montesarchio, D. Interaction of anticancer Ru(III) complexes with single stranded and duplex DNA model systems. *Dalton Trans.* **2015**, *44*, 13914–13925. [[CrossRef](#)] [[PubMed](#)]
86. Caterino, M.; Herrmann, M.; Merlino, A.; Riccardi, C.; Montesarchio, D.; Mroginski, M.A.; Musumeci, D.; Ruffo, F.; Paduano, L.; Hildebrandt, P.; et al. On the pH-modulated Ru-based prodrug activation mechanism. *Inorg. Chem.* **2019**, *58*, 1216–1223. [[CrossRef](#)] [[PubMed](#)]

87. Messori, L.; Merlino, A. Ruthenium metalation of proteins: The X-ray structure of the complex formed between NAMI-A and hen egg white lysozyme. *Dalton Trans.* **2014**, *43*, 6128–6131. [[CrossRef](#)] [[PubMed](#)]
88. Ravera, M.; Baracco, S.; Cassino, C.; Zanello, P.; Osella, D. Appraisal of the redox behaviour of the antimetastatic ruthenium(III) complex [ImH][RuCl<sub>4</sub>(DMSO)(Im)], NAMI-A. *Dalton Trans.* **2004**, 2347–2351. [[CrossRef](#)] [[PubMed](#)]
89. Bacac, M.; Hotze, A.C.G.; van der Schilden, K.; Haasnoot, J.G.; Pacor, S.; Alessio, E.; Sava, G.; Reedijk, J. The hydrolysis of the anti-cancer ruthenium complex NAMI-A affects its DNA binding and antimetastatic activity: An NMR evaluation. *J. Inorg. Biochem.* **2004**, *98*, 402–412. [[CrossRef](#)] [[PubMed](#)]
90. Timerbaev, A.R.; Rudnev, A.V.; Semenova, O.; Hartinger, C.G.; Keppler, B.K. Comparative binding of antitumor indazolium [trans-tetrachlorobis(1H-indazole) ruthenate(III)] to serum transport proteins assayed by capillary zone electrophoresis. *Anal. Biochem.* **2005**, *341*, 326–333. [[CrossRef](#)]
91. Chen, J.; Chen, L.; Liao, S.; Zheng, K.; Ji, L. A theoretical study on the hydrolysis process of the antimetastatic ruthenium(III) complex NAMI-A. *J. Phys. Chem. B* **2007**, *111*, 7862–7869. [[CrossRef](#)] [[PubMed](#)]
92. Besker, N.; Coletti, C.; Marrone, A.; Re, N. Aquation of the ruthenium-based anticancer drug NAMI-A: A density functional study. *J. Phys. Chem. B* **2008**, *112*, 3871–3875. [[CrossRef](#)]
93. Vargiu, A.V.; Robertazzi, A.; Magistrato, A.; Ruggerone, P.; Carloni, P. The hydrolysis mechanism of the anticancer ruthenium drugs NAMI-A and ICR investigated by DFT-PCM calculations. *J. Phys. Chem. B* **2008**, *112*, 4401–4409. [[CrossRef](#)] [[PubMed](#)]
94. Pashkunova-Martic, I.; Losantos, B.C.; Kandler, N.; Keppler, B. Studies of KP46 and KP1019 and the hydrolysis product of KP1019 in lipiodol emulsions: Preparation and initial characterizations as potential theragnostic agents. *Curr. Drug Deliv.* **2018**, *15*, 134–142. [[CrossRef](#)] [[PubMed](#)]
95. Pal, M.; Nandi, U.; Mukherjee, D. Detailed account on activation mechanisms of ruthenium coordination complexes and their role as antineoplastic agents. *Eur. J. Med. Chem.* **2018**, *150*, 419–445. [[CrossRef](#)] [[PubMed](#)]
96. Mestroni, G.; Alessio, E.; Sava, G.; Pacor, S.; Coluccia, M.; Boccarelli, A. Water-soluble ruthenium(III)-dimethyl sulfoxide complexes: Chemical behaviour and pharmaceutical properties. *Met. Based Drugs* **1994**, *1*, 41–63. [[CrossRef](#)] [[PubMed](#)]
97. Bouma, M.; Nuijen, B.; Jansen, M.T.; Sava, G.; Flaibani, A.; Bult, A.; Beijnen, J.H. A kinetic study of the chemical stability of the antimetastatic ruthenium complex NAMI-A. *Int. J. Pharm.* **2002**, *248*, 239–246. [[CrossRef](#)]
98. Sava, G.; Bergamo, A.; Zorzet, S.; Gava, B.; Casarsa, C.; Cocchietto, M.; Furlani, A.; Scarcia, V.; Serli, B.; Iengo, E.; et al. Influence of chemical stability on the activity of the antimetastasis ruthenium compound NAMI-A. *Eur. J. Cancer* **2002**, *38*, 427–435. [[CrossRef](#)]
99. Galanski, M.; Keppler, B.K. Searching for the magic bullet: Anticancer platinum drugs which can be accumulated or activated in the tumor tissue. *Anticancer Agents Med. Chem.* **2007**, *7*, 55–73. [[CrossRef](#)] [[PubMed](#)]
100. Piccolo, M.; Misso, G.; Ferraro, M.G.; Riccardi, C.; Capuozzo, A.; Zarone, M.R.; Maione, F.; Trifuoggi, M.; Stiuso, P.; D’Errico, G.; et al. Exploring cellular uptake, accumulation and mechanism of action of a cationic Ru-based nanosystem in human preclinical models of breast cancer. *Sci. Rep.* **2019**, *9*, 7006. [[CrossRef](#)]
101. Baillet, J.; Desvergnès, V.; Hamoud, A.; Latxague, L.; Barthélémy, P. Lipid and nucleic acid chemistries: Combining the best of both worlds to construct advanced biomaterials. *Adv. Mater.* **2018**, *30*, 1705078. [[CrossRef](#)] [[PubMed](#)]
102. Vaccaro, M.; Del Litto, R.; Mangiapia, G.; Carnerup, A.M.; D’Errico, G.; Ruffo, F.; Paduano, L. Lipid based nanovectors containing ruthenium complexes: A potential route in cancer therapy. *Chem. Commun.* **2009**, 1404–1406. [[CrossRef](#)] [[PubMed](#)]
103. Simeone, L.; Mangiapia, G.; Irace, C.; Di Pascale, A.; Colonna, A.; Ortona, O.; De Napoli, L.; Montesarchio, D.; Paduano, L. Nucleolipid nanovectors as molecular carriers for potential applications in drug delivery. *Mol. Biosyst.* **2011**, *7*, 3075–3086. [[CrossRef](#)]
104. Simeone, L.; Irace, C.; Di Pascale, A.; Ciccarelli, D.; D’Errico, G.; Montesarchio, D. Synthesis, self-aggregation and bioactivity properties of a cationic aminoacyl surfactant, based on a new class of highly functionalized nucleolipids. *Eur. J. Med. Chem.* **2012**, *57*, 429–440. [[CrossRef](#)]

105. Simeone, L.; Mangiapia, G.; Vitiello, G.; Irace, C.; Colonna, A.; Ortona, O.; Montesarchio, D.; Paduano, L. Cholesterol-based nucleolipid-ruthenium complex stabilized by lipid aggregates for antineoplastic therapy. *Bioconj. Chem.* **2012**, *23*, 758–770. [[CrossRef](#)] [[PubMed](#)]
106. Mangiapia, G.; Vitiello, G.; Irace, C.; Santamaria, R.; Colonna, A.; Angelico, R.; Radulescu, A.; D’Errico, G.; Montesarchio, D.; Paduano, L. Anticancer cationic ruthenium nanovectors: From rational molecular design to cellular uptake and bioactivity. *Biomacromolecules* **2013**, *14*, 2549–2560. [[CrossRef](#)] [[PubMed](#)]
107. Montesarchio, D.; Mangiapia, G.; Vitiello, G.; Musumeci, D.; Irace, C.; Santamaria, R.; D’Errico, G.; Paduano, L. A new design for nucleolipid-based Ru(III) complexes as anticancer agents. *Dalton Trans.* **2013**, *42*, 16697–16708. [[CrossRef](#)]
108. Luchini, A.; Irace, C.; Santamaria, R.; Montesarchio, D.; Heenan, R.K.; Szekely, N.; Flori, A.; Menichetti, L.; Paduano, L. Phosphocholine-decorated superparamagnetic iron oxide nanoparticles: Defining the structure and probing in vivo applications. *Nanoscale* **2016**, *8*, 10078–10086. [[CrossRef](#)]
109. Riccardi, C.; Fàbrega, C.; Grijalvo, S.; Vitiello, G.; D’Errico, G.; Eritja, R.; Montesarchio, D. AS1411-decorated niosomes as effective nanocarriers for Ru(III)-based drugs in anticancer strategies. *J. Mater. Chem. B* **2018**, *6*, 5368–5384. [[CrossRef](#)]
110. Riccardi, C.; Musumeci, D.; Capuozzo, A.; Irace, C.; King, S.; Russo Krauss, I.; Paduano, L.; Montesarchio, D. “Dressing up” an old drug: An aminoacyl lipid for the functionalization of Ru(III)-based anticancer agents. *ACS Biomater. Sci. Eng.* **2018**, *4*, 163–174. [[CrossRef](#)]
111. Fischer, B.; Heffeter, P.; Kryeziu, K.; Gille, L.; Meier, S.M.; Berger, W.; Kowol, C.R.; Keppler, B.K. Poly (lactic acid) nanoparticles of the lead anticancer ruthenium compound KP1019 and its surfactant-mediated activation. *Dalton Trans.* **2014**, *43*, 1096–1104. [[CrossRef](#)] [[PubMed](#)]
112. Konstantinova, T.; Riabtseva, A.; Kowol, C.R.; Jungwith, U.; Heffeter, P.; Yanchuk, I.; Zaichenko, A.; Körner, W.; Senkiv, Y.; Berger, W.; et al. Nanoformulation improves activity of the (pre)clinical anticancer ruthenium complex KP1019. *J. Biomed. Nanotechnol.* **2014**, *10*, 877–884. [[CrossRef](#)]
113. Xu, W.; Ling, P.; Zhang, T. Polymeric micelles, a promising drug delivery system to enhance bioavailability of poorly water-soluble drugs. *J. Drug Deliv.* **2013**, *2013*, 340315. [[CrossRef](#)] [[PubMed](#)]
114. Tanbour, R.M.; Martins, A.G.; Pitt, W.A.; Hussein, G. Drug delivery systems based on polymeric micelles and ultrasound: A review. *Curr. Pharm. Des.* **2016**, *22*, 2796–27807. [[CrossRef](#)] [[PubMed](#)]
115. Blunden, B.M.; Rawal, A.; Lu, H.; Stenzel, M.H. Superior chemotherapeutic benefits from the ruthenium-based anti-metastatic drug NAMI-A through conjugation to polymeric micelles. *Macromolecules* **2014**, *47*, 1646–1655. [[CrossRef](#)]
116. D’Amora, A.; Cucciolito, M.E.; Iannitti, R.; Morelli, G.; Palumbo, R.; Ruffo, F.; Tesauro, D. Pyridine ruthenium (III) complexes entrapped in liposomes with enhanced cytotoxic properties in PC-3 prostate cancer cells. *J. Drug Deliv. Sci. Technol.* **2019**, *51*, 552–558. [[CrossRef](#)]
117. Scintilla, S.; Brustolin, L.; Gambalunga, A.; Chiara, F.; Trevisan, A.; Nardon, C.; Fregona, D. Ru(III) anticancer agents with aromatic and non-aromatic dithiocarbamates as ligands: Loading into nanocarriers and preliminary biological studies. *J. Inorg. Biochem.* **2016**, *165*, 159–169. [[CrossRef](#)]
118. Escobar-Chávez, J.J.; López-Cervantes, M.; Naik, A.; Kalia, Y.N.; Quintanar-Guerrero, D.; Ganem-Quintanar, A. Applications of thermo-reversible pluronic F-127 gels in pharmaceutical formulations. *J. Pharm. Pharm. Sci.* **2006**, *9*, 339–358. [[PubMed](#)]
119. Bozzuto, G.; Molinari, A. Liposomes as nanomedical devices. *Int. J. Nanomed.* **2015**, *10*, 975–999. [[CrossRef](#)] [[PubMed](#)]
120. Sercombe, L.; Veerati, T.; Moheimani, F.; Wu, S.Y.; Sood, A.K.; Hua, S. Advances and challenges of liposome assisted drug delivery. *Front. Pharm.* **2015**, *6*, 286. [[CrossRef](#)] [[PubMed](#)]
121. Alavi, M.; Karimi, N.; Safaei, M. Application of various types of liposomes in drug delivery systems. *Adv. Pharm. Bull.* **2017**, *7*, 3–9. [[CrossRef](#)] [[PubMed](#)]
122. Yingchoncharoen, P.; Kalinowski, D.S.; Richardson, D.R. Lipid-based drug delivery systems in cancer therapy: What is available and what is yet to come. *Pharm. Rev.* **2016**, *68*, 701–787. [[CrossRef](#)] [[PubMed](#)]
123. Bulbake, U.; Doppalapudi, S.; Kommineni, N.; Khan, W. Liposomal formulations in clinical use: An updated review. *Pharmaceutics* **2017**, *9*, 12. [[CrossRef](#)] [[PubMed](#)]
124. Jani, R.K.; Gohil, K.M.; Kaushalkumar, R. Liposomal formulations in cancer therapy: Basic concepts to advanced strategies. *Int. J. Pharm. Sci. Drug Res.* **2018**, *10*, 386–393. [[CrossRef](#)]

125. Felice, B.; Prabhakaran, M.P.; Rodríguez, A.P.; Ramakrishna, S. Drug delivery vehicles on a nano-engineering perspective. *Mater. Sci. Eng. C* **2014**, *41*, 178–195. [[CrossRef](#)] [[PubMed](#)]
126. Fanciullino, R.; Ciccolini, J. Liposome-encapsulated anticancer drugs: Still waiting for the magic bullet? *Curr. Med. Chem.* **2009**, *16*, 4361–4371. [[CrossRef](#)] [[PubMed](#)]
127. Hang, Z.; Cooper, M.A.; Ziora, Z.M. Platinum-based anticancer drugs encapsulated liposome and polymeric micelle formulation in clinical trials. *Biochem. Compd.* **2016**, *4*, 1. [[CrossRef](#)]
128. Stoyanova, E.; Petrov, P.; Karadjova, I.; Momekov, G.; Koseva, N. Cisplatin delivery vehicles based on stabilized polymeric aggregates comprising poly (acrylic acid) chains. *Polym. J.* **2017**, *49*, 607–615. [[CrossRef](#)]
129. Caracciolo, G. Clinically approved liposomal nanomedicines: Lessons learned from the biomolecular corona. *Nanoscale* **2018**, *10*, 4167–4172. [[CrossRef](#)]
130. Stathopoulos, G.P.; Boulikas, T. Lipoplatin formulation review article. *J. Drug Deliv.* **2012**, *2012*, 581363. [[CrossRef](#)]
131. Qi, P.; Cao, M.; Song, L.; Chen, C.; Liu, M.; Li, N.; Wu, D.; Peng, J.; Hu, G.; Zhao, J. The biological activity of cationic liposomes in drug delivery and toxicity test in animal models. *Environ. Toxicol. Pharm.* **2016**, *47*, 159–164. [[CrossRef](#)] [[PubMed](#)]
132. Lukowski, J.K.; Weaver, E.M.; Hummon, A.B. Analyzing liposomal drug delivery systems in three-dimensional cell culture models using MALDI imaging mass spectrometry. *Anal. Chem.* **2017**, *89*, 8453–8458. [[CrossRef](#)] [[PubMed](#)]
133. Walde, P.; Ichikawa, S. Enzymes inside lipid vesicles: Preparation, reactivity and applications. *Biomol. Eng.* **2001**, *18*, 143–177. [[CrossRef](#)]
134. Irace, C.; Misso, G.; Capuozzo, A.; Piccolo, M.; Riccardi, C.; Luchini, A.; Caraglia, M.; Paduano, L.; Montesarchio, D.; Santamaria, R. Antiproliferative effects of ruthenium-based nucleolipidic nanoaggregates in human models of breast cancer in vitro: Insights into their mode of action. *Sci. Rep.* **2017**, *7*, 45236–45249. [[CrossRef](#)] [[PubMed](#)]
135. John, R. Masters HeLa cells 50 years on: The good, the bad and the ugly. *Nat. Rev. Cancer* **2002**, *2*, 315–319. [[CrossRef](#)]
136. Grobbs, B.; De Deyn, P.P.; Slegers, H. Rat C6 glioma as experimental model system for the study of glioblastoma growth and invasion. *Cell Tissue Res.* **2002**, *310*, 257–270. [[CrossRef](#)] [[PubMed](#)]
137. Miniaci, M.C.; Irace, C.; Capuozzo, A.; Piccolo, M.; Di Pascale, A.; Russo, A.; Lippiello, P.; Lepre, F.; Russo, G.; Santamaria, R. Cysteine prevents the reduction in keratin synthesis induced by iron deficiency in human keratinocytes. *J. Cell. Biochem.* **2016**, *117*, 402–412. [[CrossRef](#)]
138. Ji, L.; Zheng, W.; Lin, Y.; Wang, X.; Lü, S.; Hao, X.; Luo, Q.; Li, X.; Yang, L.; Wang, F. Novel ruthenium complexes ligated with 4-anilinoquinazoline derivatives: Synthesis, characterisation and preliminary evaluation of biological activity. *Eur. J. Med. Chem.* **2014**, *77*, 110–120. [[CrossRef](#)]
139. Nikolova, A.; Momekov, G.; Bakalova, A.; Nikolova, K.; Ivanov, D. Novel Ru(III) complexes with some benzothiazole derivatives: Synthesis, physicochemical and pharmacological investigations. *Drug Res.* **2015**, *65*, 317–322. [[CrossRef](#)]
140. Dömötör, O.; de Almeida, R.F.M.; Côrte-Real, L.; Matos, C.P.; Marques, F.; Matos, A.; Real, C.; Kiss, T.; Enyedy, É.A.; Helena Garcia, M.; et al. Studies on the mechanism of action of antitumor bis(aminophenolate) ruthenium(III) complexes. *J. Inorg. Biochem.* **2017**, *168*, 27–37. [[CrossRef](#)]
141. Sahyon, H.A.; El-Bindary, A.A.; Shoair, A.F.; Abdellatif, A.A. Synthesis and characterization of ruthenium(III) complex containing 2-aminomethyl benzimidazole, and its anticancer activity of in vitro and in vivo models. *J. Mol. Liq.* **2018**, *255*, 122–134. [[CrossRef](#)]
142. Hutchinson, L. Breast cancer: Challenges, controversies, breakthroughs. *Nat. Rev. Clin. Oncol.* **2010**, *7*, 669–670. [[CrossRef](#)]
143. Dai, X.; Li, T.; Bai, Z.; Yang, Y.; Liu, X.; Zhan, J.; Shi, B. Breast cancer intrinsic subtype classification, clinical use and future trends. *Am. J. Cancer Res.* **2015**, *5*, 2929–2943.
144. Akram, M.; Iqbal, M.; Daniyal, M.; Khan, A.U. Awareness and current knowledge of breast cancer. *Biol. Res.* **2017**, *50*, 33. [[CrossRef](#)]
145. Lacroix, M.; Leclercq, G. Relevance of breast cancer cell lines as models for breast tumours: An update. *Breast Cancer Res. Treat.* **2004**, *83*, 249–289. [[CrossRef](#)]
146. Holliday, D.L.; Speirs, V. Choosing the right cell line for breast cancer research. *Breast Cancer Res.* **2011**, *13*, 215. [[CrossRef](#)]

147. Dai, X.; Cheng, H.; Bai, Z.; Li, J. Breast cancer cell line classification and its relevance with breast tumor subtyping. *J. Cancer* **2017**, *8*, 3131–3141. [[CrossRef](#)]
148. Brabec, V.; Nováková, O. DNA binding mode of ruthenium complexes and relationship to tumor cell toxicity. *Drug Resist. Update* **2006**, *9*, 111–122. [[CrossRef](#)]
149. Bergamo, A.; Sava, G. Ruthenium complexes can target determinants of tumour malignancy. *Dalton Trans.* **2007**, *36*, 1267–1272. [[CrossRef](#)]
150. Coppola, C.; Paciello, A.; Mangiapià, G.; Licen, S.; Boccalon, M.; De Napoli, L.; Paduano, L.; Tecilla, P.; Montesarchio, D. Design, synthesis and characterisation of a fluorescently labelled CyPLOS ionophore. *Chemistry* **2010**, *16*, 13757–13772. [[CrossRef](#)]
151. De Tito, S.; Morvan, F.; Meyer, A.; Vasseur, J.J.; Cummaro, A.; Petraccone, L.; Pagano, B.; Novellino, E.; Randazzo, A.; Giancola, C.; et al. Fluorescence enhancement upon G-quadruplex folding: Synthesis, structure, and biophysical characterization of a dansyl/cyclodextrin-tagged thrombin binding aptamer. *Bioconj. Chem.* **2013**, *24*, 1917–1927. [[CrossRef](#)]
152. Riccardi, C.; Russo Krauss, I.; Musumeci, D.; Morvan, F.; Meyer, A.; Vasseur, J.J.; Paduano, L.; Montesarchio, D. Fluorescent thrombin binding aptamer-tagged nanoparticles for an efficient and reversible control of thrombin activity. *ACS Appl. Mater. Interfaces* **2017**, *9*, 35574–35587. [[CrossRef](#)]
153. Li, C.; Ip, K.-W.; Man, W.-L.; Song, D.; He, M.-L.; Yiu, S.-M.; Lau, T.-C.; Zhu, G. Cytotoxic (salen) ruthenium(III) anticancer complexes exhibit different modes of cell death directed by axial ligands. *Chem. Sci.* **2017**, *8*, 6865–6870. [[CrossRef](#)]
154. Krysko, D.V.; Vanden Berghe, T.; D’Herde, K.; Vandenabeele, P. Apoptosis and necrosis: Detection, discrimination and phagocytosis. *Methods* **2008**, *44*, 205–221. [[CrossRef](#)]
155. Chatterjee, S.; Kundu, S.; Bhattacharyya, A.; Hartinger, C.G.; Dyson, P.J. The ruthenium(II)-arene compound RAPTA-C induces apoptosis in EAC cells through mitochondrial and p53-JNK pathways. *J. Biol. Inorg. Chem.* **2008**, *1*, 1149–1155. [[CrossRef](#)]
156. De Lima, A.P.; Pereira, F.D.C.; Vilanova-Costa, C.A.S.T.; Soares, J.R.; Pereira, L.C.G.; Porto, H.K.P.; Pavanin, L.A.; Dos Santos, W.B.; Silveira-Lacerda, E.D.P. Induction of cell cycle arrest and apoptosis by ruthenium complex cis-(dichloro)tetramineruthenium(III) chloride in human lung carcinoma cells A549. *Biol. Trace Elem. Res.* **2012**, *147*, 8–15. [[CrossRef](#)]
157. Xia, Y.; Chen, Q.; Qin, X.; Sun, D.; Zhang, J.; Liu, J. Studies of ruthenium(II)-2,2’-bisimidazole complexes on binding to G-quadruplex DNA and inducing apoptosis in HeLa cells. *New J. Chem.* **2013**, *37*, 3706–3715. [[CrossRef](#)]
158. Vilanova-Costa, C.A.S.T.; Porto, H.K.P.; Pereira, F.D.C.; De Lima, A.P.; Dos Santos, W.B.; Silveira-Lacerda, E.D.P. The ruthenium complexes cis-(dichloro)tetramineruthenium(III) chloride and cis-tetraammine(oxalato)ruthenium(III) dithionate overcome resistance inducing apoptosis on human lung carcinoma cells (A549). *BioMetals* **2014**, *27*, 459–469. [[CrossRef](#)]
159. Berndsen, R.H.; Weiss, A.; Abdul, U.K.; Wong, T.J.; Meraldi, P.; Griffioen, A.W.; Dyson, P.J.; Nowak-Sliwinska, P. Combination of ruthenium(II)-arene complex [Ru( $\eta^6$ -p-cymene)Cl<sub>2</sub> (pta)] (RAPTA-C) and the epidermal growth factor receptor inhibitor erlotinib results in efficient angiostatic and antitumor activity. *Sci. Rep.* **2017**, *7*, 43005. [[CrossRef](#)]
160. Popolin, C.P.; Reis, J.P.B.; Becceneri, A.B.; Graminha, A.E.; Almeida, M.A.P.; Corrêa, R.S.; Colina-Vegas, L.A.; Ellena, J.; Batista, A.A.; Cominetti, M.R. Cytotoxicity and anti-tumor effects of new ruthenium complexes on triple negative breast cancer cells. *PLoS ONE* **2017**, *12*, e0183275. [[CrossRef](#)]
161. Popolin, C.P.; Cominetti, M.R. A review of ruthenium complexes activities on breast cancer cells. *Mini-Rev. Med. Chem.* **2017**, *17*, 1435–1441. [[CrossRef](#)]
162. Misso, G.; Giuberti, G.; Lombardi, A.; Grimaldi, A.; Ricciardiello, F.; Giordano, A.; Tagliaferri, P.; Abbruzzese, A.; Caraglia, M. Pharmacological inhibition of HSP90 and ras activity as a new strategy in the treatment of HNSCC. *J. Cell. Physiol.* **2013**, *228*, 130–141. [[CrossRef](#)]
163. Okamura, M.; Hashimoto, K.; Shimada, J.; Sakagami, H. Apoptosis-inducing activity of cisplatin (CDDP) against human hepatoma and oral squamous cell carcinoma cell lines. *Anticancer Res.* **2004**, *24*, 655–661.
164. Jänicke, R.U.; Sprengart, M.L.; Wati, M.R.; Porter, A.G. Caspase-3 is required for DNA fragmentation and morphological changes associated with apoptosis. *J. Biol. Chem.* **1998**, *273*, 9357–9360. [[CrossRef](#)]

165. Devarajan, E.; Sahin, A.A.; Chen, J.S.; Krishnamurthy, R.R.; Aggarwal, N.; Brun, A.M.; Sapino, A.; Zhang, F.; Sharma, D.; Yang, X.H.; et al. Down-regulation of caspase 3 in breast cancer: A possible mechanism for chemoresistance. *Oncogene* **2002**, *21*, 8843–8851. [[CrossRef](#)]
166. Oberhammer, F.; Wilson, J.W.; Dive, C.; Morris, I.D.; Hickman, J.A.; Wakeling, A.E.; Walker, P.R.; Sikorska, M. Apoptotic death in epithelial cells: Cleavage of DNA to 300 and/or 50 kb fragments prior to or in the absence of internucleosomal fragmentation. *EMBO J.* **1993**, *12*, 3679–3684. [[CrossRef](#)]
167. Liang, Y.; Yan, C.; Schor, N.F. Apoptosis in the absence of caspase 3. *Oncogene* **2001**, *20*, 6570–6578. [[CrossRef](#)]
168. Delbridge, A.R.D.; Grabow, S.; Strasser, A.; Vaux, D.L. Thirty years of BCL-2: Translating cell death discoveries into novel cancer therapies. *Nat. Rev. Cancer* **2016**, *16*, 99–109. [[CrossRef](#)]
169. Zheng, J.H.; Viacava Follis, A.; Kriwacki, R.W.; Moldoveanu, T. Discoveries and controversies in BCL-2 protein-mediated apoptosis. *FEBS J.* **2016**, *283*, 2690–2700. [[CrossRef](#)]
170. Abate, M.; Festa, A.; Falco, M.; Lombardi, A.; Luce, A.; Grimaldi, A.; Zappavigna, S.; Sperlongano, P.; Irace, C.; Caraglia, M.; et al. Mitochondria as playmakers of apoptosis, autophagy and senescence. *Semin. Cell Dev. Biol.* **2019**. [[CrossRef](#)]
171. Lopez, J.; Tait, S.W.G. Mitochondrial apoptosis: Killing cancer using the enemy within. *Br. J. Cancer* **2015**, *112*, 957–962. [[CrossRef](#)]
172. Delbridge, A.R.D.; Strasser, A. The BCL-2 protein family, BH3-mimetics and cancer therapy. *Cell Death Differ.* **2015**, *22*, 1071–1080. [[CrossRef](#)]
173. Sturm, I.; Papadopoulos, S.; Hillebrand, T.; Benter, T.; Lück, H.J.; Wolff, G.; Dörken, B.; Daniel, P.T. Impaired BAX protein expression in breast cancer: Mutational analysis of the BAX and the p53 gene. *Int. J. Cancer* **2000**, *27*, 517–521. [[CrossRef](#)]
174. Merino, D.; Lok, S.W.; Visvader, J.E.; Lindeman, G.J. Targeting BCL-2 to enhance vulnerability to therapy in estrogen receptor-positive breast cancer. *Oncogene* **2016**, *35*, 1877–1887. [[CrossRef](#)]
175. Kiraz, Y.; Adan, A.; Kartal Yandim, M.; Baran, Y. Major apoptotic mechanisms and genes involved in apoptosis. *Tumor Biol.* **2016**, *37*, 8471–8486. [[CrossRef](#)]
176. Qian, C.; Wang, J.Q.; Song, C.L.; Wang, L.L.; Ji, L.N.; Chao, H. The induction of mitochondria-mediated apoptosis in cancer cells by ruthenium(II) asymmetric complexes. *Metallomics* **2013**, *5*, 844–854. [[CrossRef](#)]
177. Fulda, S.; Debatin, K.M. Extrinsic versus intrinsic apoptosis pathways in anticancer chemotherapy. *Oncogene* **2006**, *25*, 4798–4811. [[CrossRef](#)]
178. Lima, A.P.; Pereira, F.C.; Almeida, M.A.P.; Mello, F.M.S.; Pires, W.C.; Pinto, T.M.; Delella, F.K.; Felisbino, S.L.; Moreno, V.; Batista, A.A.; et al. Cytotoxicity and apoptotic mechanism of ruthenium(II) amino acid complexes in sarcoma-180 tumor cells. *PLoS ONE* **2014**, *9*, e105865. [[CrossRef](#)]
179. Pietrocola, F.; Pol, J.; Vacchelli, E.; Baracco, E.E.; Levesque, S.; Castoldi, F.; Maiuri, M.C.; Madeo, F.; Kroemer, G. Autophagy induction for the treatment of cancer. *Autophagy* **2016**, *12*, 1962–1964. [[CrossRef](#)]
180. Condello, M.; Pellegrini, E.; Caraglia, M.; Meschini, S. Targeting autophagy to overcome human diseases. *Int. J. Mol. Sci.* **2019**, *20*, E725. [[CrossRef](#)]
181. Ryter, S.W.; Mizumura, K.; Choi, A.M.K. The impact of autophagy on cell death modalities. *Int. J. Cell Biol.* **2014**, *2014*, 502676. [[CrossRef](#)]
182. Mancias, J.D.; Kimmelman, A.C. Mechanisms of selective autophagy in normal physiology and cancer. *J. Mol. Biol.* **2016**, *428*, 1659–1680. [[CrossRef](#)]
183. Gozuacik, D.; Kimchi, A. Autophagy as a cell death and tumor suppressor mechanism. *Oncogene* **2004**, *23*, 2891–2906. [[CrossRef](#)]
184. Mizushima, N.; Komatsu, M. Autophagy: Renovation of cells and tissues. *Cell* **2011**, *147*, 728–741. [[CrossRef](#)]
185. Ozpolat, B.; Benbrook, D.M. Targeting autophagy in cancer management-strategies and developments. *Cancer Manag. Res.* **2015**, *7*, 291–299. [[CrossRef](#)]
186. Lippai, M.; Szatmári, Z. Autophagy—from molecular mechanisms to clinical relevance. *Cell Biol. Toxicol.* **2017**, *33*, 145–168. [[CrossRef](#)]
187. Marinković, M.; Šprung, M.; Buljubašić, M.; Novak, I. Autophagy modulation in cancer: Current knowledge on action and therapy. *Oxid. Med. Cell. Longev.* **2018**, *2018*, 8023821. [[CrossRef](#)]
188. Dikic, I.; Elazar, Z. Mechanism and medical implications of mammalian autophagy. *Nat. Rev. Mol. Cell Biol.* **2018**, *19*, 349–364. [[CrossRef](#)]
189. Lin, L.; Baehrecke, E.H. Autophagy, cell death, and cancer. *Mol Cell Oncol.* **2015**, *2*, e985913. [[CrossRef](#)]

190. Fitzwalter, B.E.; Thorburn, A. Recent insights into cell death and autophagy. *FEBS J.* **2015**, *282*, 4279–4288. [[CrossRef](#)]
191. Sambhi, M.; Haq, S.; Samuel, V.; Qorri, B.; Haxho, F.; Hill, K.; Harless, W.; Szewczuk, M.R. Alternative therapies for metastatic breast cancer: Multimodal approach targeting tumor cell heterogeneity. *Breast Cancer Targets Ther.* **2017**, *9*, 85–93. [[CrossRef](#)]
192. Lim, B.; Hortobagyi, G.N. Current challenges of metastatic breast cancer. *Cancer Metastasis Rev.* **2016**, *35*, 495–514. [[CrossRef](#)]
193. Turashvili, G.; Brogi, E. Tumor heterogeneity in breast cancer. *Front. Med.* **2017**, *4*, 227. [[CrossRef](#)]
194. Wong, C.H.; Iskandar, K.B.; Yadav, S.K.; Hirpara, J.L.; Loh, T.; Pervaiz, S. Simultaneous induction of non-canonical autophagy and apoptosis in cancer cells by ROS-dependent ERK and JNK activation. *PLoS ONE* **2010**, *5*, e9996. [[CrossRef](#)]
195. Ojha, R.; Ishaq, M.; Singh, S. Caspase-mediated crosstalk between autophagy and apoptosis: Mutual adjustment or matter of dominance. *J. Cancer Res. Ther.* **2015**, *11*, 514–524. [[CrossRef](#)]
196. Ueno, T.; Masuda, N.; Kamigaki, S.; Morimoto, T.; Saji, S.; Imoto, S.; Sasano, H.; Toi, M. Differential involvement of autophagy and apoptosis in response to chemoendocrine and endocrine therapy in breast cancer: JBCRG-07TR. *Int. J. Mol. Sci.* **2019**, *20*, E984. [[CrossRef](#)]
197. Radogna, F.; Dicato, M.; Diederich, M. Cancer-type-specific crosstalk between autophagy, necroptosis and apoptosis as a pharmacological target. *Biochem. Pharm.* **2015**, *94*, 1–11. [[CrossRef](#)]
198. Yuan, J.; Lei, Z.; Wang, X.; Zhu, F.; Chen, D. Ruthenium complex  $\Lambda$ -WH0402 induces hepatocellular carcinoma LM6 (HCCLM6) cell death by triggering the Beclin-1-dependent autophagy pathway. *Metallomics* **2015**, *7*, 896–907. [[CrossRef](#)]
199. Chen, L.; Li, G.; Peng, F.; Jie, X.; Dongye, G.; Cai, K.; Feng, R.; Li, B.; Zeng, Q.; Lun, K.; et al. The induction of autophagy against mitochondria-mediated apoptosis in lung cancer cells by a ruthenium (II) imidazole complex. *Oncotarget* **2016**, *7*, 80716–80734. [[CrossRef](#)]
200. Maier, K.E.; Levy, M. From selection hits to clinical leads: Progress in aptamer discovery. *Mol. Ther. Methods Clin. Dev.* **2016**, *5*, 16014–16023. [[CrossRef](#)]
201. Grimaldi, A.; Santini, D.; Zappavigna, S.; Lombardi, A.; Misso, G.; Boccellino, M.; Desiderio, V.; Vitiello, P.P.; Di Lorenzo, G.; Zoccoli, A.; et al. Antagonistic effects of chloroquine on autophagy occurrence potentiate the anticancer effects of everolimus on renal cancer cells. *Cancer Biol. Ther.* **2015**, *16*, 567–579. [[CrossRef](#)]
202. Decuypere, J.P.; Parys, J.B.; Bultynck, G. Regulation of the autophagic bcl-2/beclin 1 interaction. *Cells* **2012**, *1*, 284–312. [[CrossRef](#)]
203. Fujii, T.; Yajima, R.; Tatsuki, H.; Oosone, K.; Kuwano, H. Anticancer effect of rapamycin on MCF-7 via downregulation of VEGF expression. *Vitr. Cell. Dev. Biol. Anim.* **2016**, *52*, 45–48. [[CrossRef](#)]
204. Tanida, I.; Waguri, S. Measurement of autophagy in cells and tissues. *Methods Mol. Biol.* **2010**, *648*, 193–214. [[CrossRef](#)]
205. Tanida, I.; Ueno, T.; Kominami, E. LC3 and autophagy. *Methods Mol. Biol.* **2008**, *445*, 77–88. [[CrossRef](#)]
206. Zhou, F.; Yang, Y.; Xing, D. Bcl-2 and Bcl-xL play important roles in the crosstalk between autophagy and apoptosis. *FEBS J.* **2011**, *278*, 403–413. [[CrossRef](#)]
207. Fu, L.L.; Cheng, Y.; Liu, B. Beclin-1: Autophagic regulator and therapeutic target in cancer. *Int. J. Biochem. Cell Biol.* **2013**, *45*, 921–924. [[CrossRef](#)]
208. Jung, Y.Y.; Lee, Y.K.; Koo, J.S. The potential of Beclin 1 as a therapeutic target for the treatment of breast cancer. *Expert Opin. Ther. Targets* **2016**, *20*, 167–178. [[CrossRef](#)]
209. Zarzynska, J.M. The importance of autophagy regulation in breast cancer development and treatment. *Biomed. Res. Int.* **2014**, *2014*, 710345. [[CrossRef](#)]
210. Zhang, X.D.; Wang, Y.; Wu, J.C.; Lin, F.; Han, R.; Han, F.; Fukunaga, K.; Qin, Z.H. Down-regulation of Bcl-2 enhances autophagy activation and cell death induced by mitochondrial dysfunction in rat striatum. *J. Neurosci. Res.* **2009**, *87*, 3600–3610. [[CrossRef](#)]
211. Oh, S.; Xiaofei, E.; Ni, D.; Pirooz, S.D.; Lee, J.Y.; Lee, D.; Zhao, Z.; Lee, S.; Lee, H.; Ku, B.; et al. Downregulation of autophagy by Bcl-2 promotes MCF7 breast cancer cell growth independent of its inhibition of apoptosis. *Cell Death Differ.* **2011**, *18*, 452–464. [[CrossRef](#)]
212. Adams, J.M.; Cory, S. The BCL-2 arbiters of apoptosis and their growing role as cancer targets. *Cell Death Differ.* **2018**, *25*, 27–36. [[CrossRef](#)]

213. Uchegbu, I.F.; Florence, A.T. Non-ionic surfactant vesicles (niosomes): Physical and pharmaceutical chemistry. *Adv. Colloid Interface Sci.* **1995**, *58*, 1–55. [[CrossRef](#)]
214. Uchegbu, I.F.; Vyas, S.P. Non-ionic surfactant based vesicles (niosomes) in drug delivery. *Int. J. Pharm.* **1998**, *172*, 33–70. [[CrossRef](#)]
215. Marianecchi, C.; Di Marzio, L.; Rinaldi, F.; Celia, C.; Paolino, D.; Alhaique, F.; Esposito, S.; Carafa, M. Niosomes from 80 s to present: The state of the art. *Adv. Colloid Interface Sci.* **2014**, *205*, 187–206. [[CrossRef](#)]
216. Grimaldi, N.; Andrade, F.; Segovia, N.; Ferrer-Tasies, L.; Sala, S.; Veciana, J.; Ventosa, N. Lipid-based nanovesicles for nanomedicine. *Chem. Soc. Rev.* **2016**, *45*, 6520–6545. [[CrossRef](#)]
217. Khan, R.; Irchhaiya, R. Niosomes: A potential tool for novel drug delivery. *J. Pharm. Investig.* **2016**, *46*, 195–204. [[CrossRef](#)]
218. Ag Seleci, D.; Seleci, M.; Walter, J.G.; Stahl, F.; Scheper, T. Niosomes as nanoparticulate drug carriers: Fundamentals and recent applications. *J. Nanomater.* **2016**, *2016*, 1–13. [[CrossRef](#)]
219. Grijalvo, S.; Puras, G.; Zárate, J.; Sainz-Ramos, M.; Qtaish, N.A.L.; López, T.; Mashal, M.; Attia, N.; Díaz, D.; Pons, R.; et al. Cationic niosomes as non-viral vehicles for nucleic acids: Challenges and opportunities in gene delivery. *Pharmaceutics* **2019**, *11*. [[CrossRef](#)]
220. Moghassemi, S.; Hadjizadeh, A. Nano-niosomes as nanoscale drug delivery systems: An illustrated review. *J. Control. Release* **2014**, *185*, 22–36. [[CrossRef](#)]
221. Hua, S. Lipid-based nano-delivery systems for skin delivery of drugs and bioactives. *Front. Pharm.* **2015**, *6*, 219–224. [[CrossRef](#)]
222. Marianecchi, C.; Paolino, D.; Celia, C.; Fresta, M.; Carafa, M.; Alhaique, F. Non-ionic surfactant vesicles in pulmonary glucocorticoid delivery: Characterization and interaction with human lung fibroblasts. *J. Control. Release* **2010**, *147*, 127–135. [[CrossRef](#)]
223. Abdelkader, H.; Alani, A.W.G.; Alany, R.G. Recent advances in non-ionic surfactant vesicles (niosomes): Self-assembly, fabrication, characterization, drug delivery applications and limitations. *Drug Deliv.* **2014**, *21*, 87–100. [[CrossRef](#)]
224. Asthana, G.S.; Sharma, P.K.; Asthana, A. In vitro and in vivo evaluation of niosomal formulation for controlled delivery of clarithromycin. *Scientifica* **2016**, *2016*, 6492953. [[CrossRef](#)]
225. Junyaprasert, V.B.; Teeranachaideekul, V.; Supaperm, T. Effect of charged and non-ionic membrane additives on physicochemical properties and stability of niosomes. *AAPS PharmSciTech* **2008**, *9*, 851–859. [[CrossRef](#)]
226. Redondo-Morata, L.; Giannotti, M.I.; Sanz, F. Influence of cholesterol on the phase transition of lipid bilayers: A temperature-controlled force spectroscopy study. *Langmuir* **2012**, *28*, 12851–12860. [[CrossRef](#)]
227. Bates, P.J.; Reyes-reyes, E.M.; Malik, M.T.; Murphy, E.M.; Toole, M.G.O.; Trent, J.O. G-quadruplex oligonucleotide AS1411 as a cancer-targeting agent: Uses and mechanisms. *BBA Gen. Subj.* **2017**, *1861*, 1414–1428. [[CrossRef](#)]
228. Guo, J.; Gao, X.; Su, L.; Xia, H.; Gu, G.; Pang, Z.; Jiang, X.; Yao, L.; Chen, J.; Chen, H. Aptamer-functionalized PEG-PLGA nanoparticles for enhanced anti-glioma drug delivery. *Biomaterials* **2011**, *32*, 8010–8020. [[CrossRef](#)]
229. Zhang, J.; Chen, R.; Chen, F.; Chen, M.; Wang, Y. Nucleolin targeting AS1411 aptamer modified pH-sensitive micelles: A dual-functional strategy for paclitaxel delivery. *J. Control. Release* **2015**, *213*, e137–e138. [[CrossRef](#)]
230. Zhang, J.; Chen, R.; Fang, X.; Chen, F.; Wang, Y.; Chen, M. Nucleolin targeting AS1411 aptamer modified pH-sensitive micelles for enhanced delivery and antitumor efficacy of paclitaxel. *Nano Res.* **2015**, *8*, 201–218. [[CrossRef](#)]
231. Li, F.; Lu, J.; Liu, J.; Liang, C.; Wang, M.; Wang, L.; Li, D.; Yao, H.; Zhang, Q.; Wen, J.; et al. A water-soluble nucleolin aptamer-paclitaxel conjugate for tumor-specific targeting in ovarian cancer. *Nat. Commun.* **2017**, *8*, 1390. [[CrossRef](#)]
232. Gao, H.; Qian, J.; Cao, S.; Yang, Z.; Pang, Z.; Pan, S.; Fan, L.; Xi, Z.; Jiang, X.; Zhang, Q. Precise glioma targeting of and penetration by aptamer and peptide dual-functionalized nanoparticles. *Biomaterials* **2012**, *33*, 5115–5123. [[CrossRef](#)]
233. Tao, W.; Zeng, X.; Wu, J.; Zhu, X.; Yu, X.; Zhang, X.; Zhang, J.; Liu, G.; Mei, L. Polydopamine-based surface modification of novel nanoparticle-aptamer bioconjugates for in vivo breast cancer targeting and enhanced therapeutic effects. *Theranostics* **2016**, *6*, 470–484. [[CrossRef](#)]
234. Xu, G.; Yu, X.; Zhang, J.; Sheng, Y.; Liu, G.; Tao, W.; Mei, L. Robust aptamer-polydopamine-functionalized M-PLGA-TPGS nanoparticles for targeted delivery of docetaxel and enhanced cervical cancer therapy. *Int. J. Nanomed.* **2016**, *11*, 2953–2965. [[CrossRef](#)]

235. Chen, D.; Li, B.; Cai, S.; Wang, P.; Peng, S.; Sheng, Y.; He, Y.; Gu, Y.; Chen, H. Dual targeting luminescent gold nanoclusters for tumor imaging and deep tissue therapy. *Biomaterials* **2016**, *100*, 1–16. [[CrossRef](#)]
236. Xing, H.; Tang, L.; Yang, X.; Hwang, K.; Wang, W.; Yin, Q.; Wong, N.Y.; Dobrucki, L.W.; Yasui, N.; Katzenellenbogen, J.A.; et al. Selective delivery of an anticancer drug with aptamer-functionalized liposomes to breast cancer cells in vitro and in vivo. *J. Mater. Chem. B* **2013**, *1*, 5288–5297. [[CrossRef](#)]
237. Zhang, H.; Hou, L.; Jiao, X.; Yandan, J.; Zhu, X.; Hongji, L.; Chen, X.; Ren, J.; Xia, Y.; Zhang, Z. In vitro and in vivo evaluation of antitumor drug-loaded aptamer targeted single-walled carbon nanotubes system. *Curr. Pharm. Biotechnol.* **2014**, *14*, 1105–1117. [[CrossRef](#)]
238. Zhang, B.; Luo, Z.; Liu, J.; Ding, X.; Li, J.; Cai, K. Cytochrome c end-capped mesoporous silica nanoparticles as redox-responsive drug delivery vehicles for liver tumor-targeted triplex therapy in vitro and in vivo. *J. Control. Release* **2014**, *192*, 192–201. [[CrossRef](#)]
239. Li, X.; Yu, Y.; Ji, Q.; Qiu, L. Targeted delivery of anticancer drugs by aptamer AS1411 mediated Pluronic F127/cyclodextrin-linked polymer composite micelles. *Nanomed. Nanotechnol. Biol. Med.* **2015**, *11*, 175–184. [[CrossRef](#)]
240. Peng, L.H.; Zhang, Y.H.; Han, L.J.; Zhang, C.Z.; Wu, J.H.; Wang, X.R.; Gao, J.Q.; Mao, Z.W. Cell membrane capsules for encapsulation of chemotherapeutic and cancer cell targeting in vivo. *ACS Appl. Mater. Interfaces* **2015**, *7*, 18628–18637. [[CrossRef](#)]
241. Trinh, T.L.; Zhu, G.; Xiao, X.; Puszyk, W.; Sefah, K.; Wu, Q.; Tan, W.; Liu, C. A synthetic aptamer-drug adduct for targeted liver cancer therapy. *PLoS ONE* **2015**, *10*, e0136673. [[CrossRef](#)]
242. Liao, Z.X.; Chuang, E.Y.; Lin, C.C.; Ho, Y.C.; Lin, K.J.; Cheng, P.Y.; Chen, K.J.; Wei, H.J.; Sung, H.W. An AS1411 aptamer-conjugated liposomal system containing a bubble-generating agent for tumor-specific chemotherapy that overcomes multidrug resistance. *J. Control. Release* **2015**, *208*, 42–51. [[CrossRef](#)]
243. Li, X.; Zhu, X.; Qiu, L. Constructing aptamer anchored nanovesicles for enhanced tumor penetration and cellular uptake of water soluble chemotherapeutics. *Acta Biomater.* **2016**, *35*, 269–279. [[CrossRef](#)]
244. Liu, X.; Wu, L.; Wang, L.; Jiang, W. A dual-targeting DNA tetrahedron nanocarrier for breast cancer cell imaging and drug delivery. *Talanta* **2018**, *179*, 356–363. [[CrossRef](#)]
245. Taghdisi, S.M.; Danesh, N.M.; Ramezani, M.; Lavaee, P.; Jalalian, S.H.; Robati, R.Y.; Abnous, K. Double targeting and aptamer-assisted controlled release delivery of epirubicin to cancer cells by aptamers-based dendrimer in vitro and in vivo. *Eur. J. Pharm. Biopharm.* **2016**, *102*, 152–158. [[CrossRef](#)]
246. Velikyan, I. Molecular imaging and radiotherapy: Theranostics for personalized patient management. *Theranostics* **2012**, *2*, 424–426. [[CrossRef](#)]
247. Bao, G.; Mitragotri, S.; Tong, S. Multifunctional nanoparticles for drug delivery and molecular imaging. *Annu. Rev. Biomed. Eng.* **2013**, *15*, 253–282. [[CrossRef](#)]
248. Ochoa, G.P.; Sesma, J.Z.; Díez, M.A.; Díaz-Tahoces, A.; Avilés-Trigeros, M.; Grijalvo, S.; Eritja, R.; Fernández, E.; Pedraz, J.L. A novel formulation based on 2,3-di(tetradecyloxy)propan-1-amine cationic lipid combined with polysorbate 80 for efficient gene delivery to the retina. *Pharm. Res.* **2014**, *31*, 1665–1675. [[CrossRef](#)]
249. Grijalvo, S.; Alagia, A.; Puras, G.; Zárata, J.; Pedraz, J.L.; Eritja, R. Cationic vesicles based on non-ionic surfactant and synthetic aminolipids mediate delivery of antisense oligonucleotides into mammalian cells. *Colloids Surf. B Biointerfaces* **2014**, *119*, 30–37. [[CrossRef](#)]
250. Mariadason, J.M.; Arango, D.; Shi, Q.; Wilson, A.J.; Corner, G.A.; Nicholas, C.; Aranes, M.J.; Lesser, M.; Schwartz, E.L.; Augenlicht, L.H. Gene expression profiling-based prediction of response of colon carcinoma cells to 5-fluorouracil and camptothecin. *Cancer Res.* **2003**, *63*, 8791–8812.
251. Jorge, A.F.; Aviñó, A.; Pais, A.A.C.C.; Eritja, R.; Fàbrega, C. DNA-based nanoscaffolds as vehicles for 5-fluoro-2'-deoxyuridine oligomers in colorectal cancer therapy. *Nanoscale* **2018**, *10*, 7238–7249. [[CrossRef](#)]
252. Ojeda, E.; Puras, G.; Agirre, M.; Zárata, J.; Grijalvo, S.; Pons, R.; Eritja, R.; Fernández, E.; Pedraz, J.L. Niosomes based on synthetic cationic lipids for gene delivery: The influence of polar head-groups on the transfection efficiency in HEK-293, ARPE-19 and MSC-D1 cells. *Org. Biomol. Chem.* **2015**, *13*, 1068–1081. [[CrossRef](#)]
253. Luchini, A.; Vitiello, G.; Rossi, F.; Ruiz De Ballesteros, O.; Radulescu, A.; D'Errico, G.; Montesarchio, D.; de Julián Fernández, C.; Paduano, L. Developing functionalized Fe<sub>3</sub>O<sub>4</sub>-Au nanoparticles: A physico-chemical insight. *Phys. Chem. Chem. Phys.* **2015**, *17*, 6087–6097. [[CrossRef](#)]
254. Luchini, A.; Vitiello, G. Understanding the nano-bio interfaces: Lipid-coatings for inorganic nanoparticles as promising strategy for biomedical applications. *Front. Chem.* **2019**, *7*, 1–16. [[CrossRef](#)]

255. Estelrich, J.; Sánchez-Martín, M.J.; Busquets, M.A. Nanoparticles in magnetic resonance imaging: From simple to dual contrast agents. *Int. J. Nanomed.* **2015**, *10*, 1727–1741. [[CrossRef](#)]
256. Alvares, R.D.A.; Szulc, D.A.; Cheng, H.L.M. A scale to measure MRI contrast agent sensitivity. *Sci. Rep.* **2017**, *7*, 15493. [[CrossRef](#)]
257. Boni, A.; Bardi, G.; Bertero, A.; Cappello, V.; Emdin, M.; Flori, A.; Gemmi, M.; Innocenti, C.; Menichetti, L.; Sangregorio, C.; et al. Design and optimization of lipid-modified poly (amidoamine) dendrimer coated iron oxide nanoparticles as probes for biomedical applications. *Nanoscale* **2015**, *7*, 7307–7317. [[CrossRef](#)]
258. Riccardi, C.; Musumeci, D.; Russo Krauss, I.; Piccolo, M.; Irace, C.; Paduano, L.; Montesarchio, D. Exploring the conformational behaviour and aggregation properties of lipid-conjugated AS1411 aptamers. *Int. J. Biol. Macromol.* **2018**, *118*, 1384–1399. [[CrossRef](#)]



© 2019 by the authors. Licensee MDPI, Basel, Switzerland. This article is an open access article distributed under the terms and conditions of the Creative Commons Attribution (CC BY) license (<http://creativecommons.org/licenses/by/4.0/>).